UNIVERSITÉ DE GENÈVE FACULTÉ DES SCIENCES

Section de chimie et biochimie
Département de chimie minérale et analytique Professeur E. Bakker

Ultrasensitive Capacitive Readout for Ion-Selective Electrodes

THÈSE

présentée à la Faculté des sciences de l'Université de Genève
pour obtenir le grade de Docteur ès sciences, mention chimie

par

Pitchnaree KRAIKAEW

de

Nakhon Si Thammarat (Thailand)

Thèse Nº 5650

GENÈVE
Repromail
2022

UNIVERSITÉ DE GENÈVE
FACULTÉ DES SCIENCES

DOCTORAT ÈS SCIENCES, MENTION CHIMIE

Thèse de Madame Pitchnaree KRAIKAEW

intitulée :

«Ultrasensitive Capacitive Readout for Ion-Selective Electrodes»

La Faculté des sciences, sur le préavis de Monsieur E. BAKKER, professeur ordinaire et directeur de thèse (Département de chimie minérale et analytique), Monsieur R. D. MILTON, professeur assistant (Département de chimie minérale et analytique), Monsieur J. BOBACKA, professeur (Laboratory of Molecular Science and Engineering, Faculty of Science and Engineering, Abo Akademi University, Turku, Finland), autorise l'impression de la présente thèse, sans exprimer d'opinion sur les propositions qui y sont énoncées.

Genève, le 11 mai 2022

Thèse - 5650 -

Le Doyen

N.B. - La thèse doit porter la déclaration précédente et remplir les conditions énumérées dans les "Informations relatives aux thèses de doctorat à l'Université de Genève".

Abstract

Potentiometric pH probes remain the gold standard for the detection of pH but are not sufficiently sensitive to reliably detect ocean acidification at adequate frequency. In **Chapter 2**, potentiometric probes are made dramatically more sensitive by placing a capacitive electronic component in series to the pH probe while imposing a constant potential over the measurement circuit. Each sample change now triggers a capacitive current transient that is easily identified between the two equilibrium states, and is integrated to reveal the accumulated charge. This affords dramatically higher precision than with traditional potentiometric probes. pH changes down to 0.001 pH units are easily distinguished in buffer and seawater samples at a precision (standard deviation) of 28 μpH and 67 μpH, respectively. This is orders of magnitude better than what is possible with potentiometric pH probes.

A constant potential capacitive readout of solid-contact ion-selective electrodes (SC-ISE) allows one to obtain easily identifiable current transients that can be integrated to obtain a charge vs logarithmic activity relationship. The resulting readout can therefore be much more sensitive than traditional open-circuit potentiometry. Unfortunately, however, comparatively long measurement times and significant baseline current drifts make it currently difficult to fully realize the promise of this technique. We show in **Chapter 3** that this challenge is overcome by placing the SC-ISE in series with an electronic capacitor, with pH probes as examples. Kirchhoff's law is shown to be useful to choose an adequate range of added capacitances so that it dominates the overall cell value. Two different ion-to-electron transducing materials, functionalized single-wall carbon nanotubes (f-SWCNTs) and poly(3-octylthiophene) (POT), were explored as solid-contact transducing layers. The established SC-ISE-based f-SWCNT transducer is found to be compatible with a wide range of external capacitances up to 100 μF, while POT layers require a narrower range of 1− 4.7 μF. Importantly, the time for a charging transient to reach equilibrium was found to be less than 10 s, which is dramatically faster than without added electronic component. Owing to the ideal behavior of capacitor, the response current decays rapidly to zero, making the determination of the integrated charge practically applicable.

Constant potential capacitive readout of ion-selective membranes offers better sensitivity than traditional potentiometry by giving an easily identifiable transient current spike, which can be integrated to give a charge proportional to logarithmic of ion activity. Some concerns of this technique include complex fluidic handling, longer measurement times, baseline drifts and memory effects arising from excess charge accumulation on the capacitor. **Chapter 4** describes an electronic circuit strategy to automate the switching

procedure, resulting in rapid and reproducible measurements. In contrast to earlier work, alternating to a reference solution is no longer required for establishing a new current baseline. The open-circuit potential is measured before performing chronoamperometry and its value is applied directly to the sample solution. The intermittent discharging of the capacitor by the electronic circuit assures that the potential difference across the capacitor returns again to zero. This electronic capacitive readout system was applied to measure sodium concentration using a 10 μF capacitor to amplify the signal. The precision was found to be improved over direct potentiometry, corresponding to 0.11 mmol L^{-1} 1 NaCl and 0.13 mmol L^{-1} 1 NaCl for standard solutions and pooled serum sample, respectively. Using the automated electronic system for ion measurement makes the system more robust while resulting in fast and reliable quantitative measurements.

In **Chapter 5**, the development of a portable device for constant-potential coulometry is presented. A small potentiostat along with dedicated electronic circuits are integrated and fitted in a small box (18.5 cm width × 10.7 cm length × 3.6 cm height with a weight of 370 g). A range of capacitors (22 – 220 μF) are included in the device, which can be automatically chosen by the control software. The device, the so-called PotentioCap, was evaluated in standard pH solutions and stabilized seawater samples using a hydrogen-selective electrode placed in series with a capacitor. The results of transient current and integrated charge over time correlates well with that from capacitive readout using a benchtop potentiostat with an external electronic circuit (Chapter 4). Furthermore, a mathematical model is presented to describe the effects of constant and exponential decay currents on ion-selective membranes using the Nernst-Planck equation. Numerical simulations are used for estimating the concentration polarization of the ion-ionophore complex and the ion-exchanger in the space and time domains within the membrane. The mathematical models were tested with experiments involving current polarized membranes. The calculated phase boundary potential appears to drift in the same manner as that observed experimentally. In order to improve the measurement procedure, the characteristics of membrane regeneration by the controlled constant potential is simulated. By applying a constant open-circuit potential for 1 min, the precision is found to be 40 times better than without regeneration. Furthermore, a new capacitive model according to RC constant is proposed by considering the resulting potential change with time. The model results were successfully compared with the associated current spike obtained from the established RC charging equation and the experimental data. Electric migrations are shown not to be a significant contribution to the transient current.

Résumé

Les sondes de pH potentiométriques demeurent la référence absolue pour la détection du pH, mais elles ne sont pas suffisamment sensibles pour détecter de façon fiable l'acidification des océans à une fréquence adéquate. Dans le **Chapitre 2**, les sondes potentiométriques sont rendues beaucoup plus sensibles en plaçant un composant électronique capacitif en série avec la sonde de pH, tout en imposant un potentiel constant sur le circuit de mesure. Chaque changement d'échantillon déclenche maintenant un transitoire de courant capacitif qui est facilement identifié entre les deux états d'équilibre, et qui est intégré pour révéler la charge accumulée. Les changements de pH jusqu'à 0,001 unité de pH sont facilement distingués dans les solutions tampon et d'eau de mer avec une précision (écart type) de 28 μpH et 67 μpH, respectivement. Cela représente des ordres de grandeur supérieurs à ce qui est possible avec les sondes de pH potentiométriques.

Une lecture capacitive à potentiel constant des électrodes sélectives d'ions à contact solide (SC-ISE) permet d'obtenir des transitoires de courant facilement identifiables qui peuvent être intégrés pour obtenir une relation charge/activité logarithmique. La lecture qui en résulte peut donc être beaucoup plus sensible que la potentiométrie traditionnelle en circuit ouvert. Malheureusement, les temps de mesure relativement longs et les dérives significatives du courant au niveau de la ligne de base rendent actuellement difficile la réalisation concrète de cette technique prometteuse. Nous montrons au **Chapitre 3** que ce défi est surmonté en plaçant la SC-ISE en série avec un condensateur électronique, en prenant pour exemple les sondes pH. Nous montrons que la loi de Kirchhoff est utile pour choisir une gamme adéquate de capacités ajoutées afin qu'elle domine la valeur globale de la cellule. Deux matériaux différents de transduction ion à électron, les nanotubes de carbone à paroi simple fonctionnalisés (f-SWCNT) et le poly(3-octylthiophène) (POT), ont été étudiés comme couches de transduction à contact solide. Les f-SWCNT, un transducteur classique des SC-ISE, s'est révélé compatible avec une large gamme de capacités externes allant jusqu'à 100 μF, tandis que les couches basées sur POT nécessitent une gamme plus étroite de 1 à 4,7 μF. Il est important de noter que le temps nécessaire à un transitoire de charge pour atteindre l'équilibre est inférieur à 10 s, ce qui est nettement plus rapide que sans composant électronique ajouté. En raison du comportement idéal du condensateur, le courant de réponse décroît rapidement jusqu'à zéro, ce qui rend la détermination de la charge intégrée applicable en pratique.

La lecture capacitive à potentiel constant des membranes sélectives d'ions offre une meilleure sensibilité que la potentiométrie traditionnelle en donnant un pic de courant transitoire facilement identifiable, qui peut

être intégré pour donner une charge proportionnelle au logarithme de l'activité ionique. Cette technique présente quelques inconvénients, notamment une manipulation fluidique complexe, des temps de mesure plus longs, des dérives de la ligne de base et des effets de mémoire dus à l'accumulation d'une charge excessive sur le condensateur. Le **Chapitre 4** décrit une stratégie de circuit électronique permettant d'automatiser la procédure de commutation, ce qui permet d'obtenir des mesures rapides et reproductibles. Contrairement aux travaux antécédents, il n'est plus nécessaire d'alterner avec une solution de référence pour établir une nouvelle ligne de base du courant. Le potentiel en circuit ouvert est mesuré avant d'effectuer la chronoampérométrie et sa valeur est appliquée directement à la solution d'échantillon. La décharge intermittente du condensateur par le circuit électronique garantit que la différence de potentiel aux bornes du condensateur revienne à zéro. Ce système de lecture capacitif électronique a été appliqué pour mesurer la concentration de sodium en utilisant un condensateur de 10 µF pour amplifier le signal. La précision a été améliorée par rapport à la potentiométrie directe, correspondant à 0,11 mmol L^{-1} 1 NaCl et 0,13 mmol L^{-1} 1 NaCl pour les solutions standard et des échantillons de sérum, respectivement. L'utilisation du système électronique automatisé pour la mesure d'ions rend le système plus robuste tout en permettant des mesures quantitatives rapides et fiables.

Le **Chapitre 5** présente le développement d'un appareil portable pour la coulométrie à potentiel constant. Un petit potentiostat doté de ses propres circuits électroniques intégrés est placé dans une petite boîte (18,5 cm de largeur ,10,7 cm de longueur, 3,6 cm de hauteur avec un poids de 370 g). Une gamme de condensateurs (22 - 220 µF) est incluse dans le dispositif, qui peut être automatiquement choisie par le logiciel de contrôle. Le dispositif, appelé PotentioCap, a été évalué dans des solutions de pH standard et des échantillons d'eau de mer stabilisés à l'aide d'une électrode sélective d'hydrogène placée en série avec un condensateur. Les résultats du courant transitoire et de la charge intégrée dans le temps sont bien corrélés avec ceux de la lecture capacitive utilisant un potentiostat traditionnel avec un circuit électronique externe (chapitre 4). En outre, un modèle mathématique est présenté pour décrire les effets des courants constants et à décroissance exponentielle sur les membranes sélectives d'ions en utilisant l'équation de Nernst-Planck. Des simulations numériques sont utilisées pour estimer la polarisation de la concentration du complexe ion-ionophore et de l'échangeur d'ions dans les domaines spatiaux et temporels au sein de la membrane. Les modèles mathématiques ont été testés avec des expériences impliquant des membranes polarisées par un courant. Le potentiel de limite des phases calculé semble dériver de la même manière que celui observé expérimentalement. Afin d'améliorer la procédure de mesure, les caractéristiques de la régénération de la membrane par le potentiel constant contrôlé sont simulées. En appliquant un potentiel constant en circuit ouvert pendant 1 min, on constate que la précision est 40 fois meilleure que sans régénération. De plus, un

nouveau modèle capacitif selon la constante RC est proposé en considérant le changement de potentiel résultant avec le temps. Les résultats du modèle ont été comparés avec succès avec le pic de courant associé obtenu à partir de l'équation de charge RC établie et des données expérimentales. Il est démontré que les migrations électriques ne constituent pas une contribution significative au courant transitoire.

List of Publications

1. Kraikaew, P.; Jeanneret, S.; Soda, Y.; Cherubini, T.; Bakker, E., Ultrasensitive Seawater pH Measurement by Capacitive Readout of Potentiometric Sensors. *ACS Sensors* **2020**, 5 (3), 650-654.
2. Kraikaew, P.; Sailapu, S. K.; Bakker, E., Rapid Constant Potential Capacitive Measurements with Solid-Contact Ion-Selective Electrodes Coupled to Electronic Capacitor. *Anal. Chem.* **2020**, 92 (20), 14174-14180.
3. Kraikaew, P.; Sailapu, S. K.; Bakker, E., Electronic control of constant potential capacitive readout of ion-selective electrodes for high precision sensing. *Sens. Actuators B Chem.* **2021**, 344, 130282
4. Kraikaew, P.; Bakker, E. Ultra-Sensitive Measurement of Ocean PH: Highlights of Analytical Sciences in Switzerland. *Chimia* **2020**, *74*, 1021.

Acknowledgements

The works presented in this dissertation were carried out at the department of Inorganic and Analytical Chemistry, University of Geneva under the supervision of Prof. Eric Bakker since 2017 to 2022. I would like to acknowledge for Swiss National Science Foundation (SNSF) for supporting of chemicals, equipments and research activities. Grant from the Development and Promotion of Science and Technology Talents Project (DPST) of Thailand for financial support throughout my PhD is gratefully acknowledged.

I would like to express my gratitude and appreciation to Prof. Eric Bakker for all of his guidance, dedication, patience, understanding and encouragement during my PhD. Thank you very much for giving me the opportunity to do my doctoral degree under your supervision. I really appreciate your patience in teaching and advising me to improve my academic and research skills. He is a role model and inspires me of being a good researcher and a teacher. I would like to thank you for providing healthy laboratory environment as well as research ideas and discussions. I am very grateful to Prof. Johan Bobacka from the Åbo Akademi University and Prof. Ross Milton from the University of Geneva for having accepted the request to review my thesis and join as jury for my defense.

I would like to thank my co-authors for their great contributions to this work and reviewing the manuscripts. I especially thank Dr. Sunil Kumar Sailapu for teaching me basic electronics and helping me develop research projects. Many thanks to Stephane Jeanneret and Thomas Cherubini for working hard on device fabrication and software development. I would like to acknowledge Yoshiki Soda for your support with scientific discussions. I am thankful to Serge Rodak and Guy Lecoultre for their technical assistance and support. I very much thank Magali Cissokho for her administrative management and kindness.

I would like to thank my colleagues and my friends here:, Gabriel Junquetti Mattos, Robin Nussbaum, Ayian Speck, Nikolai Tiuftiakov, Yaotian Wu, Nicolas Layglon, Tanguy Gressard, Yoshiki Soda, Tara Forrest, Kye Robinson, Elena Zdrachek, Polina Damala, Sunil Sailapu, Melina Abduo, Nadezda Pankratova, Sutida Jansod, Suphasinee Sateanchok, Supacha Wirojsaengthong, Zdenka Jarolimova, Wenyue Gao, Lu Wang, Dajing Yuan, Marie-Lou Tercier-Waeber, and Maria Cuartero for having wonderful time together, and especially Canwei Mao for being my office and apartment roommate during my PhD.

I express my gratitude and appreciation to my family members who stand for me in my difficult times and their endless love. Special thanks to intimate friends: Panyapon Sudkaow and Sasikarn Seetasang for your encouragement and keeping in touch over 10 years. Finally, I would like to thank you Association of Thai Students in Switzerland (ATSS) and all Thai friends for make my life in Switzerland magnificent and joyful. Please forgive me if I carelessly missed the name of anyone.

University of Geneva, March 2022
Pitchnaree Kraikaew

Contents

Chapter 1: Introduction

1.1 Electrochemical sensors

Electrochemical sensors form an important class of chemical sensors that grow rapidly. Typically, a chemical sensor is used to observe responses of analyte relating to the quantity or quality of specific species. A chemical sensor consists of a transducer which converts such responses to detectable signals by an instrument. Chemical sensors can be classified according to the type of measurements such as: electrical, mass, optical, or thermal sensor[1]. Sensors are designed depending on state of analyte in solid, liquid, or gas. Compared to other sensors, electrochemical sensors are powerful analytical tools because of their high sensitivity, high selectivity, rapidity of measurement as well as their ability to make miniaturized and simplified low-cost devices[2-5]. They are widely used in important applications, i.e. environmental, clinical, industrial and agricultural analysis. Potentiometry, amperometry, and conductometry are three main types that being used in electrochemical sensors[6]. Briefly, potentiometric sensor determines the composition of the sample at the electrode interface by measuring a potential difference between an indicator and reference electrode under zero current when local equilibrium is established. Amperometric sensor is carried out by recording a current when applying a potential across a working electrode and a counter electrode with respect to a reference electrode to cause oxidation or reduction of an electroactive species. Conductometric sensors measure the conductivity of the thin electrolyte layer adjacent to the electrode surface. In this thesis we put the emphasis on potentiometric sensors using ion-selective electrodes which will be explained in next section.

1.1.1 Electrochemical cells for ion-selective potentiometry

Potentiometric ion sensors are one of the oldest device among electrochemical sensors. About a century ago, Max Cremer discovered the pH sensitive glass membrane[7] and Fritz Haber made glass bulk electrodes to monitor acid-base titrations[8]. From the commercial point of view, Beckman simplifies the use of pH glass electrode in the 1930s[9]. He developed a vacuum tube voltmeter to use with glass electrode instead of the usual galvanometer. The new era of potentiometry started when the silver iodide-based iodide selective electrode was invented by Erno Pungor in the 1960s[10]. Ross, however, pointed out that it is not possible to make a glass calcium electrode because the transport rate of calcium ions through glass was too slow. This brought the basic concept of the liquid membrane electrode[11]. About 1969, the liquid-membrane construct of valinomycin-based potassium selective electrode was invented[12] and used for serum measurement[13].

Since the first publications, there have been many attempts to develop new types of ion-selective electrodes (ISEs) containing selective complexing agent for example: the differential CO_2 electrodes for clinical blood-gas analyzers[14], the polyion-selective electrode for anticoagulant drug heparin and its antidote protamine[15], and the nitrate-selective electrode for water quality monitoring[16]. Today, several types of commercial ISEs are available for direct measurement of cation ion or anion ion activity (concentration) in liquid samples of different nature[17].

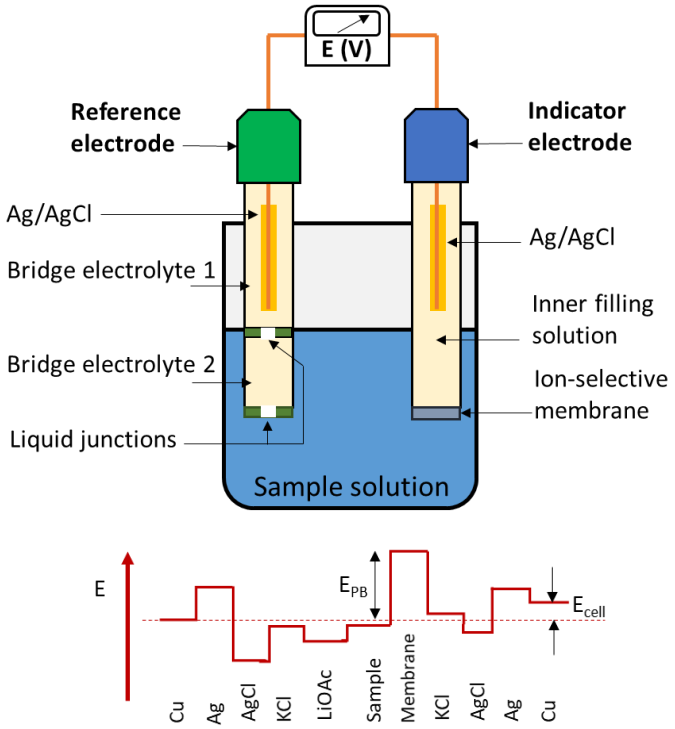

Figure 1.1. Top: potentiometric cell assembly with a conventional, liquid inner contact ion-selective membrane electrode as indicator electrode and a double junction reference electrode. Bottom: individual phase boundary potentials in the potentiometric cell assembly above.

Potentiometry is typically measured under zero current conditions in a galvanic cell. The setup of potentiometric measurements consists of an indicator electrode and a reference electrode connected to a high input impedance voltmeter. Here, we focus on ion-selective electrodes (ISEs) and classical Ag/AgCl reference electrode with aqueous bridge electrolyte of saturated KCl solution immersed in the sample solution through a liquid junction. The most commonly used ion-selective electrodes are glass electrodes and liquid membrane electrodes consisting of water immiscible polymeric film loaded with a complexing agent (ionophore) and an organic ion-exchanger[18]. The polymeric membrane is attached to the tip of a cylindrical electrode body and separates the inner filling solution of ISE from the sample solution as shown

in Fig. 1.1 top. The measurement of the potential difference (electromotive force, EMF) under zero current reflects the sum of all potential difference in the cell. Those potentials are ideally largely independent of the sample except the potential at the interface of the membrane and sample solution (Fig. 1.1 bottom)[19, 20]. The potential change is proportional to the change in logarithmic ion activity according to the well-known Nernst equation. The EMF response of such membranes is normally understood as a phase-boundary potential which assumes that the distribution of ionic species across the sample-membrane interface is at local electrochemical equilibrium. The phase-boundary potential is formulated as eq. 1.1[21].

$$E_{PB} = E_I^0 + \frac{RT}{z_I F} \ln \frac{a_I(aq)}{a_I(org)} \qquad 1.1$$

where R is the universal gas constant, T the absolute temperature, F the Faraday constant, z_I the charge of the primary ion and $a_I\,(aq)$ and $a_I\,(org)$ are the activities of the ion I in the organic and aqueous phase boundaries. E_I^0 is chemical standard potential in both phases:

$$E_I^0 = \frac{\mu_I^0(aq) - \mu_I^0(org)}{z_I F} \qquad 1.2$$

At room temperature (298 K), equation 1.1 can be simplified to Nernst equation for ion-selective electrodes as:

$$EMF = K + \frac{s}{z_I} \ln a_I(aq) \qquad 1.3$$

where s is Nernst slope of 59.18 mV, which is divided by the charge of the primary ion. A Nernstian response slope is accomplished by the assistance of an ion-exchanger in the ion-selective membrane to maintain permselectivity of the membrane and to keep $a_I\,(org)$ constant[22]. The addition of a selective receptor (or ionophore) in the polymeric membrane helps to suppress spontaneous ion-exchange with competing ions of the same charge sign as the analyte ion[18, 23].

1.1.2 Ion-selective membrane

The composition of ion-selective membranes (ISMs) is carefully prepared with the right proportion of high-purity compounds. ISMs typically consist of a water insoluble polymeric matrix with plasticizer, ion-exchanger, and ionophore. The molar ratio of ionophore to ion-exchanger is often 3:1 to assure that free ionophore is in molar excess[18]. An organic supporting electrolyte such as ETH 500 (tetradodecylammonium

tetrakis-(4-chlorphenyl)-borate) may be added into membrane to reduce the electrical resistance[24]. Tetrahydrofuran (THF) is a solvent used for dissolving the membrane cocktail homogenously. The membrane cocktail solution is poured onto an inert surface such as glass to allow the solvent to evaporate, resulting in the formation of a polymer layer with a thickness of 150-200 µm. For conventional ISEs, the membrane is punched to circular shape (~5 mm) and is attached to an electrode containing the inner filling solution[25]. In another design, the membrane cocktail solution is drop cast on top of a transducer surface of a solid-state electrode, depending upon the choice of sensor[26]. The polymer materials regularly used as a membrane substrate is high molecular weight poly (vinyl chloride) (PVC) doped with a plasticizer (e.g. bis(2ethylhexyl) sebacate (DOS), 2-nitrophenyl octyl ether (o-NPOE)) with a ratio of 1:2 to promote its plasticity and flexibility of the polymer[27].

1.1.3 Selectivity of ion-selective electrodes

As mentioned above, the ion-selective membrane is doped with a salt of a lipophilic ion, for instance, tridodecylmethylammonium chloride (TDMAC) as anion exchanger and sodium tetrakis[3,5-bis(trifluoromethyl)phenyl] borate (NaTFPB) as cation exchanger. The structures of ion-exchangers are shown in Fig 1.2. Before use, the membranes are conditioned in a solution of reasonably high concentration (millimolar or higher) of the cation or anion of interest. In this manner, the initial counterion of the ion-exchanger is replaced by the ion of interest. The extraction by simple membranes containing only an ion-exchanger always favors more lipophilic ion over less lipophilic ones[28]. The selectivity sequence of such membranes follows the so-called Hofmeister sequence:

Anion-selective membranes: $R^- > ClO_4^- > I^- > NO_3^- > Br^- > Cl^- > F^-$

Cation-selective membranes: $R^+ > Cs^+ > Rb^+ > K^+ > Na^+ > Li^+$

where R^- and R^+ denotes an organic anion and organic cation, respectively. Membranes containing only an ion-exchanger exhibit limited selectivity for hydrophilic species[28]. Therefore, modern ISMs are comprised of an additional ionophore to enhance its selectivity for the analyte ion[29]. The ionophore is a compound that selectively binds to specific ion over others, e.g. valinomycin for potassium-selective membranes, tridodecylamine for hydrogen-selective membranes, and 4-tert-butylcalix[4]arene-tetraacetic acid tetraethyl ester for sodium-selective membranes. The chemical structures of these mentioned ionophores are illustrated in Fig 1.2.

NaTFPB TDMAC Valinomycin

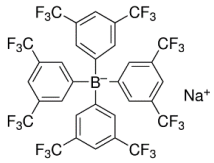

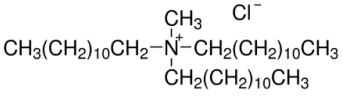

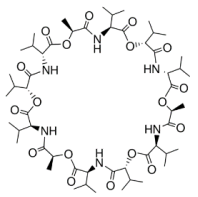

Tridodecylamine 4-tert-Butylcalix[4]arene-tetraacetic acid tetraethyl ester

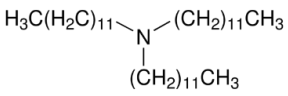

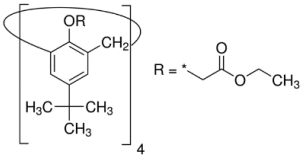

Figure 1.2. The chemical structures of ion-exchangers and select ionophores.

The addition of a selective ionophore in the membrane leads to smaller $a_I\,(org)$ in eq. 1.1, resulting in a greater phase boundary potential at the outer interface[18]. The selectivity of the membrane is expressed by the selectivity coefficient (K_{IJ}^{pot}). Its dependence on the standard potential difference and ratios of ion activities in the organic phase boundaries is described by eq. 1.4[30].

$$K_{IJ}^{pot} = \frac{a_I(org)}{a_J(org)}\left\{\frac{z_I F}{RT} exp\left(E_J^0 - E_I^0\right)\right\} \qquad 1.4$$

where I is the primary ion (analyte) and J is the interfering ion. Smaller K_{IJ}^{pot} value indicates better selectivity for the primary ion over the interfering ion.

1.1.4 Detection limit of ISEs

The traditional approach to define the detection limit of ISEs is the intersection of the two extrapolated linear segments of the calibration curve. It means that the detection limit is determined by the potential response of the background solution containing interfering ion J (absent of primary ion I) compared with the Nernstian response of the ISE to the primary ion I, predicted by eq. 1.1. In this manner, the lower detection limit (LDL) is given by[31]:

$$a_I(LDL) = K_{IJ}^{pot} a_J^{z_I/z_J} \qquad 1.5$$

In case of high selectivity, the use of eq. 1.5 on the basic of thermodynamic displacement (ion-exchanger) may not be practical for calculation of the lower detection limit. The ion-exchange process at the sample side creates counterdiffusion ion fluxes at zero current. Primary ions exchanged from the membrane diffuse away from the membrane to the sample bulk while interfering ions diffuse in the opposite direction. Thus, the kinetic low detection limit in the case of all monovalent ions may be estimated by[32]:

$$C_I(LDL) = \left(q c_R^m \sum_{J \neq I} K_{I,J}^{pot} a_J\right)^{1/2} \quad 1.6$$

where $c_R{}^m$ is the concentration of ion-exchanger (molar) in the membrane and q is the permeability ratio given by[32]:

$$q = \frac{D_m \delta_{aq}}{D_{aq} \delta_m} \quad 1.7$$

where D and δ are the diffusion coefficient and diffusion layer thickness of membrane (*m*) and aqueous phase (*aq*).

1.1.5 Solid-contact ion-selective sensor

Further developments of ion-selective electrode were made to improve the detection limit by replacing the conventional inner filling solution with a solid-contact material. In this case, an optimization of inner filling solution is no longer required. In earlier solid-contact electrodes there was a challenge of poor adhesion due to the formation of a water layer between the electrode surface and the polymeric membrane,[33, 34] which prevented solid-contact ion-selective electrodes (SC-ISEs) from achieving a low detection limit and resulted in potential drift[35]. Major improvement of SC-ISEs were achieved by placing a transducing material that serves as an ion-to-electron translator from selective membrane to electron conductor that gave operationally stable potentials[36-39]. In order to obtain a stable electrode potential, the following three conditions for the solid-contact material need to be met: (1) reversibility and equilibrium stability of the transition from ionic to electronic conductivity; (2) exchange currents that are sufficiently high in comparison to the current passed during measurement (3) The absence of parallel side reactions to the main electrode reaction[40]. The use of well-defined SC-ISEs makes potentiometric sensors more robust and practicable for miniaturization. Materials often used as transducers are conducting polymers [41]and carbon materials[42] which are both adequate materials but exhibit different mechanisms of ion-to-electron transduction.

1.1.5.1 Solid-contact based conducting polymers.

Among conducting polymer materials (CPs), poly(3, 4-ethylenedioxythiophene) (PEDOT), poly(3-octylthiophene) (POT), and polypyrrole (PPy) are the oldest CPs used for SC-ISEs[41]. Those substrates stabilize the potential at inner interface (metallic electrode/CP layer) by a reversible redox reaction coupled with ionic transference in the selective membrane. Bobacka's group investigated the potential stability of all-solid-state K^+-ISEs using PEDOT doped with polystyrenesulfonate (PSS^-) as a model electrode[40]. Chronopotentiometric measurements of a K^+-ISE with PEDOT(PSS) showed that it has negligible potential drift over time (change in slope of $\Delta E/\Delta t$) compared to a so-called coated-wired K^+-ISE (without conducting polymer). The potential drift was found to be proportional to the capacitance (*C*) of the solid-contact material and the current (*i*) as follows[40]:

$$\text{Potential drift} = \frac{\Delta E}{\Delta t} = \frac{i}{C} \qquad 1.8$$

According to this relationship, a thicker layer of CP results in a higher capacitance, which enhances potential stability. The optimization of the capacitance of CPs was studied by Maksymiuk's group[43]. The effective capacitance of a PEDOT solid contact decreased in the presence of the selective membrane due to low charge transfer onto the polymer layer/membrane interface. This limitation can be minimized by adding a significantly higher concentration of ion-exchanger into the membrane in order to increase the concentration of mobile ions and to reduce concentration polarization in the membrane. Lindner and coworkers improved the hydrophobicity of PEDOT by functionalizing with a C_{14} alkane chain (PEDOT-C_{14}) and doped with tetrakis-(pentafluorophenyl)borate[44]. Such solid contact was applied for the development of pH, Na^+ and K^+ sensors[44]. The potential drift was minimized to 0.02 ± 0.03 mV/day. For the pH sensor, the reproducibility of pH measurement was as low as ±0.002 pH units.

POT is one of the CPs that is attractive for potentiometric sensors owing to its high hydrophobicity and ease to deposit on the electrode surface (electrodeposition from the monomer or drop casting from polymer solution)[37]. POT-based ISEs were employed for measurement of both cation and anion species, for example K^+, Ca^{2+}, Cl^-, nitrate, carbonate with various polymer substrates[45]. The reported long-term potential drift with POT solid-contacts for Ca-ISE is 0.23 mV/day with a standard potential E^0 of 259.3 ± 1.3 mV[37]. Ion-to-electron transduction processes of POT have been studied by Amemiya's group[46] and Bakker's group[47]. The processes have been described as consisting of 3 major phases: (i) oxidation of POT to $POT^+ + e^-$ (ii) subsequently by incorporating with anionic lipophilic ion-exchanger (R^-) from the membrane to the POT

layer (iii) and expelling counterions M^+ from the membrane to the aqueous phase to maintain electroneutrality (Fig. 1.3). The potential at the inner membrane side is determined by the POT/POT^+ ratio. POT, on the other hand, has the disadvantage of being light-sensitive and pH-sensitive.

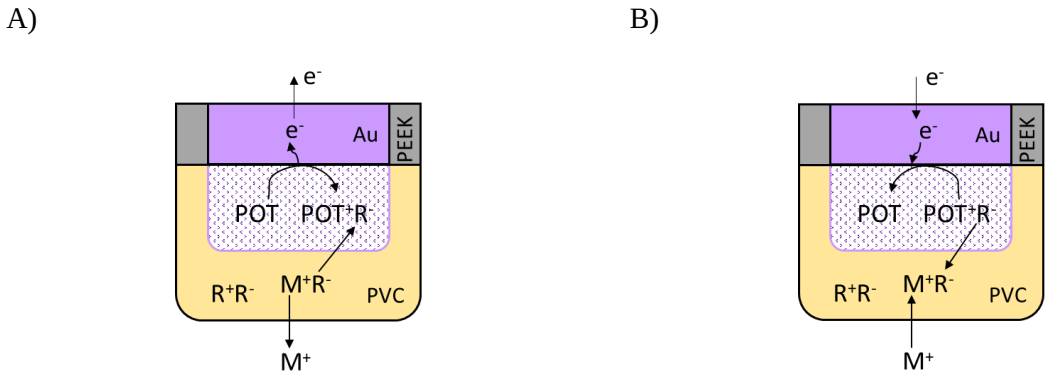

Figure 1.3. Operation of the voltammetric ISE sensor based on a bilayer consisting of a PVC layer on a poly(3-octylthiophene)-modified Au electrode. (A) is oxidation and (B) is reduction of POT.

1.1.5.2 Solid-contact based carbon materials

Compared with redox CPs, carbon materials such as graphene, graphene oxide, and carbon nanotubes (CNTs) have become well established as solid contact materials for potentiometric sensing owing to their high lipophilicity and chemical inertness. The transduction mechanism of multi-walled carbon nanotubes (MWCNTs)-based SC polymeric ion sensors has been studied by Cuartero et al[48]. The results indicate that the mechanism involves an electrical double layer coupling the capacitive behavior through adsorption/absorption of a lipophilic anion onto and into the MWCNTs SC layer, while electrons are located on the MWCNTs leading to a charging/discharging capacitive process. As evidence, the capacitive transduction mechanism of CNTs is not associated with the oxidation/reduction reaction, which is unlike conducting polymers, as shown in Fig. 1.4. Grespo and Bakker described anion-selective sensors using functionalized-MWCNTs as solid contact material[49]. In comparison to POT SC, the functionalized-MWCNTs-based sensor is light-insensitive and has medium-term stability of 0.04 mV/h for carbonate detection. For cation measurement, a Nernstian slope was achieved for K^+ using single-walled CNTs as SC with precision of 0.4 mV/decade a_{K^+}[42].

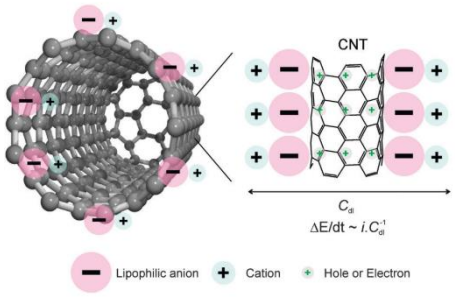

Figure 1.4. Schematic illustration of the capacitive double layer generation by adsorption of either cations or anions onto the high surface area nanostructured material. (Figure is modified from reference 42) [48]

1.2 Constant-potential coulometric method

One of the unresolved issues in zero current potentiometry of SC-ISEs is the insufficient reproducibility and stability of the standard potential E^0 due to, for example, the partitioning of solid contact material into the membrane layer and its sensitive reaction to gases (CO_2 and O_2) as well as to pH and light[50, 51]. This sort of potentiometric sensor measures an open circuit potential (OCP) as an output signal, which makes the calibration-free procedure challenging. The standard potential, on the other hand, can be adjusted by short-circuiting with the reference electrode, resulting in a potential difference near to zero[52]. This strategy is especially helpful when it comes to simplifying calibration curves. Conversely, the E^0 of SC-ISEs based CPs can be alternated by electrochemical control of applying potential or current pulse[53]. Furthermore, non-zero current measurement have been developed to broaden the application of ion-selective electrodes[4]. Thin layer coulometry of ion-selective membranes has been demonstrated as a method for potentially calibration-free ion-sensing[54]. In this method, ion transfer is triggered by an applied potential, resulting in ion-transfer current that can be integrated to the overall charge used in the process. With a known sample volume, the ion concentration in the sample can be determined. One example of thin layer coulometry was applied to microfluidic device for Ca^{2+} measurement in mineral water[55]. A strategy called tuned galvanostatic polarization was presented to improve the analytical characteristics of ISEs to achieve a lower limit of detection[56]. The procedure is carried out by recording the OCP and subsequently by recording the potential change while applying an optimized current for a certain time, after which again the potential is immediately recorded at zero current and used as a readout signal. By this technique, linear Nernstian response for Ca-ISE was obtained down to 10^{-10} M. The charge transfer process of CP based ISEs can be compensated via conditioning by galvanostatic polarization.

1.2.1 Principle of coulometric readout method

As previously stated, calibration-free sensors are highly desired as ideal analytical tools. Recently, a novel signal transduction method for SC-ISEs based on constant potential coulometry was presented by Hupa et al[57]. In this approach, the open circuit potential of the SC-ISE is recorded against a reference electrode and then kept constant throughout the measurement using a potentiostat. A conventional electrochemical cell with a double junction Ag/AgCl/ 3 M KCl/0.1 M KCl electrode as reference electrode, a glassy carbon rod as counter electrode, and a SC-ISE as working electrode was employed. The solid-contact material PEDOT(PSS) conducting polymer was used as an ion-to-electron transducer. Its redox-capacitance involves cation-exchanger processes with an assistance of cation-selective membrane as described in eq. 1.9:

$$PEDOT^{+}PSS^{-}_{(film)} + K^{+}_{(membrane)} + e^{-} \leftrightarrow PEDOT^{0}PSS^{-}\,K^{+}_{(film)} \qquad 1.9$$

The principle of constant-potential coulometric readout is shown in Fig. 1.5. Since the potential of the SC-ISE is held constant, any change in the activity of the primary ion in the sample results in a change in the potential difference between the SC-ISE and the reference electrode (RE). The potential difference will be compensated by an opposite potential change at the PEDOT(PSS) layer, leading to a transient current through the counter electrode (CE) until a new equilibrium is reached. The transient current causes the oxidation/reduction of PEDOT(PSS) (see eq. 1.9), which can be integrated into charge-time information. Vanamo et al. showed that the total cumulated charge is linearly proportional to the change of the logarithm of the primary ion activity[58]. An attractive feature of this method is that the reading signal could be amplified by increasing the redox-capacitance (thickness) of the conducting polymer solid contact.

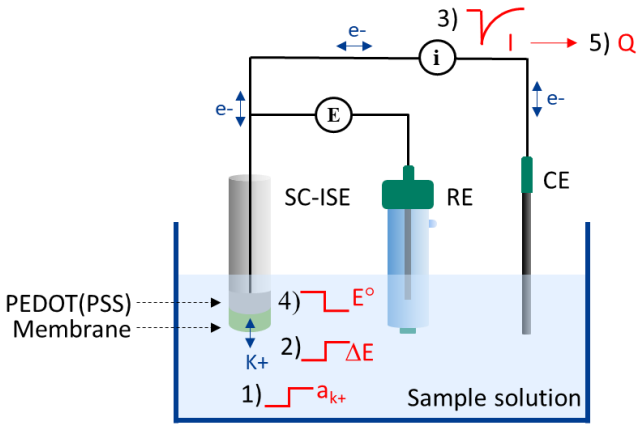

Figure 1.5. Schematic illustration of principle of constant-potential coulometric readout.

1.2.2 Development of coulometric readout

As mentioned earlier, the coulometric readout method is based on a redox process of the solid-contact conducting polymer and also of the diffusion of primary ions in the membrane. With greater charge passed, a longer time for the transient current to reach the zero baseline is required. This results in long measurement times. Han and coworkers, however, found that the electrode geometry of SC-ISEs influences the response time[59]. When the capacitance of CPs and the thickness of the covering membrane remained constant, a larger electrode diameter gave faster response times. This is due to the fact that a small electrode diameter is unable to convert the entire change of ion activity into charge at a given time. Spin-coating the thin ion-selective membrane (ISM) instead of drop-casting has been shown to minimize resistance resulting in a shortened response time of SC-ISEs[60]. The remarkable property of coulometric transduction method is that it provides better sensitivity than conventional potentiometry. By using an optimized K^+-SCISE, the technique was shown to detect 0.1% change in K^+ in activity and small pH change within 5 min of each equilibrium. It is clear that increasing the PEDOT (PSS) capacitance (by altering the thickness) from 1 mC to 10 mC can amplify the signal, but at the cost of a response time longer than 5 min. According to impedance data, the transduction process of the K^+-SCISE is restricted by diffusion even for thin ISMs. H^+-SCISEs, on the other hand, give a faster response, possibily due to a higher mobility of H^+ in H^+-ISM[60]. This method shows promising results of K^+ and pH measurement in serum and seawater samples[60]. Furthermore, PEDOT(PSS) based SC-ISEs were tested for measurement of divalent ions of Ca^{2+} and Pb^{2+}[61]. The redox-capacitance reaction of PEDOT(PSS) is assumed to follow eq. 1.10. A linearity of accumulated charge (Q) with logarithmic divalent ion activity was obtained, but the slope (Q vs log a_{a2+}) vs capacitance value does not increase proportionally since the current signal does not reach zero baseline. In comparison with monovalent ions of K^+-SCISE, the result deviates from the theoretical expectation that Q of monovalent ions (K^+) is not twice larger than Q of divalent ions (Pb^{2+}) at a given time. This appearance could be due to ion transport limitations or a difference in redox capacitance in the presence of Pb^{2+} compared to K^+. Impedance studies confirm that the coulometric response of Pb^{2+} is limited mainly by charge transfer due to interactions between Pb^{2+} and PEDOT(PSS).

$$2PEDOT^+PSS^-_{(film)} + Pb^{2+}_{(membrane)} + 2e^- \leftrightarrow (PEDOT^0PSS^-)_2\, Pb^{2+}_{(film)} \qquad 1.10$$

The use of constant-potential coulometric technique for anion measurement was also presented by Han and coworkers for nitrate, perchlorate, and sulfate[62]. Contrary to cation measurements, PEDOT doped with small anions including Cl^-, NO_3^-, SO_4^{2-}, and ClO_4^- was utilized as an ion-to-electron transducer for SC-ISEs. The mechanism of PEDOT(NO_3) based nitrate-selective membrane was proposed with eq. 1.11.

$$PEDOT^{n+}(NO_3^-)_n + xe^- \leftrightarrow PEDOT^{(n-x)+}(NO_3^-)_{n-x} + xNO_3^- \quad 1.11$$

The principle of coulometric transduction is analogous but the observed current is of opposite sign. Cyclic voltammetry shows that the capacitive currents of 10 mC GC/PEDOT electrodes give rise to the following order: PEDOT(Cl) ≈ PEDOT(SO_4) < PEDOT(NO_3) < PEDOT(ClO_4), which may be attributed to hydrophobicity (Hofmeister series) or anion size. However, PEDOT(Cl) is relatively independent of supporting electrolytes, making it an effective solid contact material for anion SC-ISEs. The response time of anion detection is significantly faster than that of cation detection when a spin-costed ISM (thin membrane) is used. Transient currents of NO_3^--SCISE and SO_4^{2-}-SCISE stabilize with 2 min and 1 min, respectively. Identical to cation SC-ISEs, the coulometric signal is amplified by increasing polymerization charge (thickness of PEDOT film), which is proportional to the change in anion activity.

Constant potential coulometry, a new readout method based on non-zero current, has been shown to improve sensitivity over direct potentiometry. The oxidation/reduction of conducting polymers is, however, limited by ion transport in the ISMs and also the charge transfer at the CP layer. Different interactions between primary ions and CPs lead to difference in redox capacitance, which influence the response time. In order to obtain the most effective coulometric readout for each interest ion, the characteristics of SC-ISEs e.g. capacitance (thickness of SC), types of transducer as well as thickness of ISMs need to be optimized prior to starting the measurement, making this approach not obviously suitable for on-field analysis.

1.2.3 Capacitive model for coulometric readout

The first capacitive model for coulometric signal transduction readout of SC-ISEs with conducting polymers was presented by Jarolimova and coworkers[63]. They showed that the capacitive model correlates well with SC-ISEs using PEDOT(Cl) as ion-to-electron transducer. As mentioned previously on the principle of the approach, the constant potential the ISE with a capacitive transducing layer is held at corresponds to the open circuit potential of the initial solution, resulting in an initial zero current. A change in the analyte ion activity at time t_0 will cause a potential change at the membrane-sample boundary as described by the Nernst equation:

$$\Delta E_{pb}(sample) = \frac{s}{z_i} \log \frac{a_i(final)}{a_i(initial)} \quad 1.12$$

where *s* is 59.2 mV for 25 °C and z_i is the charge of the analyte ion. The change at the inner membrane side (inner transducing layer) must be exactly opposite as follows:

$$\Delta E_{pb}(inner\ side) = \frac{s}{z_i}\log\frac{a_i(initial)}{a_i(final)} \quad 1.13$$

The observed current response is defined in the same way to a constant potential step at a capacitor, which is expressed as:

$$i(t) = \frac{\Delta E_{pb}(inner\ side)}{R_{cell}} e^{t-t_0/C_{cp}R_{cell}} \quad 1.14$$

where C_{cp} is the capacitance of the inner transducing layer and R_{cell} is the resistance of the electrochemical cell. Equation 1.13 is substituted into eq. 1.14 to determine the relationship between current transient and activity change in a sample as shown below:

$$i(t) = \frac{s}{z_i R_{cell}}\log\left(\frac{a_i(initial)}{a_i(final)}\right) e^{t-t_0/C_{cp}R_{cell}} \quad 1.15$$

Equation 1.15 explains that a current spike is generated when the sample ion activity is altered. The transient current decays with an RC time constant as a function of the capacitance of the inner transducer and resistance of the cell. A SC-ISE covered with a thicker ion-selective membrane has a generally higher resistance, which results in a longer RC time constant and a smaller magnitude of current. Thus, a well-defined thin membrane may improve the signal-to-noise ratio and also the response time. At t = 0, the maximum current can be calculated by:

$$i(t) = \frac{s}{z_i R_{cell}}\log\left(\frac{a_i(initial)}{a_i(final)}\right) \quad 1.16$$

As evidenced in eq. 1.14 and eq. 1.15, the transient current depends not only on the Nernst function but also the cell resistance. If the resistance of the membrane does not dominate the cell resistance, this could be a source of measurement uncertainty. To overcome this problem, the current may be integrated over time to obtain charge (Q) information as shown in eq. 1.17 where C_{cp} is the capacitance of the conducting polymer.

$$Q = C_{cp}\frac{s}{z_i}\log\left(\frac{a_i(initial)}{a_i(final)}\right) \quad 1.17$$

Theoretically, an integrated charge should be proportional to the logarithmic ion activity change. The sensitivity of observed Q may be improved by increasing C_{cp} by the thickness of the conducting polymer. This theoretical prediction agrees well with experimental detection of K^+ ion as mentioned earlier using the coulometric readout of K^+-SCISE.

A more recent model of the coulmetric readout method was reported by Kondratyeva and coworkers[64]. Since the current flow across the ion-selective membrane results in concentration polarization, the previous theoretical equation (eq. 1.15) may not always allow for a good fit. Hence, this behavior is taken into account by adding a Cottrellian term to obtain modified equations for chronoamperometric measurements and coulometric measurements, respectively, as follows:

$$i(t) = \frac{RT}{z_i F} \ln \frac{a_i(initial)}{a_i(final)} \left[\frac{1}{R_{cell}} e^{-t/C_{cp}R_{cell}} + \left(\frac{N}{2}\right) t^{-1/2} \right] \quad 1.18$$

$$Q(t) = \frac{RT}{z_i F} \ln \frac{a_i(initial)}{a_i(final)} \left[C_{cp}\left(1 - e^{-t/C_{cp}R_{cell}}\right) + N t^{1/2} \right] \quad 1.19$$

The parameter $N = 2\pi^{-1/2} (F/RT) A_E C_I D_I$ where A_E is the electrode cross-section area, C_I is the concentration of the ionic species in the membrane, and D_I their diffusion coefficient. The modified equation was shown to be a better fitting than the simple equation based RC constant for both current-time and charge-time information[64]. A robust theoretical description is useful for predictions of chronoamperometric data (current) and coulometric data (charge) so that the measurement does not need to reach the equilibrium state (zero-current baseline). From a practical point of view, this interpretation method is important since it allows for short measurement times, resulting in higher throughput analysis.

1.3 Fundamental electronic circuits

1.3.1 Ohm's law

Materials, usually, have a characteristic behavior of resisting the flow of electric charge (current) known as resistance (*R*). It is measured in ohms (Ω). In the electronic components, a resister is a passive element. The relationship between current and voltage for a resistor is explained by Ohm's law: the voltage (*V*) across a resistor is proportional to the current (*i*) flowing through the resistor as described below:

$$V = iR \quad 1.20$$

A circuit symbol for resistance is illustrated in Fig. 1.6. In this example, the circuit consists of a battery connecting to 5 kΩ, which allows a current flow.

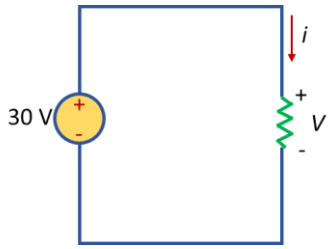

Figure 1.6. An example of simple electronic circuit including battery, resistor, and current.

1.3.2 Kirchhoff's laws

Kirchhoff's laws were first introduced in 1847 by the German physicist Gustav Robert Kirchhoff. They are used to quantify how the current flows through a circuit and how voltage varies around a loop in a circuit. The laws consist of Kirchhoff's current law (KCL) and Kirchhoff's voltage law (KVL), which is extended for analyzing the resistance as well as capacitance in the circuits[65]. The fundamental concept in physics states that charge will be always conserved in the environment. Consequently, Kirchhoff's current law explains that the current flowing into a node (or a junction) must be equal to the current flowing out of it. An example of current travelling down wires is depicted in Fig. 1.8. The sum of the currents in Fig.1.7 indicates that

$$I_1 + I_2 = I_3 \qquad 1.21$$

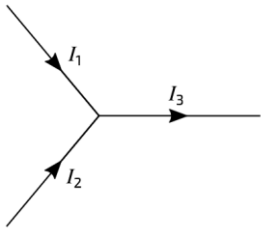

Figure 1.7. Three wires connect at a node. Different currents is flowing thought each wire.

Mathematically, the total current can be generalized in case of n wires connected to a node as:

$$\sum_{n=1}^{n} I_n = 0 \qquad 1.22$$

Kirchhoff's voltage states that in a closed loop with applied electrical energy, the sum of all voltages within a circuit across a component must be equal to the sum of all voltages across another component. Consequently, conservation of charge and energy must occur. Figure 1.8 shows how a 6 V potential from a battery is applied to a loop containing two resistors of 2 Ω and 1Ω is distributed over the individual elements.

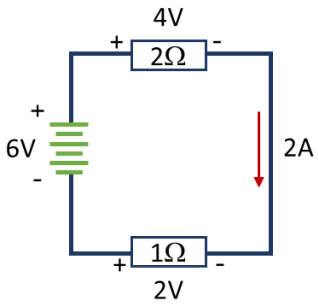

Figure 1.8. Overall voltage in a closed circuit when electrical energy is supplied through resistors leading to current generation.

Kirchhoff's voltage law is applicable to any loop *n* with any number of components. It can be written in a general manner as follows:

$$\sum_{n=1}^{n} V_n = 0 \qquad 1.23$$

1.3.3.1 Series and parallel resistors

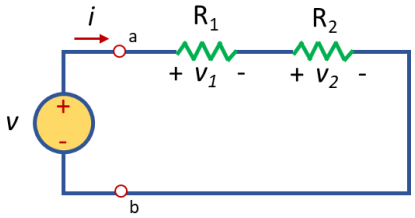

Figure 1.9. A single-loop circuit with two resistors in series.

A combination of resistances is needed when a circuit is comprised of more than one resistor. As illustrated in Fig. 1.9, the two resistors are in series such that the same current flows across the circuit. By applying Ohm's law and KVL, the equivalent resistance R_{eq} is sum of the individual resistance (resistors) connected in series as shown in eq. 1.24.

$$R_{eq} = R_1 + R_2 + \cdots + R_n = \sum_{n=1}^{n} R_n \qquad 1.24$$

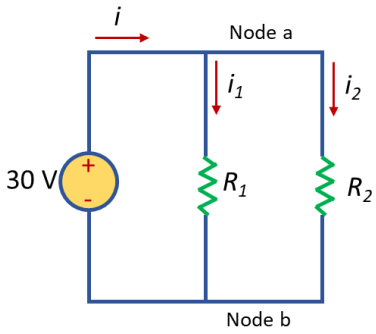

Figure 1.10. A circuit with two resistors in parallel at node a and b.

In the event of a circuit consisting of two nodes where resistors are placed in parallel as seen in Fig. 1.10. The same voltage across them is the same however the current generation may be difference depending on each resistance. According to Ohm's law and KCL, the equivalent resistance R_{eq} of resistors in parallel is equal to the sum of the reciprocal of the resistance 1 to N as expressed in eq. 1.25.

$$\frac{1}{R_{eq}} = \frac{1}{R_1} + \frac{1}{R_2} + \cdots + \frac{1}{R_N} \qquad 1.25$$

1.3.3 Capacitor

A) B)

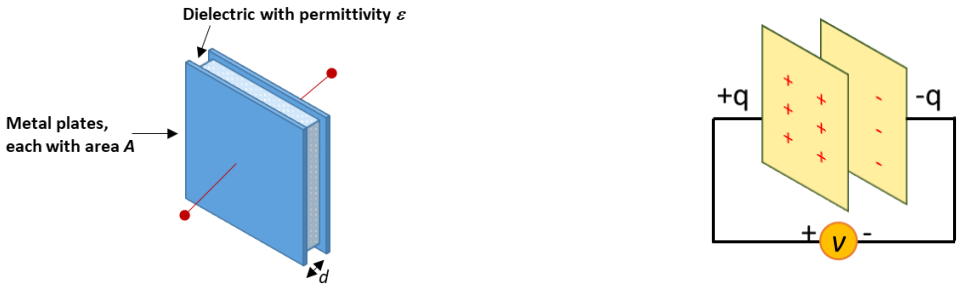

Figure 1.11. (A) Construction of a typical capacitor and (B) characteristic of a capacitor with applied voltage V.

A capacitor is a passive element and a well-known electrical energy storage unit. A typical capacitor consists of two conducting plates which are separated by an insulator (or a dielectric) as depicted in Fig. 1.11A. Figure 1.11B shows that when a voltage source is connected to the capacitor, a positive charge ($+q$)

deposits on one plate and a negative charge (-*q*) on the other. Charge accumulation (*q*) in the capacitor is proportional to the applied voltage (*V*) as follows:

$$q = CV \tag{1.26}$$

where *C* is the capacitance of the capacitor in units of farad (*F*). The capacitance is the ratio of the charge on one plate of a capacitor divided by the voltage difference between the two plates where 1 farad = 1 coulomb/volt. The capacitance of a capacitor depends on the dimensional parameters as given in eq. 1.27.

$$C = \frac{\epsilon_0 A}{d} \tag{1.27}$$

where A is the surface area of each plate, d is the distance between the two plates, and ϵ_0 is the permittivity of the dielectric material between the plates with value 8.85×10^{-12} F m^{-1}. The current-voltage relationship of the capacitor can be calculated by taking the derivative of both sides of $I = dq/dt$ as:

$$i = C\frac{dV}{dt} \tag{1.28}$$

1.3.4.1 Series and Parallel capacitors

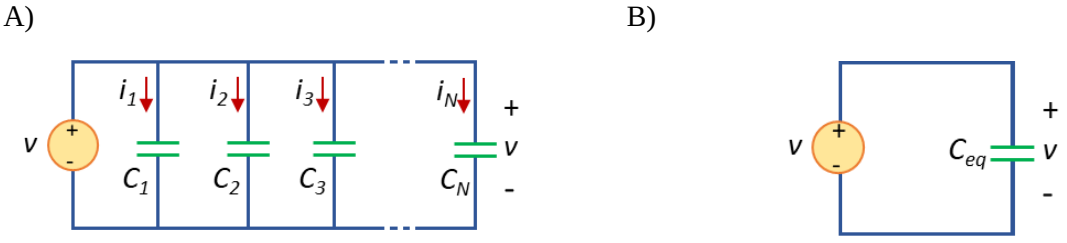

Figure 1.12. (A) Parallel-connected N capacitors and (B) equivalent circuit for the parallel capacitors.

The series-parallel combination of circuit elements provides advantages to simplify circuits. This technique can be used to extend the series-parallel connections of capacitors[65]. The circuit in Fig. 1.12A shows that when N capacitors are placed in parallel the voltage across the capacitors is the same. In order to obtain the equivalent circuit in Fig. 1.12B, KCL and eq. 1.28 were considered for the equivalent capacitance. As a result, the equivalent capacitance of capacitors *N* connected in parallel is the sum of the individual capacitances as shown in eq. 1.29.

$$C_{eq} = C_1 + C_2 + C_3 \cdots + C_N \qquad 1.29$$

A) B)

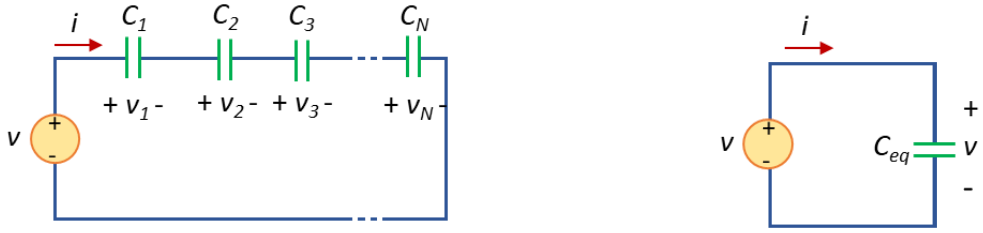

Figure 1.13. (A) Series-connected *N* capacitors and (B) equivalent circuit for the series capacitor.

Next, capacitors connected in series is illustrated in Fig. 1.13A and compared to the situation with the equivalent circuit in Fig. 1.13B. Here, the same current *i*, which is carrying the same charge, flows through the capacitors. Considering KVL to the loop in Fig. 1.13A, the equivalent capacitance of capacitors connected in series is the reciprocal of the sum of the reciprocals of the individual capacitances:

$$\frac{1}{C_{eq}} = \frac{1}{C_1} + \frac{1}{C_2} + \frac{1}{C_3} \cdots + \frac{1}{C_N} \qquad 1.30$$

1.3.4 RC circuit

An RC circuit is a series combination of a resistor (*R*) and a capacitor (*C*) which are connected to a DC battery supply as shown in Fig. 1.14. At time zero, initial conditions of the capacitor are $i = 0$ and $q = 0$. When the switch is closed, the capacitor progressively charges up through the resistor until the voltage across the capacitor (V_c) reaches the supply voltage (V_s). Figure 1.15 shows the plots of capacitor voltage and capacitor current.

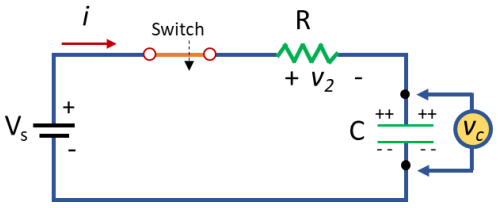

Figure 1.14. Schematic illustration of simple RC circuit consists of a battery (V_s), a resistor (*R*), a capacitor (*C*), and a switch for open or close circuit.v_c is voltage across the capacitor.

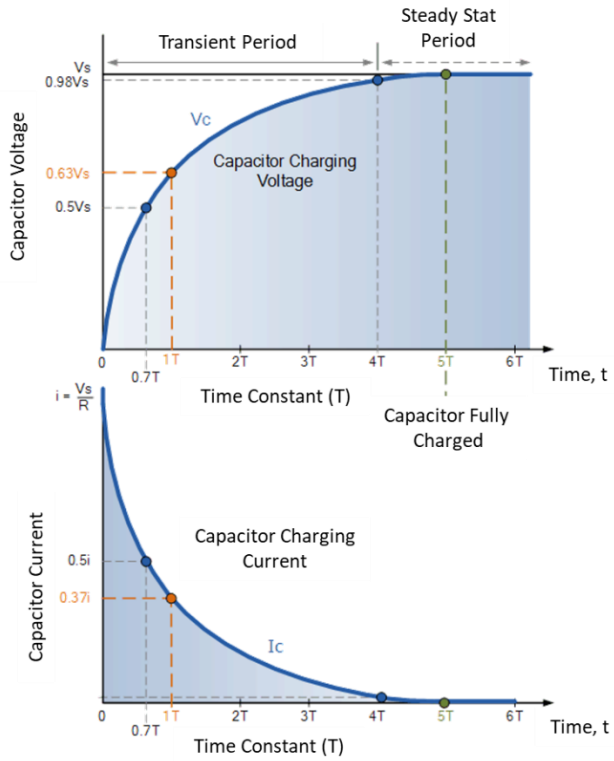

Figure 1.15. Step response of an RC circuit with initially uncharged capacitor: (top) voltage response, (bottom) current response (The figure modified from www.electronics-tutorials.ws).

Charging up the capacitor (*C*) through the resistor suffers from the RC time delay[66]. As time increases, the voltage of the capacitor increases toward steady state (Fig. 1.15 top). The rate by which the voltage increases is expressed in terms of the time constant, denoted by tau (τ), The time constant of a circuit is the time required for the response to gain to a factor of 1- e^{-1} (at t = τ) or 63.2 percent of initial voltage value as eq. 1.31:

$$V(t) = V_s\left(1 - e^{-t/\tau}\right) \qquad 1.31$$

or

$$\tau = RC \qquad 1.32$$

As the sine voltage across the capacitor is equal to zero at the initial state, the capacitor behaves as a short-circuit resulting in maximum current flow at t = 0. Such current can be calculated by Ohm's law. The current continuously generates until the potential difference of the capacitor approaching zero. At t > 0, however, the current decay exponentially called charging current as depicted in Fig.1.15 (bottom). The rate of current decay is obtained from eq. 1.31 and using $i(t) = CdV/dt$[65], thus

$$i(t) = \frac{V_s}{R} e^{-t/\tau} \quad 1.33$$

At 63% of capacitor charging voltage results in the current decay to 37% of the maximum value. The current that is produced before reaching five time constants (5τ, 98% Volt) is called transient current[66]. After 5τ, the capacitor is considered to be fully charged where t = ∞ and $V_c = V_s$. At this point, there is no more charging current flow (i = 0). This period is known as steady state where the capacitor acts like an open circuit.

1.4 Electrochemical measurements

1.4.1 Potentiometry

A typical potentiometric measurement involves a two-electrode cell consisting of an indicator electrode and a reference electrode. A high input impedance voltmeter allows one to measure precise EMF values in units of volts at so-called zero current. The potential of the ISE as indicator electrode is proportional to the activity of the primary ion while the reference electrode should give a stable and sample-independent potential. Potential-time changes at ISEs are complex time-dependent phenomena that depend on the electroactive material (membrane/film) and the bulk solution as well as the membrane|solution interface and its composition and thermodynamic and kinetic properties[30]. In this work, potentiometric measurements were used to evaluate ISEs to confirm that they provide a Nernstian response in which the potential vs log a_i is close to 59.2 mV/decade for a monovalent ion. Potentiometry was also utilized as a standard method of chronoamperometry and coulometry in order to compare its sensitivity and its reproducibility (Chapters 1, 3).

1.4.2 Chronoamperometry and coulometry

Chronoamperometry is an alternative electrochemical method to zero current measurements. In this technique the current is measured while a constant potential is applied for a certain time. In our work the transient current generated from the potential difference is recorded until it reaches a new electrochemical equilibrium state[25, 67]. Here, the chronoamperometric measurements are carried out in a three-electrode cell consisting of a working electrode (ISE in series with a capacitor), a reference electrode and a counter electrode. The potential of the working electrode against the reference electrode is kept constant by a potentiostat and the current flow between the counter electrode and the working electrode is measured. The

coulometric method is an integration of the chronoamperometric current over time to obtain charge-time information. This technique is recorded at a constant applied potential and is therefore called constant potential coulometry. Coulometric readout is also used to confirm the performance of an ISE connected in series with a capacitor, which will be evaluated by theoretical predictions involving RC circuit elements.

1.4.3 Electrochemical impedance spectroscopy

Electrochemical impedance spectroscopy (EIS) is an electrochemical technique in which a system is perturbed with a small time-dependent sinusoidal potential wave at varying frequency where $E = E_0 \sin(\omega t)$.[68] Normally, a 10mV potential amplitude, E_0, is applied, resulting in frequency-dependent amplitude and phase shift of the resulting current. This output signal is related to the function of $I = I_0 sin\{(\omega + \varphi)t\}$ where φ is the phase angle. A complex number is the ratio *E/I*, which determines the impedance at the corresponding frequency[69]. The EIS measurement is performed in a three-electrode system consisting of a working electrode, counter electrode and reference electrode. The Nyquist plot expresses the conductive behavior (a resistor or a capacitor) that occurs for the real and imaginary components of impedance denoted as Z_{real} (x-axis) and Z_{im} (y-axis), and the phase angle at a given frequency range as shown in Fig. 1.16A.

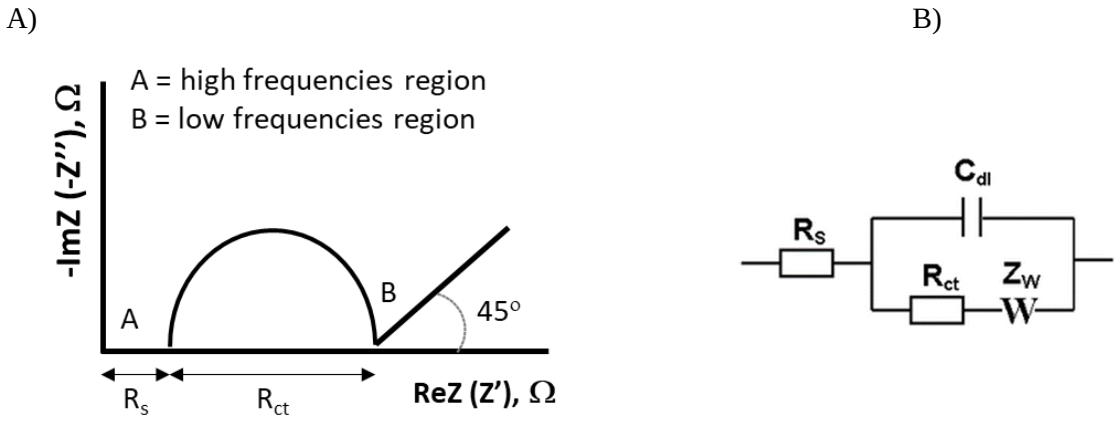

Figure 1.16. Schematic of typical A) Nyquist plot and B) Randles circuit.

The EIS response of electrode|electrolyte systems can be modelled as an equivalent circuit. As shown in Fig. 1.16B, the simplest circuit for a faradaic reaction is the Randles circuit. The faradaic reaction is occurring in parallel with the charging of the double layer at the electrode surface. Therefore, the charge transfer resistance, R_{ct}, associated with the faradaic reaction is in parallel with C_{dl}. The rate of the faradaic reaction is controlled by a diffusion of the reactants to the electrode surface. The diffusional resistance

element (the Warburg impedance, Z_w) is hence in series with R_{ct}. Here, EIS is used to characterize liquid-contact ISE in series with a capacitor and solid-contact ISE in series with a capacitor. Charge transfer kinetics and double-layer contributions at the ISM|solution interface was also investigated. Ideally, at low frequencies, a vertical line (phase angle at 90°) indicates the domain of capacitive behavior of the electronic capacitor or transducing material that acts as a pure capacitor.[70] A diffusion control process will cause a phase angle shift at 45° at intermediate frequencies. At high frequencies, a semicircle indicates the resistance of the ISM which can refer to a kinetic control of the double-layer charging and the charge transfer at the ISM|solution interface. This work proposes an extension of the Randles circuit when the working electrode is connected to an electronic capacitor as shown in the relevant chapters.

Chapter 2: Ultrasensitive seawater pH measurement by capacitive readout of potentiometric sensors

2.1 Development pH measurements

The measurement of pH is of enormous importance in most chemical, biological and environmental processes.[71-74] Atmospheric carbon dioxide (CO_2) output from anthropogenic sources including fossil fuel combustion and deforestation results in its gradual absorption by marine systems. This oceanic uptake serves to moderate atmospheric CO_2 but causes a reduction of surface ocean pH.[75] This significantly alters the chemical balance of the marine carbonate system, with a potentially dramatic impact to marine biota and ocean ecosystems.[76, 77] To accurately understand how ocean acidification impacts marine life, it is necessary to quantify seawater pH variability at an adequate measurement frequency.

While they remain the gold standard, the precision of potentiometric pH probes is limited because potential drifts/uncertainties (up to 0.02 pH units per day) may become difficult to distinguish from the desired change in pH.[78, 79] Potentiometric seawater pH measurements have been found to exhibit a precision of about 0.003 pH units,[80] or about 0.2 mV. Ion-selective field-effect transistors (ISFET) on the other hand, gave a precision better than 0.0005 pH units over hours and 0.005 over weeks for the same application.[81, 82] Similar to conventional glass electrode, ISFETs are still required regular calibration using standard pH buffer.[83] Spectrophotometry by indicator dye solution affords improved precision, giving a variability of just 0.4 mpH units for seawater.[84, 85] For this, the indicator solution must be adequately stored to ensure long-term stability[86] and the indicator needs to be highly purified to reduce errors in the pH calculated from absorbance data.[87, 88] However, spectrophotometric pH is not the same as pH reported by potentiometry because very different assumptions are involved in the measurement. With pH indicator dyes the activity coefficient of the dye depends on solution ionic strength and there is no liquid junction potential.

Here, the determination of pH at very high precision is achieved by modifying the electronic readout of electrochemical pH probes. Instead of observing potentials over time, which are difficult to distinguish from unrelated potential drifts, one allows a transient current to occur for a given pH change by placing an electronic capacitor component in series to the pH probe and holding the cell potential constant. The small current excursions can be easily identified, background-subtracted and integrated to give a charge that serves as sensor signal.

The approach proposed here builds on earlier work by the group of Bobacka[57, 60] on the basis of a conducting polymer, poly(3,4-ethylenedioxythiophene) (PEDOT) doped with poly(styrenesulfonate) (PSS), that serves as capacitive layer between electrode and ion-selective membrane. Vanamo et al. demonstrated that the measured current signal can be amplified by increasing the thickness, and therefore the redox capacitance, of the solid contact conducting polymer.[58] The theory for this transduction method suggests that an increasing capacitance, *C*, results in a larger measured charge, *Q*, as follows.[63]

$$Q = C\frac{s}{z_i}log\left(\frac{a_i(initial)}{a_i(final)}\right) \qquad 2.1$$

Where *s* is the Nernstian slope (59.2 mV at 25°C), z_i is the charge of the detected ion (for hydrogen ions, $z_i = 1$), $a_i(initial)$ and $a_i(final)$ are the activity of the detection ion *i* before and after the sample composition change.

2.2 Experimental and preparation for capacitive readout method

Materials and reagents Potassium chloride (KCl), sodium chloride (NaCl), hydrogen ionophore I, high molecular weight poly(vinyl chloride) (PVC), 2-Nitrophenyl octyl ether (o-NPOE), sodium tetrakis[3,5-bis(trifluoromethyl)phenyl]borate (NaTFPB), tetrakis(4-chlorophenyl)borate tetradodecylammonium salt (ETH 500), and tetrahydrofuran (THF) were purchased from Sigma-Aldrich. Ultrapure Tris-(hydroxymethyl)aminomethane (Tris) and 0.1 M sodium hydroxide (NaOH) volumetric solution were purchased from PanReac AppliChem. 1 M hydrochloric acid (HCl) volumetric solution was purchased from Fisher Scientific.

Instrumentation and Measurements An Ag/AgCl electrode with electrode diameter of 3.00 ± 0.01 mm and a hydrogen ion-selective electrode (H^+-ISE) were use as working electrodes in a conventional three-electrode system. A double junction Ag/AgCl/3 M KCl/1 M LiOAc electrode (Metrohm, Switzerland) and a platinum rod (Metrohm, Switzerland) were used as reference electrode and counter electrode, respectively. The working electrode was directly connected in series with a commercially available capacitor ranging from 4.7 to 470 µF. Electrode bodies (Oesch Sensor Technology, Sargans, Switzerland) were used to mount the polymeric membranes for the H^+-ISEs. For potentiometry, the H^+-ISEs were measured and calibrated with a high impedance input 16-channel EMF monitor potentiometer (Lawson Laboratories, Inc., Malvern, PA) at zero current. Chronoamperometric measurements were performed with a PGSTAT302N Autolab (Metrohm Autolab B.V., Switzerland) controlled by Nova 2.1.4 software. The

open circuit potential (OCP) of the working vs reference electrode was determined and enforced as a constant value by the potentiostat during the chronoamperometric measurements. The measured current signal was integrated over time to obtain the charge-time relationship. Cumulated charge was then plotted vs the logarithm of ion concentration (activity). Potentiometric experiments were performed with a high impedance input 16-channel potentiometer as mentioned before. The EMF vs the logarithm of ion activity was recorded. All experiments were carried out at ambient laboratory temperature.

Sample preparation Aqueous solutions were prepared by dissolving the respective salts in deionized water (>18 MΩ cm). All chemicals were of at least analytical grade. 0.1 mM KCl solution was prepared in 10 mM KNO_3 background electrolyte and was used as reference solution for measuring the OCP for chloride ions analysis. The concentration of KCl in a range of 0.1 mM to 3.3 mM was used for this experiment with 0.2 mM increment. For pH measurement, 0.1 M Tris-HCl buffer solution pH 7.00 was prepared in 10 mM NaCl background electrolyte and was used as reference solution of OCP measurement. Seawater from Arcachon Bay (France) with salinity of 28.4 was used as sample solution. After filtration the seawater sample was prepared in 0.1 M Tris-HCl buffer to maintain the pH at 8.0 and used as reference solution. The desired pH was adjusted by addition of NaOH solution (see Methods in main text).

Preparation of the Electrodes Ag/AgCl electrode was prepared by electrochemical oxidation of an Ag electrode in 1 M HCl for 1 h at constant anodic current of 1 mA/cm^2. The coated electrode was washed with deionized water prior to use. A PVC based ion-selective membrane was used for pH measurements, which was composed of 15 mmol kg^{-1} hydrogen ionophore I, 5 mmol kg^{-1} NaTFPB ion-exchanger, 90 mmol kg^{-1} ETH 500, 118 mg o-NPOE and 59 mg PVC (total mass of 200 mg). The cocktail was dissolved in 2.0 mL of THF and poured into glass ring (22 mm ID) affixed onto a glass slide. The solution was allowed to evaporate overnight. This initial membrane was cut with a hole-puncher into small pieces of 8 mm diameter and mounted into Ostec electrode bodies. The electrodes were conditioned overnight in the 10 mM Tris-HCl and 10 mM NaCl pH 7.0 inner filling solution. For seawater experiment, seawater sample in 10 M Tris-buffer (pH 8.0, salinity 28.4) was used as inner filling solution**.**

In-line measurement The solution was delivered by peristaltic pumps (ISMATEC, model ISM935c, Clattbrug, Switzerland) equipped with tygon tubing (ISMATEC, inner diameter 1.42 mm). An air gap was used to separate each solution plug at a flow rate of 333 µL/min. The tygon tube installed on the pumps was connected to the electrochemical flow cell using PTFE tube (BOLA, inner diameter 0.8 mm). The tip of the working electrode was inserted into a wall-jet flow cell which allowed the solution stream to flow through. The open circuit potential (OCP) was determined for the reference solution flow prior the measurement.

The chronoamperometric experiments were carried out with the same continuous flow system. The fully automated system was controlled by LabVIEW 10.0. Small pH change of 0.1 M Tris-HCl buffer solution in bulk solution (500 mL) was prepared by automatic titration by a 765-Dosimat (Metrohm, Switzerland). The bulk solution was stirred continuously. 1 mL of each sample solution and reference solution were switched and separated by 11 μL air. Signals were automatically recorded by Nova software (Autolab, Metrohm, Switzerland). The flow path was flushed with new sample solution before the next measurement. The same methodology as standard solution was applied to measure pH in seawater sample. Small pH change was imposed by adding NaOH to seawater sample in 0.1 M Tris-HCl buffer (500 mL). Seawater sample in Tris-HCl buffer is also used as reference solution.

To avoid deteriorating signals from trapped air bubbles, the air gap was removed before measurement by a debubbler placed just before the wall-jet cell. Small, well defined changes of pH were achieved by automatic titration, delivering precise amounts of NaOH into a 0.1 M Tris-HCl buffer. The required volume of NaOH was determined from potentiometric titration of the buffer and used to achieve the desired change of pH as a function of added NaOH volume from the Henderson-Hasselbalch equation. A large buffer volume of 500 mL was used to minimize uncertainties. Each new sample composition was aspirated to the detection cell for measurement illustrated in Scheme S2.1. After each measurement the residual volume of the Tris-HCl buffer was corrected for calculating the precise amount of NaOH needed for the following pH change. Each new sample composition was passed through the cell for sufficient time to eliminate error from carry-over of the previous sample composition. The OCP was measured in the reference solution stream of Tris-HCl buffer and subsequently imposed for the sample as well. The OCP was re-measured before changing to a new pH value to minimize drift. The seawater sample from Arcachon bay with a salinity of 28.4 was filtered and prepared in 0.1 M Tris-HCl buffer to give a pH of 8.07 by adding NaOH solution. The automated system consisted of i) sample preparation: Tris-HCl buffer bulk solution was titrated by 0.1 M NaOH by a 765 Dosimat liquid delivery system (Metrohm, Switzerland). ii) Fluidics: the solutions were delivered by a peristaltic pump (ISMATEC, Switzerland) with tygon tubing (ISMATEC, I.D. 1.42 mm) at a flow rate of 333 μL/min to the detection cell. A switching valve (VICI, USA) was used to switch between solutions and air. iii) Detection: chronoamperometry was performed by NOVA software (Autolab, Metrohm, Switzerland) to record current-time signals and their integration to charge-time information. The open circuit potential (OCP) of the working electrode vs reference electrode was determined and subsequently enforced unto the cell by the potentiostat during the chronoamperometric measurements.

2.3 Results and discussion

Here, ultra-sensitive pH measurements are achieved by using, for the first time, electronic capacitor components instead of conducting polymer layers. This likely provides better stability and further gives exquisite control for tuning the sensitivity of the method to the pH change of interest. Scheme 2.1 shows the capacitive readout principle with an ion-selective membrane element connected in series with an electronic capacitor. The initial open circuit potential (OCP) of the measurement cell is kept constant. A change in ion activity results in a potential change at the indicator electrode in agreement with the Nernst equation, which must be compensated by an opposite potential change of the capacitor. For measuring small pH changes, the compositional change must reach the indicator electrode abruptly to achieve well resolved current transients that can be subtracted from the background. A segmented flow separates the sample solution from a reference solution with an air gap[89-91] to minimize dispersion. Each measurement involves a sequential alternation of sample (S1) and reference solution (Ref), giving a sharp transition that reflects the ion activity change (see top right in Scheme 2.1).

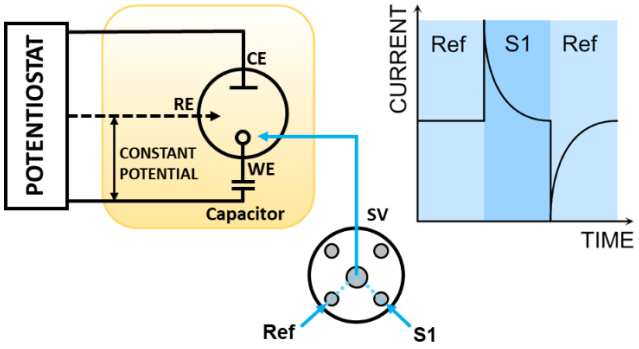

Scheme 2.1. The potential change observed at a pH electrode is compensated over a capacitive element placed in series as the overall cell potential is held constant. The alternating introduction of a reference (Ref) and sample solution (S1) results in current transients that are easily identified and quantified to make ultra-sensitive pH measurements possible. The important application for this advance is the monitoring of ocean acidification at high time resolution. SV: switching valve.

Potentiometric probes consisting of an Ag/AgCl sensing element served as an initial model system because their potential is resistant to the passage of current. The detection protocol involves the measurement of the open circuit potential (OCP) in the reference solution, which is then imposed at the same amplitude over the course of the experiment. When a sample of different concentration reaches the electrode, a transient current spike is observed (Fig. 2.1A). Decreasing sample concentrations result in a reversible change in the

opposite direction. Integration of the transient currents provide the corresponding cumulated charge over time (Fig. 2.1B).

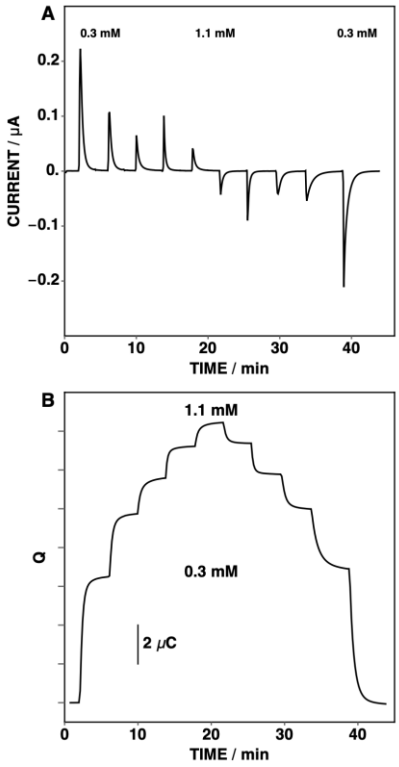

Figure 2.1. (A) observed current transients and (B) integrated charge upon increasing the chloride concentration from 0.1-1.1 mM in 0.2 mM steps, and back to 0.1 mM, using the chloride sensitive Ag/AgCl electrode as initial model system to demonstrate the principle.

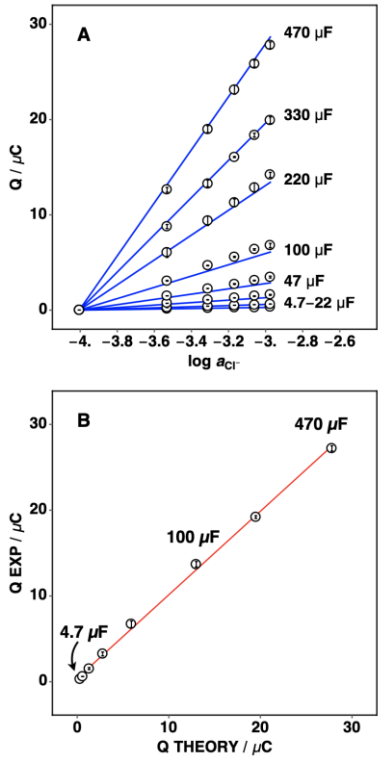

Figure 2.2. (A) Calibration curves for integrated charge vs. logarithmic chloride activity for the indicated capacitances, using an Ag/AgCl sensing element as model system. Blue lines are theoretical based on eq. 2.1. (B) Correspondence between theoretical (eq. 2.1) and observed charge upon a 10-fold activity change in the sample for the same range of capacitances (4.7 µF to 470 µF).

A range of commercially available capacitors (4.7 to 470 µF) was evaluated. As shown in Figure 2.2A, a linear dependence of accumulated charge on the logarithmic chloride activity is obtained with the Ag/AgCl electrode in agreement with eq. 2.1 and using the known capacitance of the electronic element (solid lines are predicted from nominal capacitances). Figure 2.2A, B shows that the observed slopes for charge Q vs. loga_{Cl^-} agree well with those predicted from eq. 2.1 for a wide range of capacitances. Larger capacitances result in a greater charge, proportional to Csz_i^{-1} in eq. 2.1, which can therefore be amplified for better sensitivity. An excessive charge passing through the cell should be avoided to minimize sample and

membrane perturbations. For this reason, larger capacitances are best suited for small sample concentration changes to limit the resulting charge.

The constant-potential coulometric approach integrated into an automated air-segmented flow system was applied to demonstrate the reversible detection of pH change using an H^+-selective electrode. The high resistance of commercial glass pH probes (50 to 500 MΩ) make it too difficult to pass appreciable charge and result in RC time constants on the order of hours. The membranes used here were polymeric membrane electrodes containing tridodecylamine as lipophilic H^+-ionophore for long-term measurement over period of weeks (see Supporting Information and Figure S2.1 for detail). The membrane electrode chosen here is of the aqueous inner solution type, and future work will evaluate whether the approach can be made applicable to solid-contact membrane electrodes. Small, well-defined changes of pH were achieved by automatic titration, delivering precise volumes of NaOH into a 0.1 M Tris buffer. Figure 2.3 illustrates the observed reversible transient current spikes over time for pH changes that range from 0.001 to 0.005 pH units relative to the reference solution, using a 100 µF capacitor for improved sensitivity. The measurement of reference solution – sample – reference solution gives two current transients, one positive and one negative. The first peak is used as the signal while the reversal peak serves to establish the new current baseline for subsequent measurements. The transients are found to be sufficiently sharp, see Fig. 2.3A. Linear regression of charge and ΔpH is shown in Fig. 2.4A, described by $Q = 1.37\times10^{-9}\ C + 56.7\times10^{-7}\ C\times\Delta pH$ and r^2 of 0.9993. Equation 2.1 may be rewritten to represent pH change instead of ion activity as follows:

$$Q = Cs\Delta pH \qquad 2.2$$

where s is electrode slope (ideally 58.6 mV at 22 °C) and C is the capacitance used. For the data in Fig. 2.3A, s is near-Nernstian at 56.7 mV (see calibration curve in Fig. 2.4A) and in good agreement with eq. 2.2. The observed reproducibility (average standard deviations, shown as error bars in Fig. 2.4A) is found as 28×10^{-6} pH units, which in potentiometry would correspond to a potential change of a mere 1.7 µV.

The proposed method was compared with zero current potentiometry using the same pH electrode (without capacitor) in otherwise the same measurement setup, sequentially comparing each sample to the reference solution. The corresponding EMF vs time traces are shown in Fig 2.3B. For the smallest pH changes, it becomes difficult to distinguish the individual potential responses, while for larger ones, the differences become evident, but so is the influence of potential drift on the pH data. Figure S2.2 shows the corresponding plot of measured EMF change vs. ΔpH, with the slope (sensitivity) indicated as a solid line

($\Delta EMF = -0.04mV - 37.0mV \times \Delta pH$ and $r^2 = 0.98$), which is significantly sub-Nernstian which contrasts to the expected behavior over a wide pH range (Fig. S2.3). The average standard deviation is found as 0.012 mV or 1.4 mpH units, which is about 2 orders of magnitude worse than with the approach introduced here. The systematic error originating in the deviation from Nernstian response slope further exacerbates this uncertainty. Based on the data presented here, the capacitive readout allows one to achieve ultra-precise pH readings that significantly surpass that of potentiometry for the determination of pH.

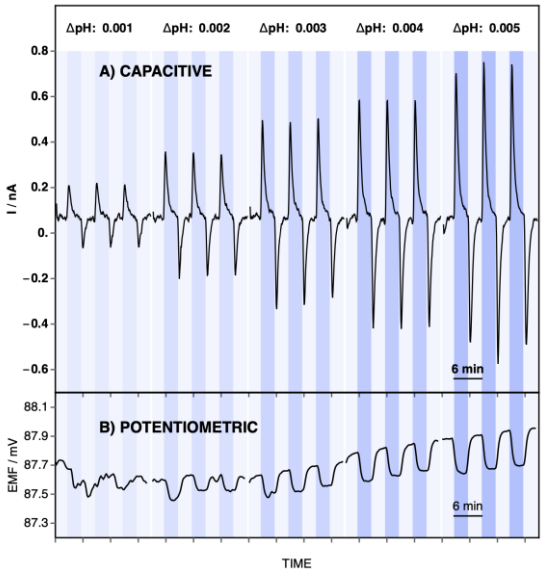

Figure 2.3. (A) Measurement of small pH change in the range of 0.001 to 0.005 units with a 100-µF capacitance. Detection of the reference sample (light background color) is followed by the sample of increasing pH (darker background), repeated three times for each pH value. Negative current transients indicate return to reference solution of lower pH. (B) Same measurement as for (A), but using zero current potentiometry as readout in the absence of capacitive element.

Fluctuations in seawater pH are mainly driven by an increase in atmospheric CO_2, shifting the carbonate buffer system and adversely impacting the development of marine species, particularly calcifying organisms. Since the industrial revolution, the average ocean surface pH has decreased by 0.1 pH units[92] at a current rate of 0.002 pH units per year.[93, 94] Capturing pH variations at a detection frequency in the order of days is important to assess ocean acidification dynamics. The precision of potentiometric pH probes is not adequate for this task.

The proposed method is demonstrated to measure ultra-small pH changes of seawater that was sourced from Arcachon Bay near Bordeaux in Southwestern France. To eliminate potential sources of error from CO_2 re-equilibration with the atmosphere, which contrasts to the expected behavior over a wide pH range

(Figure S2.4), the seawater samples were treated with Tris buffer to stabilize their pH values. The total pH scale was used where sulfate ion is also considered by titration to identify the pKa value (Figure S2.5). Figure 2.4B shows the observed integrated charge as a function of pH for seawater under otherwise the same experimental conditions as for Fig. 2.4A. Regression analysis gives $Q = 0.01\times10^{-9}\,C + 65.5\times10^{-7}\,C\times\Delta pH$ ($r^2 = 0.9999$) corresponding to a near-Nernstian slope of 65.5 mV with the 100 µF capacitive elements used here (eq 2.2). The reproducibility calculated as the average of the standard deviations is 67 µpH, which compares well to the data in Fig. 2.4A. The same samples assessed potentiometrically (Fig. S2.6) give potential traces that are too difficult to distinguish reliably. While the observed EMF visibly drifts, the ΔEMF versus ΔpH curve plotted as a function of time in Fig. S2.6 (inset) gives a calculated standard deviation of 0.7 mpH or 0.017 mV. Given the sub-Nernstian response slope for this data, the actual error is expected to be larger.

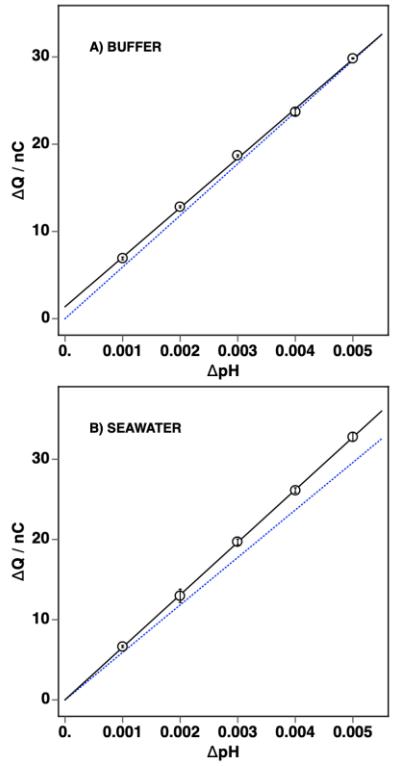

Figure 2.4. (A) Calibration curve of integrated charge from the current transients shown in Figure 2.3A as a function of pH change. Error bars are standard deviations (n = 3), corresponding to an average of 28 µpH units. (B) Calibration curve from the same type of experiment as in (A), but with seawater sample from Arcachon Bay (average standard deviation of 67 µpH). Blue dashed lines are theoretical based on eq. 2.1 and deviate slightly more for seawater, likely given by the limited extrapolation precision to find the pH change. The seawater sample pH was stabilized to minimize systematic errors (see text).

2.4 Supporting information

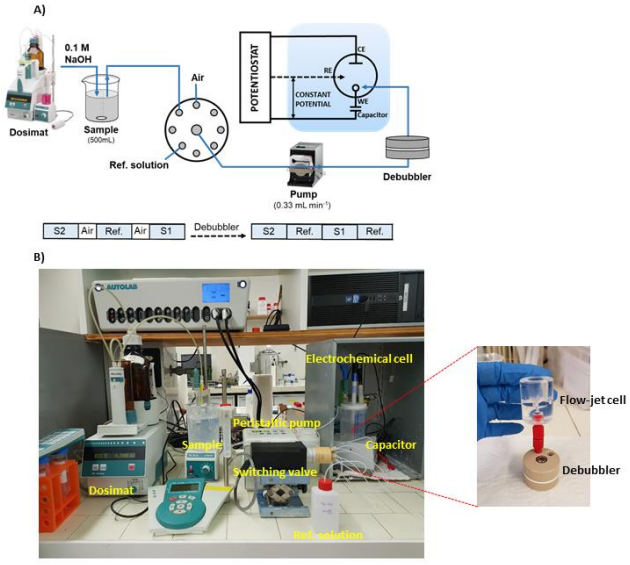

Scheme S2.1. (A) Schematic illustration and (B) photos of fully automated system for determination of small pH change. The system consists of a dosimat for preparing the sample solution, a peristaltic pump equipped with a switch valve for delivering all solutions to the detection cell, a debubbler device for eliminating the air bubble just before measurement, and an electrochemical system for recording the signal controlled by Nova software. The lower chart shows the sequence of the flow of analytes and air-gap before and after passing though the debubbler; S1 and S2 are sample 1 and sample 2, Ref. is the reference solution.

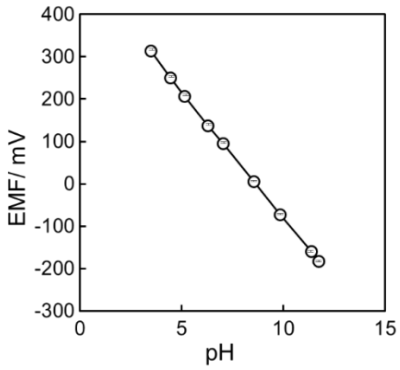

Figure S2.1. Long-term stability test of used polymeric membraned electrode based tridodecylamine (TDDA). The membrane electrodes were used for several experiments in seawater sample and stored for 3 months before this test. A Calibration curve between EMF and pH with linear regression (solid line) shows Nernstian behavior with $EMF = 515.79\ mV + 59.61\ mV \times pH$, $r^2 = 0.9998$.

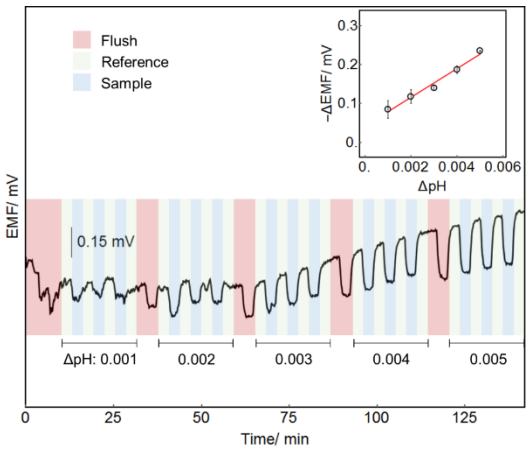

Figure S2.2. Repeatability of potentiometric measurement of small pH change utilizing the fully automated system for Tris buffer solution. Inset: Correlation between EMF change and ΔpH (open circles) together with linear regression (solid line, EMF = -0.04mV-37.0mV×pH and r^2 = 0.98). The sub-Nernstian slope results from potential drifts, see also Nernstian behaviour in a wide range of pH for the same electrode in Figure S2.3.

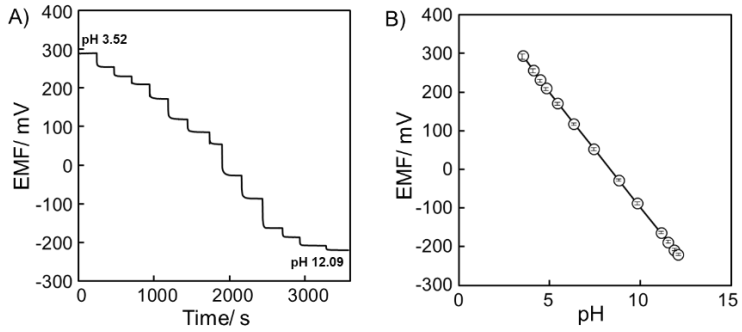

Figure S2.3. (A) Potentiometric measurement of wide range pH change using hydrogen-selective membrane electrode in universal buffer and 10 mM NaCl, demonstrating Nernstian response slope (compare to Figure S2.2 above where a narrow pH range gives an undesired sub-Nernstian slope). (B) Corresponding calibration curve of EMF versus pH. Nernstian response is observed with a linear regression of EMF = 499mV-59.7 mV×pH and r^2 = 0.9999.

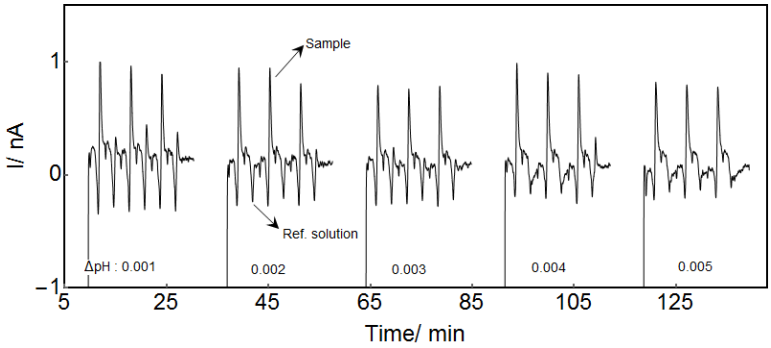

Figure S2.4. Chronoamperometric measurement of small pH change in the range of 0.001 to 0.005 units of unmodified seawater sample using polymeric membrane electrode assembled with 100-µF electronic capacitor. Increasing sample

pH (positive current) was switched to reference solution (seawater, negative current) by continuous flow system. Each sample was repeated three times.

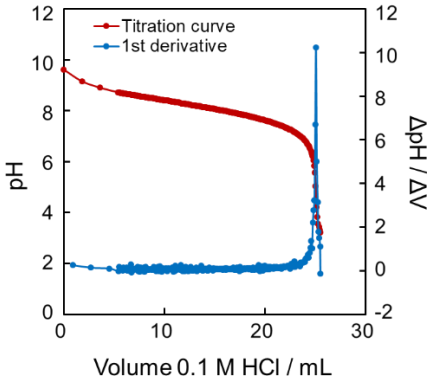

Figure S2.5. Potentiometric titration curve of Tris buffer in seawater sample (red) and first derivative plot (blue). Concentration of Tris buffer of 0.084 M was obtained respected to the pKa value of 8.24.

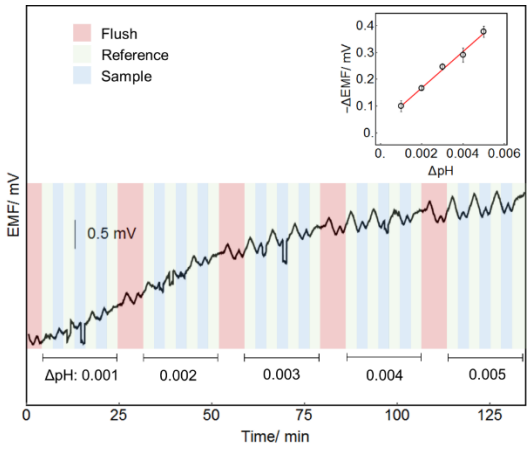

Figure S2.6. Repeatability of potentiometric measurement of small pH change of seawater sample in Tris-HCl buffer utilizing the fully automated system. Inset: Correlation between EMF change and ΔpH (open circles) together with linear regression (solid line, EMF = -0.03mV-67.7 mV×pH and $r^2 = 0.99$).

Chapter 3: Rapid constant potential capacitive measurements with solid-contact ion-selective electrodes coupled to electronic capacitor

3.1 Development of solid-contact ion-selective electrodes for capacitive readout

Ion selective electrodes (ISEs) are established in analytical applications including environmental monitoring, clinical diagnostics, and industrial processes. Classical ISEs based on polymeric membrane containing ionophores and with an inner filling solution of optimized conditions may give low detection limits,[95] high ruggedness as well as high selectivity. Such ISEs have seen significant a research activity for their use as potentiometic sensors but also with alternative readout principles.[96] More recently, the inner filling solution has been eliminated and replaced with an ion-to-electron transducing material placed between electrode substrate and membrane to realize all-solid-state ion selective electrodes.[97, 98]

Numerous publications have reported the use of conducting polymers (CPs) as solid-contact material aiming to achieve robust potentiometric sensors. The most common CPs include polypyrrole (PPy)[36], poly(3,4-ethylenedioxythiophene) (PEDOT)[40], and poly(3-octylthiophene) (POT)[37]. However, CPs may be sensitive to light or pH, resulting in potential drifts and undesirable aging.[50] Nanomaterials have also been found promising as solid-contact ion transducer, e.g., carbon nanotubes (CNTs),[99] graphene,[100] and gold nanoparticles.[101]

The research cited above has chiefly aimed for a zero current potentiometric readout of these sensors. In that case, however, the sensitivity is limited by the Nernst equation. For instance, oceanographic research for tracing pH change of seawater requires high sensitivity and precision.[82] Clinical analysis of electrolytes in biological fluids also exhibits a narrow concentration interval that results in a small potential change.[38] The sensitivity to divalent or multivalent ions is also significantly decreased, described by z_i in the term RT/z_iF.[102]

To overcome the limitation from the Nernstian slope, an alternative readout with conducting polymer transducing materials as a capacitive layer has been introduced by Bobacka's group[57, 58]. It is coined "constant-potential coulometry" and gives rise to current transients that are easily identifiable and integrated, which is in contrast with zero current potentiometric traces. In this method the redox capacitance of poly(3,4-ethylenedioxythiophene) (PEDOT) doped with poly(styrene sulfonate) (PSS) in SC-ISE assists in the transduction of ion activity to an electrical current and charge.

To achieve this, the potential of the SC-ISE is enforced to a constant value by an external power source (see Scheme 3.1). A change of ion activity results in a potential change at the sample–membrane interface. Since the cell potential is constant, this is compensated by charging a capacitive solid contact layer with the same potential of opposite sign, until the new equilibrium state is established. From this, a transient current is observed and integrated to give accumulated charge as sensing readout. This charge is expected to be proportional to the logarithmic ion activity change. A simple theoretical model for the capacitive readout has been described, giving good agreement with experimental results.[63] Polarizations at the ion-selective membrane have recently also been considered by an extended theoretical equation.[64] The charge is proportional to the thickness of the transducing layer.[58] A coulometric readout therefore allows one to amplify the analytical signal by increasing the capacitive thickness of the solid contact. The coulometric readout of this transient current should depend on the RC time constant, chiefly given by the capacitance of transducing layer and the resistance of the membrane.[63]

The main drawback of coulometric readout is the relatively long measurement time and a drifting of the current that makes reliable integration difficult. In recent work, increasing the geometric surface area of electrode[59] or using thin membranes[60] gave significantly shorter response times. For this reason, Kondratyeva et al. proposed to use a fixed cutoff time to obtain a reasonably linear dependence of charge vs logarithmic ion activity.[64] The approach showed promising results of K^+ ion measurements in serum samples when the charge accumulation time was over 300 s. Unfortunately, however, the linearity of the resulting calibration curve was rather poor. In a compromise between sensitivity and sampling rate, an optimization of such SC-ISE would be needed to give a coulometric mode that is truly analytically useful.

Very recently, a method for improving the precision and sensitivity of potentiometric pH probes was presented by our group[25] that is based on the principle of constant-potential coulometry.[58] The capacitive readout was carried out with liquid-contact ISEs and a commercially available electronic capacitor placed in series instead of a chemical transducing material. The sensitivity of pH measurement in stabilized seawater was found to be dramatically improved, down to a precision of 67 µpH units. The uniqueness of the approach is its simplification by adding the external capacitor to match the desired application. The use of electronic components also appeared to overcome the drifting currents and long response times mentioned above. Those results suggest that solid-contact transducers may not behave as ideally as electronic components and might be the source of this nonideality. We postulate here that an electronic capacitor may be added to a SC-ISE to dominate the constant potential coulometric readout of a sensor of interest.

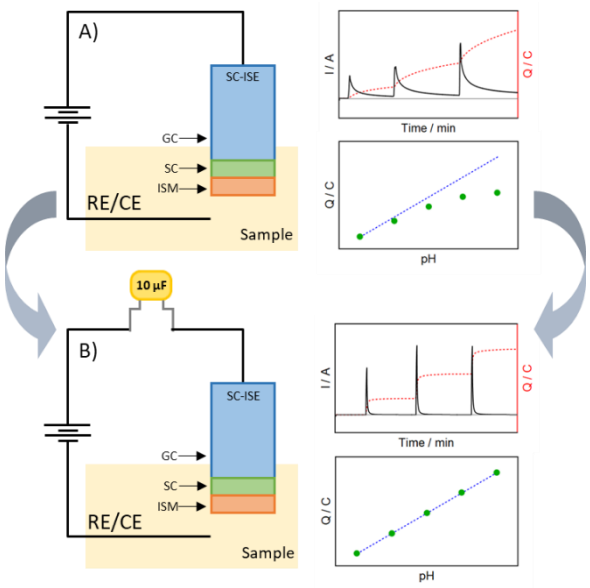

Scheme 3.1. Large improvement of constant potential coulometric readout by solid contact ion-selective electrodes (SC-ISEs) by connecting an electronic capacitor in series. (A) The potential change at a SC-ISE is compensated over a capacitive SC layer material. The nonideality of this material gives rise to slow current transients and significant drift, giving moderate linearity of the calibration curve. (B) Placing an electronic capacitor in series imposes its capacitance on the cell and rectifies the non-idealities observed in (A).

In this work, two types of solid-contact materials were explored, with POT as redox material and functionalized-CNT as capacitive material. Sample pH changes were investigated with PVC-based H^+-selective solid contact electrodes. As expected, the approach gave dramatically shorter measurement times and allow for an improved sampling rate using established macroelectrode membrane geometries (3 mm dia.) and thicknesses. Instead of having to optimize the solid contact layer thickness, the added electronic capacitor was found to be responsible for gaining sensitivity. Importantly, the error of charge integration originating from the drifting current baseline was largely eliminated.

3.2 Experimental and preparation for capacitive readout method

Materials and Reagents. Octadecylamine functionalized single-walled carbon nanotube (f-SWCNT, 0.5-200 µm length and 30-50 nm diameter), regioregular poly(3-octylthiophene-2.5-diyl) (POT) with a weight-average molecular weight of ca. 34 000 g mol^{-1}, sodium chloride (NaCl), acetic acid, phosphoric acid, boric acid, hydrogen ionophore I, high molecular weight poly(vinyl chloride) (PVC), 2-nitrophenyl octyl ether (o-NPOE), tetrakis(4-chlorophenyl)borate tetradodecylammonium salt (ETH 500), sodium tetrakis[3,5-bis(trifluoromethyl)phenyl]borate (NaTFPB), and tetrahydrofuran (THF) were purchased from Sigma-

Aldrich. Chloroform (analytical grade), 1 M sodium hydroxide (NaOH) volumetric solution and 1 M hydrochloric acid (HCl) volumetric solution was purchased from Fisher Scientific. A mixed solution of acetic acid, phosphoric acid, and boric acid was dissolved in 10 mM NaCl to obtain universal buffer at 10 mM final concentration. pH 7.0 served as initial pH, which was adjusted by NaOH or HCl to give the final pH. All aqueous solutions were prepared in deionized water (>18 MΩ cm).

Preparation of Electrodes. Glassy carbon electrodes were modified by f-SWCNTs[26, 49] or POT[103] with a similar protocol as described. A 1 mg mL^{-1} of f-SWCNT solution was dispersed in 1 mL THF and a 4.2 mg mL^{-1} of POT solution was dissolved in 1 mL chloroform. A film of each transducing materials was deposited on top of each electrode by drop casting one to eight layers (20 µL for each layer) for f-SWCNT electrode denoted as GC/CNT/H-ISM or 1 layer (10 µL) for POT electrodes denoted as GC/POT/H-ISM. A silicone mask was placed on the electrode surface to confine the drop cast area to the underlying electrode. Each layer was left to dry for 10 min and 30 min for f-SWCNT and POT, respectively, before the next layer was deposited. The membrane cocktail was composed of 15 mmol kg^{-1} hydrogen ionophore I, 5 mmol kg^{-1} NaTFPB ion-exchanger, 90 mmol kg^{-1} ETH 500, and a 1:2 ratio of PVC and o-NPOE (total mass of 200 mg). The cocktail was dissolved in 2.0 mL of THF. Then, 150 µL of the membrane cocktail was drop-cast on top of the f-MWCNT or POT film (3 × 50 µL), and each layer was allowed to dry for 20 min. Finally, the electrodes were conditioned in universal buffer pH 7.0 overnight before use.

Electrochemical Measurements. Glassy carbon (GC) electrodes with electrode diameter of 3.00 ± 0.05 mm (Metrohm, Switzerland), a double junction Ag/AgCl/3 M KCl/1 M LiOAc electrode (Metrohm, Switzerland) and a platinum rod (Metrohm, Switzerland) were used in a three-electrode cell. A solid-contact ion-selective electrode (SC-ISE) was connected in series with a commercially available capacitor in a range of 1-100 µF. A PGSTAT302N Autolab (Metrohm Autolab B.V., Switzerland) controlled by Nova 2.1.4 software was used to perform chronoamperometry and electrochemical impedance spectroscopy (EIS).

The open circuit potential (OCP) of the working electrode vs reference electrode at pH 7.0 (universal buffer) was determined and subsequently enforced unto the cell by the potentiostat during the chronoamperometric measurements in universal buffer. Transient currents were recorded, while the pH was alternated by consecutively adding NaOH for basic range or HCl for acid range. The current was then integrated to obtain charge versus pH information. EIS experiment were used to explore GC/CNT/H-ISM and GC/POT/H-ISM with and without capacitor in series. Impedance spectra were recorded at OCP in 10 mM universal buffer and 10 mM NaCl with an ac excitation amplitude of 100 mV to enhance signal/noise ratio. A frequency range of 1 MHz – 0.1 Hz was used. Potentiometric measurements were performed by a high impedance

input 16-channel EMF monitor potentiometer (Lawson Laboratories, Inc., Malvern, PA) using an Ag/AgCl/3 M KCl/1 M LiOAc reference electrode (Metrohm, Switzerland).

3.3 Results and discussion

This work aims to help develop robust and reliable constant potential coulometric solid-contact (SC) ion-selective electrodes (ISEs) by exploring the use of an external capacitor. We postulate that the undesirable current drift observed with SC-ISEs is caused by the faradaic characteristics of the transducing material that allows for a residual current to be passed. If so, the placement of an electronic capacitor in series to the ion-selective electrode (see Scheme 3.1B) such that it dominates the overall cell capacitance might alleviate this important limitation. This approach is motivated by our previous work on aqueous inner-contact ISEs where an added capacitive element gave rise to rapid current transients with no appreciable drift.[25]

For this to work, the existing capacitance of the SC-ISE needs to be taken into account. Kirchhoff's law may serve as a useful starting point to estimate how the cell capacitance changes when an external capacitance is placed in series:

$$\frac{1}{C_{tot}} = \frac{1}{C_{SC}} + \frac{1}{C_{cap}} \qquad 3.1$$

Accordingly, the total capacitance value (C_{tot}) should depend on the sum of the reciprocal individual capacitors of the solid contact (SC) and the external electronic capacitor (cap). As an example, Bobacka reported on capacitances of conducting polymer solid contact layers on the order of 250 µF.[60] To keep the influence of C_{SC} to less than 10%, the added capacitor should have a 10-fold smaller value. From previous work, however, the sensitivity of the calibration curve is linearly proportional to the capacitance value of the cell:[63]

$$Q = C_{tot}\, s_I\, log\, \frac{a_I(initial)}{a_I(final)} \qquad 3.2$$

where Q is the charge from the integrated current spike, s_I is the Nernstian slope (for a monovalent ion *I*, ideally 59.2 mV), while a_I(initial) and a_I(final) are the ion activities for the sample of the initial and the final solution, respectively. The applied potential corresponds to the open-circuit potential for the reference solution. From eq. 3.2, the desired total capacitance should be as large as practically possible. This points

to a narrow, optimal range of capacitance values that combines the desired properties of fast response time and high sensitivity.

The first example studied here involves a transduction layer composed of functionalized CNTs (f-SWCNTs). The formation of electrical double layer of functionalized carbon nanotube has been confirmed to relate to a capacitive mechanism[48] while preventing an undesired water layer. The use of functionalized CNTs up to eight-layer coatings was shown to give high potential stability for use as potentiometric sensors in environmental applications.[26] This f-SWCNT material was chosen in combination with a polymeric pH electrode for the measurement of pH.

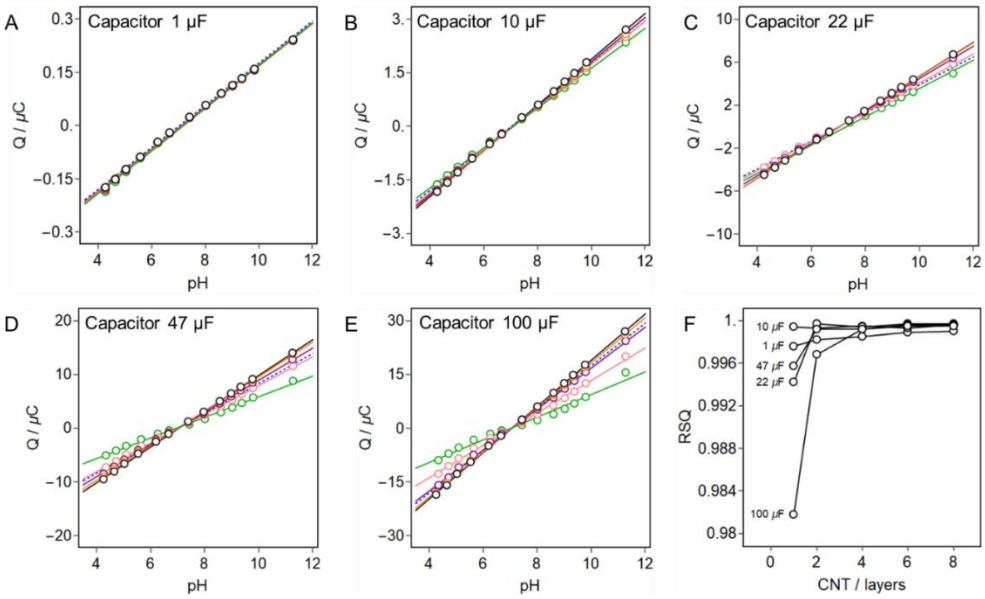

Figure 3.1. (A-E) Influence of added electronic capacitor in the range of 1-100 µF (A-E) on the response slopes for GC/CNT/H-ISEs with different transducing layer thicknesses. Shown are the accumulated charge vs pH for the following number of f-SWCNTs transducing layers: one layer (green), two layers (pink), four layers (purple), six layers (orange), and eight layers (black). Experiments are by chronoamperometry in 10 mM universal buffer and 10 mM NaCl in the pH range 4.3 to 11.3, using a pH 7 universal buffer as reference sample (a_H*(initial)* in eq 3.2). The blue dashed lines are theoretical expectations for the added capacitance value (eq 3.2). (F) Quality of linear regression (R^2) for the Q vs pH responses shown in (A-E).

A range of electronic capacitors (capacitance values between 1 µF to 100 µF) were connected in series to SC-ISEs modified with one to eight layers of f-SWCNTs (see Experimental Section) and evaluated in terms of their integrated current response as a function of sample pH. Figure 3.1A-E shows the corresponding calibration curves of charge Q vs. pH change obtained by constant-potential coulometry. Larger capacitors placed in series resulted in a larger deviation from linearity and a lower precision. This appears to be in

qualitative agreement with Kirchhoff's law (see above). On the other hand, for all studied thicknesses of the f-SWCNT layer, a capacitor of 1 µF resulted in the same response curves, independent of the value of the solid-contact capacitance (Fig. 3.1A).[25]

A thicker f-SWCNT coating (four to eight layers) could be combined with capacitances of up to 100 µF and gave better precision than thin layers (Fig. 3.1A-E). As illustrated in Fig. 3.1F, the linearity was maximal at a thickness over four layers for all added capacitances, with an R^2 value better than 0.9985. In agreement with the calibration curves, small added capacitances of 1 µF and 10 µF were applicable for all thicknesses of GC/CNT/H-ISEs (R^2 0.9976 to 0.9996). The appropriate linear fits for all GC/CNT/H-ISEs are given in Table S3.1 (Supporting Information). The reason for the observed nonlinearity for the cases where C_{SC} dominates is explained with the current response not adequately reaching zero baseline (see Fig. S3.1), which makes it difficult to properly quantify the accumulated charge. The observed slopes versus added capacitance for the data in Fig. 3.1A-E are shown in Fig. 3.2. Larger capacitances result in a greater charge. The slope can therefore be amplified by applying a larger capacitance for better sensitivity. The upper limit depends on the f-SWCNTs loading of the SC-ISE. When using GC/CNT/H-ISE with four to eight layers, Q is proportional to added capacitance in the range of 1-100 µF (see linear fits in Table S3.2).

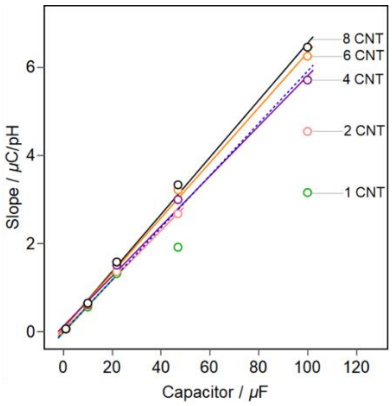

Figure 3.2. Correspondence between slope obtained from Fig. 3.1A-E and the value of the added capacitance (1-100 µF). The number of f-SWCNT layers to modify the SC-ISE is represented by color, with green (one layer), pink (two layers), purple (four layers), orange (six layers), black (eight layers). The dashed line is the theoretical expectation (eq. 3.2).

From the data in Fig. 3.2, agreement with eq 3.2 can be evaluated. For the measurement of pH, the theoretical slope of 59.2 mV agrees reasonably well with the 62.5 mV and 64.7 mV obtained for six and eight layers, respectively, when dividing the slope shown in Fig. 3.2 by the value of the added capacitance.

Thinner CNT layers and the smaller added capacitors gave 59.9 mV (one layer) and 56.6 mV (two layers), giving good agreement as well.

The nominal capacitance for the solid-contact layers were evaluated by electrochemical impedance spectroscopy (EIS). The impedance spectra for GC/CNT/H-ISM with/without a capacitor connected in series are shown in Fig. 3.3. The semicircle at high frequency relates to the bulk resistance (19.4 ± 1.9 kΩ) and geometric capacitance (130 ± 21 pF) of the membrane. The impedance response at low frequency shows a line at close to 45°, which is evidence for a diffusion process (Warburg impedance). This may indicate that the current response of GC/CNT/H-ISM is limited by ion transport into the membrane and/or f-SWCNTs, which might be the cause for current drifts in coulometric readout mode. Increasing the thickness of the CNT layer decreases the resistance at low frequency (see Table S3.3). The capacitance of each CNT thickness is estimated by equivalent circuit fitting (Fig. S3.2) as 96.1 µF, 123 µF, 202 µF, 257 µF, and 306 µF for one to eight layers, respectively. From Kirchhoff's law it becomes clear why added capacitances of 10 µF or less gave the smallest deviation from linearity (Figures 3.1 and 3.2). The impedance of GC/CNT/H-ISM with a 1 µF electronic capacitance placed in series was also evaluated (Fig. 3.3B). The semicircle impedance at high frequency was similar to that in Fig. 3.3A. However, the low-frequency response was observed as a vertical line, which is attributed to a dominant capacitive behavior, in contrast to Fig. 3.3A. By adding the external capacitor, the GC/CNT/H-ISM appears to act as an ideal capacitor even with different thicknesses of the f-SWCNT layer. Importantly, there is no evidence for this case that ion transport is limited by diffusion processes, resulting in much fast measurements.

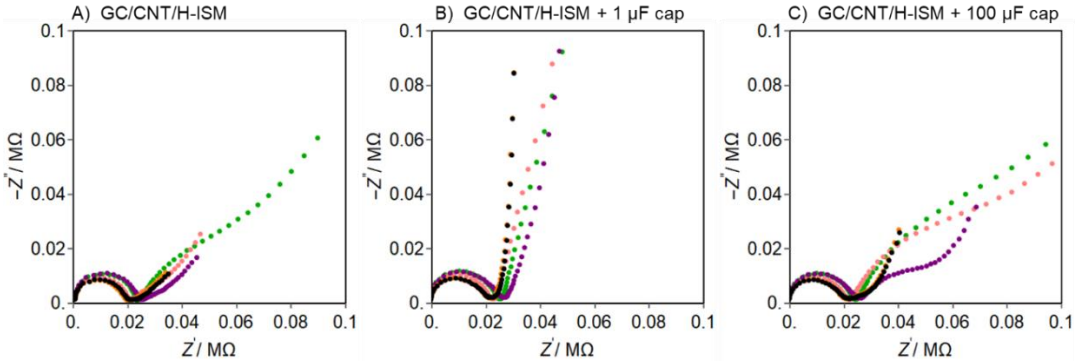

Figure 3.3. Impedance spectra for (A) GC/CNT/H-ISM without electronic capacitor, (B) GC/CNT/H-ISE + capacitor of 1 µF, and (C) GC/CNT/H-ISE + capacitor of 100 µF in 10 mM universal buffer and 10 mM NaCl (pH 7). The SC-ISEs were drop-cast with different number of f-SWCNT layers, with one layer (green), two layers (pink), four layers (purple), six layers (orange), and eight layers (black). Impedance measurements at OCP with 100 mV amplitude at a frequency range of 1 MHz to 0.1 Hz.

To compare, the addition of a higher capacitance (100 µF) is shown in Fig. 3.3C. A nonvertical line at intermediate frequency is observed for CNT thicknesses of four to eight layers (purple dotted, orange dotted, and black dotted, respectively), indicating ion transport limitation. However, a near-vertical line in the low-frequency part was observed as well, which is indicative of the behavior of the electronic capacitor. This suggests that thick CNT layers with an added large capacitor rely on both diffusion and capacitive processes. Utilizing a large capacitor for a thin layer of CNTs requires significant ion transport through the ion-selective membrane and the CNT layer to give the larger charging current, which may become rate limiting as evidenced by the nonvertical line at an angle of 45° for the thin layer f-SWCNT (Fig. 3.3C; green dotted and pink dotted). The impedance data are in agreement with the observed nonlinearity of Q vs pH data with thin layers of f-SWCNTs (see Fig. 3.1E).

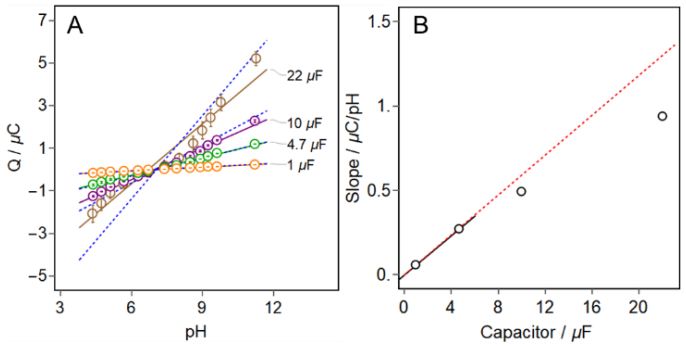

Figure 3.4. Coulometric measurement of GC/POT/H-ISE with one layer of POT. (A) Linear dependence of accumulated charge vs pH change (solid lines) by consecutive addition of NaOH or HCl to a universal buffer solution (initial pH = 7) for a range of electronic capacitances: 1 µF (orange), 4.7 µF (green), 10 µF (purple) and, 22 µF (brown). The dashed lines show theoretical behavior according to eq. 3.2 for the electronic capacitance values. (B) Relationship between experimental and theoretical slope (red dashed line) as a function of added capacitance.

POT as a solid-contact material was also explored for capacitive readout because it can be considered a model material of redox capacitance. POT can be deposited on the electrode surface by either electropolymerization or drop-casting[104]. Commercially available POT for drop-casting is mainly in its undoped, neutral form[105], which has a low conductivity (1×10^{-6} S/cm) [106]. A thin layer of POT has been shown to be sufficient to eliminate the undesired water layer.[107] Thus in this work only one layer of POT was drop-cast, using the same type of polymeric PVC membrane for pH analysis as above (see Experimental Section for electrode preparation). Figure 3.4A shows the observed calibration curves of Q vs pH obtained for GC/POT/H-ISE with a range of added capacitors (1-22 µF). The accumulated Q did not show good linearity for the entire range of capacitances, but correlation with theory (blue dashed line) was

excellent with added capacitors of 1 µF and 4.7 µF (R^2 of 0.999 and 0.996, respectively; see Table S3.4 for linear equations). Linearity becomes progressively inferior with higher capacitances (Fig. S3.3). As above, this is explained by the inability for the current to properly return to the zero baseline, resulting in an error for the integration of charge (Fig. S3.4). Figure 3.4B presents the correlation between slope of Q and capacitances in analogy to Fig. 3.2. The experimental slopes obtained for capacitors of 1 µF and 4.7 µF correlated well with the theoretical slope (red dashed line), translating to a near-Nernstian slope of 58.1 mV with eq. 3.2 (Table S3.5). This experiment demonstrates that the upper limit of added capacitance for SC-ISE modified with a thin layer of CP (POT) is 4.7 µF. If high sensitivity is required, CNT-modified electrodes seem to have superior characteristics. The capacitance value of POT SC estimated by fitting impedance spectra (Fig. S3.5; cyan dotted) with the circuit of Fig. S3.2 was 11.1 µF (Table S3.3). The impedance spectra showed dominant capacitive behavior when the capacitance of the added capacitor was smaller (1-4.7 µF) than that of POT SC, which correlates well with the results of Fig. 3.4. For larger capacitors, an ion-transport limiting process is involved, as evidenced by a Warburg line in Fig. S3.5 (purple dotted and brown dotted), in agreement with imperfect linearity shown in Fig 3.4.

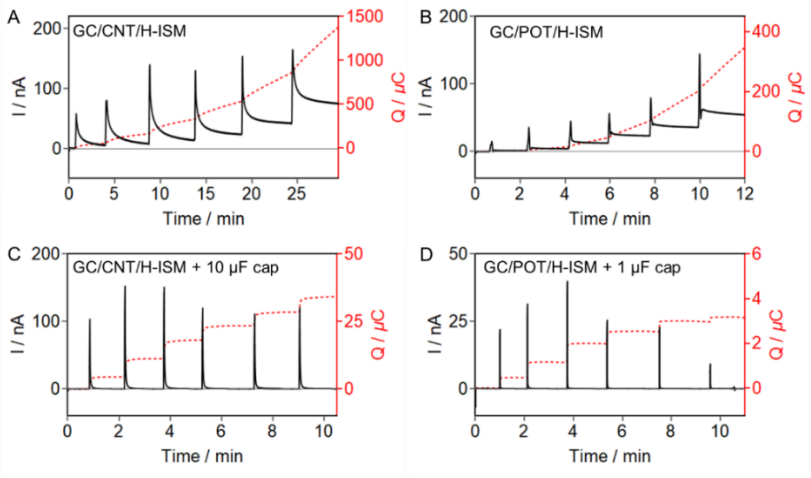

Figure 3.5. Chronoamperometric (solid black line) and chronocoulometric (dashed red line) response of (A, C) GC/CNT/H-ISE (one layer of CNT) and (B, D) GC/POT/H-ISE (one layer of POT) with (top) and without (bottom) capacitor for the measurement of pH in 10 mM universal buffer + 10 mM NaCl. A pH 7.0 buffer served as initial solution whose pH was sequentially increased to pH 7.4, 8.0, 8.6, 9.0, 9.4, and 9.8 from left to right by consecutively adding NaOH. The addition of the electronic component dramatically reduces the current transient and therefore the response time.

The time transients shown in Fig. 3.5A,B confirm that the currents for GC/CNT/H-ISE and GC/POT/H-ISE without added capacitor do not return to zero upon successive increasing of pH (black solid line), resulting in a drift for the integrated charge with time (red dashed line). The current decay did not agree

with an RC time constant, suggesting that the ion-to-electron transducer behaves as a pseudo-capacitor. Using an electronic capacitor in series with GC/CNT/H-ISE or GC/POT/H-ISE (Fig. 3.5C,D), the current transient is found to return to zero baseline, giving dramatically shorter response times. The use of an external capacitor forces the system to behave as an ideal capacitor.

The system GC/CNT/H-ISE with a capacitor of 10 µF was chosen for a more detailed evaluation because it gave the best compromise between sensitivity (amplitude of current spikes) and linearity. Based on the data shown in Fig. 3.6A for a range of different SC coatings, a coating of six layers of f-SWCNT was chosen. With this configuration, a $t_{95\%}$ of 9.6 s was observed for the response time. It agrees with the behavior of an ideal capacitor, where 3RC = 9.7 s. The current integrated between visual achievement of the equilibrium value (13.6 s) and a further 2 min only increases the signal by 1.2% (2.8 nC), which seems sufficiently attractive for practical applications.

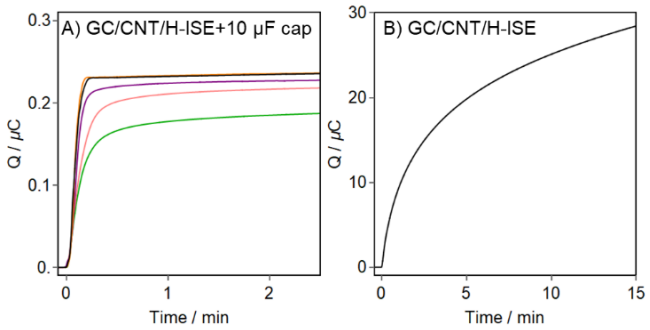

Figure 3.6. Response time of the accumulated charge Q upon changing the pH from 7.0 to 7.4 at time 0 with (A) GC/CNT/H-ISEs modified with varying f-SWCNTs layers of one (green), two (pink), four (purple), six (orange), eight (black) in series with a capacitance of 10 µF, and with (B) a GC/CNT/H-ISE modified with one layer of f-SWCNTs without added capacitor. The addition of a capacitor reduces the response time to a few seconds.

A fast response time of a few seconds is achieved with membranes of regular thickness, for which previous reports suggested tens of minutes or longer.[60, 61] To compare, the same GC/CNT/H-ISE without external capacitor was evaluated in Fig. 3.6B. For this case, the integrated charge with time did not reach an equilibrium value for 15 min. This transient behavior does not agree with an exponential RC time response (Fig. 3.5A) and it is difficult to use this signal for charge integration. While a fixed measurement time has been suggested,[64] it is rather evident that an external capacitor is preferred as it completely eliminates this undesirable characteristic.

3.4 Supporting information

Table S3.1 linear equations fitted for responses obtained with GC/CNT/H-ISEs and added electronic capacitor (in a range of 1 – 100 μF) for pH change from 4.3 to 11.3.

CNT layers	linear fit equations for added capacitive element									
	1 μF	R^2	10 μF	R^2	22 μF	R^2	47 μF	R^2	100 μF	R^2
1	Q (μC) = -0.43 + 0.0600 pH	0.9975	Q (μC) = -3.96 + 0.559 pH	0.9995	Q (μC) = -9.59 + 1.31 pH	0.9942	Q (μC) = -13.30 + 1.91 pH	0.9957	Q (μC) = -22.21 + 3.16 pH	0.9816
2	Q (μC) = -0.42 + 0.0591 pH	0.9982	Q (μC) = -4.26 + 0.600 pH	0.9992	Q (μC) = -9.52 + 1.36 pH	0.9997	Q (μC) = -18.74 + 2.67 pH	0.9991	Q (μC) = -31.93 + 4.53 pH	0.9968
4	Q (μC) = -0.42 + 0.0592 pH	0.9984	Q (μC) = -4.38 + 0.619 pH	0.9995	Q (μC) = -10.58 + 1.51 pH	0.9994	Q (μC) = -20.95 + 2.99 pH	0.9992	Q (μC) = -40.35 + 5.71 pH	0.9992
6	Q (μC) = -0.42 + 0.0592 pH	0.9990	Q (μC) = -4.42 + 0.622 pH	0.9993	Q (μC) = -11.09 + 1.58 pH	0.9997	Q (μC) = -22.48 + 3.21 pH	0.9995	Q (μC) = -44.15 + 6.25 pH	0.9995
8	Q (μC) = -0.42 + 0.0592 pH	0.9989	Q (μC) = -4.53 + 0.641 pH	0.9996	Q (μC) = -11.11 + 1.58 pH	0.9997	Q (μC) = -23.42 + 3.32 pH	0.9996	Q (μC) = -45.50 + 6.45 pH	0.9995
Theoretical calculation	Q (μC) = -0.42 + 0.0592 pH		Q (μC) = -4.16 + 0.592 pH		Q (μC) = -9.13 + 1.30 pH		Q (μC) = -19.50 + 2.78 pH		Q (μC) = -41.74 + 5.92 pH	

Table S3.2 linear equations for fitting the slope (from Table S1) vs added capacitor of GC/CNT/H-ISEs for different thicknesses of f-SWCNT.

CNT/ layers	slope vs capacitance	
	linear equation	R^2
1	S (μC pH^{-1}) = -0.14 + 59.9 C (mV pH^{-1})	0.9555
2	S (μC pH^{-1}) = 0.04 + 56.6 C (mV pH^{-1})	0.9834
4	S (μC pH^{-1}) = 0.13 + 56.8 C (mV pH^{-1})	0.9959
6	S (μC pH^{-1}) = 0.09 + 62.5 C (mV pH^{-1})	0.9972
8	S (μC pH^{-1}) = 0.08 + 64.7 C (mV pH^{-1})	0.9974
Theoretical calculation	S (μC pH^{-1}) = -0.00 + 59.2 C (mV pH^{-1})	

*S = slope obtained from Table S3.1, C = capacitance in μF.

Table S3.3 Value obtained from equivalent circuit (Fig. S3.2) fitting of impedance spectra of GC/CNT/H-ISEs and GC/POT/H-ISE without added capacitor.

SC materials	Thickness/ layers	C_g (pF)	R_m (kΩ)	Z_w ($\mu\Omega^{-1}$ s^N)	C_{SC} (μF)	$R_{overall}$ (kΩ)
f-SWCNT	1	106	19.8	14.0	96.1	89.9
	2	120	20.0	39.8	123	46.8
	4	120	22.1	46.5	202	45.3
	6	152	17.3	69.3	257	34.0
	8	154	18.0	67.1	306	34.9
POT	1	123	15.4	6.36	11.1	141.8

Table S3.4 linear equations fitted for GC/POT/H-ISEs with different capacitors in the range of 1 – 22 μF for pH change from 4.3 to 11.3.

POT/ layer	linear fit equation for different capacitors							
	1 μF	R^2	4.7 μF	R^2	10 μF	R^2	22 μF	R^2
1	Q (μC) = -0.40 + (0.0568 ± 0.0031)pH	0.9991	Q (μC) = -1.90 + (0.271 ± 0.019)pH	0.9958	Q (μC) = -3.42 + (0.492 ± 0.024)pH	0.9911	Q (μC) = -6.28 + (0.94 ± 0.26)pH	0.9521
Theoretical calculation	Q (μC) = -0.42 + 0.0592 pH		Q (μC) = -1.96 + 0.278 pH		Q (μC) = -4.18 + 0.592 pH		Q (μC) = -9.18 + 1.30 pH	

Table S3.5 linear fit equations of slope (from Table S3.4) vs added capacitor (1 - 4.7 µF) of GC/POT/H-ISEs.

POT/ layers	slope vs capacitor	
	linear equation	R^2
1	S (µC pH^{-1}) = 0.0 + 58.1 C (mV pH^{-1})	1
Theoretical calculation	S (µC pH^{-1}) = 0.0 + 59.2 C (mV pH^{-1})	

*S = slope obtained from Table S3.4, C = capacitance in µF

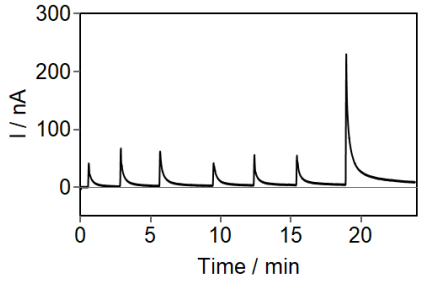

Figure S3.1. Current response over time of GC/CNT/H-ISE with 1 layer of f-SWCNTs connected in series with 100 µF of electronic capacitive element. The experiment was done by consecutive addition of NaOH in 10 mM universal buffer and 10 mM NaCl, giving a pH range of 7.0 to 11.3 from left to right.

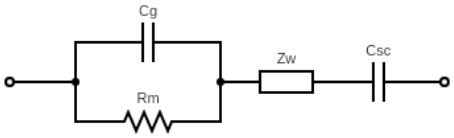

Figure S3.2. Equivalent circuit for impedance analysis of solid-contact ion-selective electrode (SC-ISE). The resistance Rm represents the resistance of the bulk membrane. The capacitor Cg is the geometric capacitance of the membrane. Zw is the Warburg impedance. The capacitor Csc is the capacitance of solid-contact material.

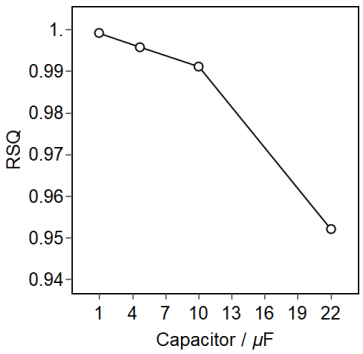

Figure S3.3. R-squared vs added capacitor in the range of 1 µF to 22 µF obtained from linear regression of charge vs pH (Table S3.4) of GC/POT/H-ISE.

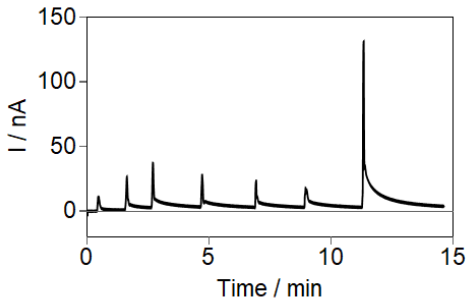

Figure S3.4. Current response with time of GC/POT/H-ISE with one layer of POT connected in series with a 22 µF electronic capacitor. The experiment was done by consecutive addition of NaOH in 10 mM universal buffer and 10 mM NaCl, resulting in a pH change from 7.0 to 11.3 (left to right).

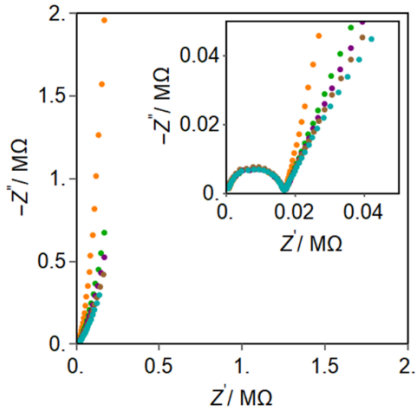

Figure S3.5. Impedance spectra of GC/POT/H-ISE with and without applying a capacitor in series: without a capacitor (cyan), with a capacitor 1 µF (orange), with a 4.7 µF (green), with a capacitor 10 µF (purple), and with a capacitor 22 µF (brown). The impedance measurements were done in 10 mM universal buffer and 10 mM NaCl at OCP with 100 mV of amplitude. A frequency range of 1 MHz to 0.1 Hz was applied. Inset is magnification at high frequency.

Impedance Analysis of ISEs containing POT as transducing layer

The EIS experiment was done with an identical GC/POT/H-ISM as illustrated in Fig. S3.5. A single layer of POT was drop cast on the electrode surface and subsequently covered with a thick H-ISM membrane in analogy to the other electrode. The impedance spectra were recorded with the same procedure as GC/CNT/H-ISM. The high-frequency semi-circle corresponds to the bulk resistance (15.4 kΩ) and geometric capacitance (123 pF) of the membrane as shown in the inset of Fig. S3.5. Warburg impedance of GC/POT/H-ISM without capacitor (cyan dotted) was noted at low frequency. It is recognized by straight line at 45° angle to the axis, which is usually due to the limitation of ionic transport by diffusion to the interface. The capacitance value of POT SC, estimated by fitting the impedance spectra

with the same circuit (Fig. S3.2), was 11.1 μF. The current recorded for coulometric measurement showed baseline drifting (Fig. 3.5B), which may be explained that POT layer may allow for a current to pass. It is reasonable that the system of GC/POT/H-ISM did not exhibit ideal capacitive behavior. In the presence of external electronic capacitor of 1 μF and 4.7 μF (orange dotted and green dotted), the impedance did not show evidence of a diffusion process but instead of a capacitive process. This is compatible with the coulometric results shown in Fig. 3.5D where pure capacitive behavior was observed. However, with large applied capacitances of 10 μF or 22 μF (purple dotted and brown dotted), the low-frequency impedance showed a non-vertical line nearly an angle of 45° and also close to original impedance of pure POT SC-ISE (cyan dotted). This implies that the system was no longer dominated by the added capacitor. This is analogous to the explanation for GC/CNT/H-ISM with large added capacitances: this case requires a comparatively large charge accumulation which is limited by the ion transport into POT layer for oxidation/reduction process. The capacity of POT at the interface may not be sufficient for to absorb the large ion to electron transduction charge required by the larger capacitor. The results for the capacitors 10 μF and 22 μF (Fig. 3.4A-B) agree with the fact that the observed charge was lower than theoretical expectations.

Chapter 4: Electronic control of constant potential capacitive readout of ion-selective electrodes for high precision sensing

4.1 Development of automatic capacitive readout system

Among diagnostic tools for the detection of electrolytes in clinical samples, the most commonly used technique is potentiometry using ion-selective electrodes (ISE). The output potential is proportional to the logarithmic ion activity in solution, expressed by the Nernst Equation [108]. Owing to the logarithmic relationship between potential and ion activity, the precision of potentiometric sensors may be negatively affected by potential drifts that make it difficult to identify signals arising from a sample composition change [78]. Biofouling of polymeric membrane-based electrochemical sensors caused by the adsorption of cells and biomolecules is a further known limitation for application in complex biological samples such as blood, serum or urine. Such biofouling may affect the sensor performance by perturbing the diffusion of analyte to the sensing interface, and as well altering ion concentration at the membrane surface owing to the bioactive film [109, 110].

Our group has recently described a method for improving the precision and sensitivity of potentiometric probes based on the principle of constant potential coulometry for a so-called capacitive readout [25], which is a further development of a concept originally introduced by Bobacka's group [57, 58, 60]. Here, the sensing electrode consists of a liquid-contact ISE in series with an electronic capacitor. The open-circuit potential (OCP) for a reference solution is measured and subsequently enforced onto the electrochemical cell, keeping it constant while changing the sample composition. Any change in analyte activity now results in a potential change over the capacitive element, which results in an identifiable current transient. The charge obtained by the integration of the current signal is proportional to the logarithmic ion activity and scales with the Nernstian slope as well as the value of the capacitive element [63].

The current transient is easier to identify and isolate from the background than a slowly drifting potential signal, as also reported by Han et al. using solid-contact ISEs [60]. This approach may give much improved sensitivity. By measuring pH using electronic components in stabilized seawater as an early example, a precision on the order of a few tens of µpH units was achieved [25]. The approach is attractive because the value of the external capacitor may be chosen to match the desired application. The use of electronic components instead of a capacitive layer of the solid-contact transducer material as reported earlier [58, 64] also drastically reduced the drifting currents caused by the non-ideality of those transducers [25, 111].

Despite these advantages, the protocol reported earlier [25] involves complex fluidic handling. Each measurement requires a sequential alternation of sample and reference solution to establish the new current baseline for the charging/discharging cycles of the electronic capacitor. Particularly, the chemical discharging step (with the help of reference solution) may result in a residual charge accumulation across the electronic capacitor over repetitive measurements, thereby leading to undesired memory effects. Such memory effects restrict one of taking complete advantage of the coulometric technique in terms of achieving lower detection limits with a superior precision and resolution. Moreover, care must be taken to achieve a sufficiently sharp transition between reference solution and sample to generate a single peak-based rapid capacitor charging event that precisely reflects the potential change. In our previous work, the partial mixing of the reference and sample solution was avoided by using an air gap, in analogy to sequential flow analysis, but this may not be practical in routine use.

In this work, the capacitive readout method described above is simplified by an automated electronic switching protocol. Instead of alternating to a reference solution between every measurement to discharge the capacitor and establish a zero-current baseline, the open-circuit potential (OCP) for the reference solution is here separately measured and stored. The discharging of the capacitor is achieved by short circuiting the element, again executed by electronic control. The stored reference OCP is subsequently applied to each sample solution, resulting in a sharp current transient. Since the capacitor is discharged electronically, the repetitive introduction of the reference solution is no longer required. As a result, the repetitive measurement of a given sample solution is conveniently possible. Because the cell is at open circuit while introducing the sample solution, charge accumulation induced memory effects at the capacitor are further suppressed and as are current baseline drifts. Furthermore, the adopted approach provides the feasibility for sample measurements at stopped flow, which is in agreement with electrochemical clinical analyzers, and gives reduced electrical noise.

As an example of clinical relevance, the concept described above is explored for the detection of sodium in serum samples. Sodium plays a key role in our body and represent the most frequent ion in extracellular fluids. It accounts for approximately 90% of the total cationic species present with a relative narrow concentration range between 135 and 145 mmol/L [112, 113]. Sodium participates in maintaining normal blood pressure and also supports the activity of the nervous, muscular, and cardiovascular systems [114, 115] . Sodium is therefore routinely determined in the clinical laboratory. Among disorders caused by fluctuation in serum sodium concentration, hyponatremia (sodium in blood < 135 mmol/L) [116] and hypernatremia (sodium in blood > 145 mmol/L) [117] are the most common. Precise, sensitive, and reliable sodium measurements are required because incorrect treatment may lead to fatalities [118-120]. Current guidelines recommend treatment

options where sodium levels should not rise faster than 0.5-0.7 mM/h [121, 122] or approximately 10 mM during 24 h [122, 123]. Routine measurements of sodium in blood serum in the clinical laboratory is mainly by ion-selective electrodes, among other possible techniques [124-132]. The reported measurement precision is about 2-5 mmol/L of sodium [124, 125, 133, 134], which this work aims to improve upon.

4.2 Experimental and preparation for capacitive readout method

Materials and Reagents Sodium ionophore X, poly (vinyl chloride) (PVC, high molecular weight), sodium tetrakis[3,5-bis-(trifluoromethyl) phenyl]borate (NaTFPB), 2-nitrophenyloctyl ether (o-NPOE), tetradodecylammonium tetrakis(4-chlorophenyl) borate (ETH 500), tetrahydrofuran (THF), sodium chloride (NaCl, ≥99.5%), and pooled human serum (human male AB plasma, USA origin, sterile-filtered) were purchased from Sigma-Aldrich. Verified human serum contains a sodium concentration of 141 mmol / L. All aqueous solutions were prepared in deionized water (>18.2 MΩ-cm). Single-in-line package (SIP) reed relays (9007 series) were purchased from Coto Technology, inc. The data acquisition device (NI USB-6009) was obtained from National Instruments Corporation. Tantalum through-hole capacitors of 10 µF (KEMET) was used for all experiments. The electronic components were connected on a breadboard.

Sample preparation The standard solutions of NaCl without background electrolyte were prepared by dissolving the respective salt in Milli-Q water. The relevant concentration range is between 135 mM and 145 mM, where 135 mM of NaCl solution was used as the reference solution for the open-circuit potential (OCP) measurement in constant-potential coulometry. The incremental NaCl concentration increase was 2.0 mM. Aliquots of the pooled serum sample were spiked with NaCl to construct a calibration curve in 2.0 mM increments. Unspiked serum sample (141 mM NaCl) was used as reference solution for OCP measurement.

Electrode preparation A PVC based ion-selective membrane was used as indicator electrode for sodium measurements, which was composed of 15 mmol kg−1 sodium ionophore X, 5 mmol kg^{-1} NaTFPB ion-exchanger, 90 mmol kg^{-1} ETH 500, 117 mg o-NPOE, and 58.5 mg PVC (total mass of 200 mg). The cocktail was dissolved in 2.0 mL of THF and poured into a glass ring (22 mm ID) affixed onto a glass slide. The solution was allowed to evaporate overnight. This parent membrane was cut with a hole-puncher into small pieces of 8 mm diameter and mounted into Ostec electrode bodies. The electrodes were conditioned overnight in a 140 mM NaCl inner filling solution. A double junction Ag/AgCl / 3 M KCl / 3 M KCl electrode (Metrohm, Switzerland) and a platinum rod (Metrohm, Switzerland) were used as reference electrode and counter electrode, respectively.

Electronic circuit A fully automated system configured for performing coulometric measurements is illustrated in Fig. S4.1 (see Supporting Information). The electronic circuit to implement the automated system is illustrated in Scheme 4.2. A commercially available 10 µF capacitor (C) is connected in series with the sensing electrode. Here, two SIP reed relays (S1 and S2) operate as electronical switches and are controlled through the data acquisition device and a custom-developed LabVIEW program. While one of the relays (S1) makes or breaks the contact between the sensing electrode and potentiostat through the capacitor C, the other relay (S2) assists in short-circuiting the capacitor in order to discharge it. For coulometric measurements, the potential of the sensing electrode (vs reference electrode) is kept constant by the potentiostat.

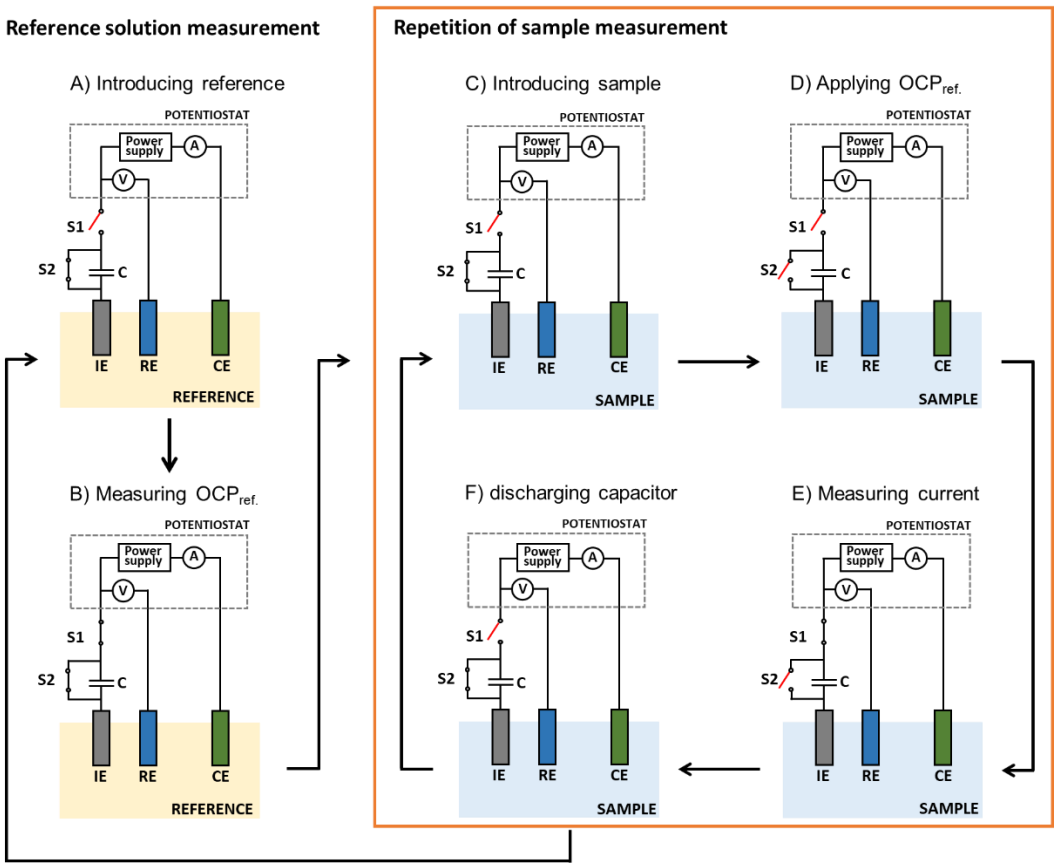

Scheme 4.1. Schematic diagram of constant potential capacitive readout by integrating the electrochemical detection cell with an electronic system. A-F describe the operational steps where S1 and S2 are reed relay switches 1 and 2. IE is the indicator electrode, RE the reference electrode and CE the counter electrode. The operation consists of 2 main parts, the measurement of the reference solution (A and B) and repetitive sample measurements (C-F).

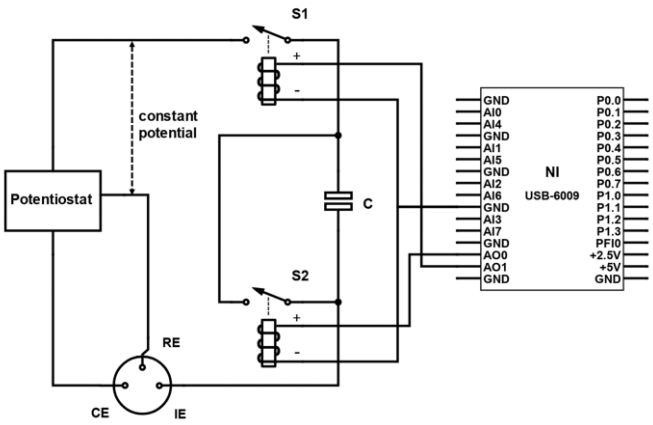

Scheme 4.2. Electronic diagram used for automatically controlling the capacitive readout system. NI USB-6009: National Instrument USB-6009; C: capacitor. For other symbols see Scheme 4.1.

Capacitive measurements of sodium activity are performed following the steps shown in Scheme 4.1; Table 4.1 shows the summary of all the operations involved in these steps. A) While the reference solution is introduced to the indicator electrode (IE), the electrical connection between the sensing electrode and potentiostat is broken to avoid current flow. The capacitor is also short-circuited to keep it discharged. B) On stopping the flow, all the relay switch connections are made for measuring OCP of the reference solution, whose value is stored by the software of the potentiostat. C) The IE is subsequently disconnected from the potentiostat while the capacitor is kept discharged for replacing the sample solution in the detection cell. Then relay switch across capacitor is opened and a reference OCP is applied to the stagnant sample solution in step D. E) The connection between IE and potentiostat is now established to allow current through the capacitor, which is measured over time by chronoamperometry. F) After each measurement, the capacitor is discharged by short-circuiting it using the relay switch. Before starting the next measurement, the same sample solution is replaced in the detection cell and the operations are repeated from step C to F (n = 5 for standard solution and n = 3 for serum sample). The reference solution can be re-measured by returning to step A whenever desired.

Chronoamperometric Measurements The reference solution was delivered by a peristaltic pump (ISMATEC, Switzerland) with tygon tubing (ISMATEC, 1.42 mm ID) at a flow rate of 1.56 mL/min for 60 s to the detection cell. When the solution reaches the sensing electrode, flow rate is reduced to 0.08 mL/min until OCP become stable (160 s). The flow was stopped and the OCP of the reference solution between the indicator electrode and the reference electrode was determined and subsequently enforced unto the cell by the potentiostat during the chronoamperometric measurements. A switching valve (VICI, USA)

was used to alternate between solutions. The sample solution was introduced into the detection cell with the same flow rates used earlier with reference solution. The flow was again stopped before applying reference potential to the sample solution. The measurements were each repeated 5 times for artificial solutions and 3 times for serum sample solutions. However, for each repetition, the sample solution in detection cell was replaced by flowing a fresh sample solution of the same concentration for a duration of 10 s at the rate of 0.08 mL/min. Constant-potential coulometry was performed using Autolab (Metrohm, Switzerland) and the obtained current was recorded with NOVA software. The current signal was subsequently integrated over measured time using the same software to obtain the charge.

Table 4.1 Steps and operations of sensing measurement.

Steps	Switch 1 (S1)	Switch 2 (S2)	Pump	Flow rate (mL min^{-1})	Operation
A	open	close	on	1.56 (60 s) 0.08 (160 s)	Flow reference solution to the detection cell
B	close	close	off	-	Measure OCP of reference solution
C	open	close	on	1.56 (60 s) 0.08 (160 s)	Introduce sample solution to the detection cell
D	open	open	off	-	Apply OCP of reference
E	close	open	off	-	Measure transient current vs time
F	open	close	off	-	Discharge the capacitor

4.3 Results and discussion

For the capacitive readout principle using an electronic capacitor with polymeric membrane ion-selective electrode reported recently by our group [25], the indicator electrode was integrated into a flow-jet cell to expose the reference and sample solution to a continuous solution flow. The concentration changes of the analyte in the sample relative to that in the reference solution resulted in a potential change that was imposed onto the capacitive element. To obtain a quantifiable current transient peak, the longitudinal dispersion between the two solutions had to be minimized. In the absence of segmented flow, allowing for a direct contact of the two solutions, the partial mixing resulted in a smearing of the current-time profile (see Fig. S4.2A in Supplementary Information). The current excursion was sluggish and had difficulty returning to

baseline, making it unreliable to integrate the charge (Figure S4.2B). In previous work, this challenge was overcome by a flow design where the aqueous solutions were separated by an air gap that was removed just prior to the detection cell by means of a debubbling device [25]. The debubbler characteristics involve a limiting air volume (11 µL) and a specific range of flow rates (0.5 mL/min to 2.0 mL/min), which may be undesired. Moreover, this arrangement added significant complexity and required the measurement of continuously flowing samples.

Here, an improved capacitive readout system is described that gives a well-defined current signal without requiring segmented flow, just by using electronic switching components. The electronic circuit used to establish a robust capacitive readout is shown in Scheme 4.2. It consists of two switching modules. One of them opens and closes the circuit between sensing electrode and potentiostat to avoid undesired current flow through the cell. Another switch is placed across the electronic capacitor itself. If the connection is made, the capacitor is short circuited and allowed to discharge. This alleviates the need to discharge the electronic capacitor by alternating to a reference solution. Repeated measurement pulses can now be imposed onto the same sample by using the potential value for the reference solution stored in memory.

The operational steps for a constant potential coulometric measurement are summarized as follows (see Scheme 4.1 and Experimental Section). The initial potential of indicator electrode in contact with the reference solution is first observed and stored while short circuiting the capacitor (Scheme 4.1B). The cell is then maintained at open circuit while introducing the sample solution (Scheme 4.1C). In the next step (1D), the switch across the capacitor is opened to place the element in series with the indicator electrode. The potential stored in the first step is now applied to the cell, the current transient is recorded and subsequently integrated to give the analytical signal. The last step involves again the short circuiting of the capacitor to discharge it and placing the cell in open circuit so that the sample can be replaced with another one (return to previous step) or with the reference solution (first step of the cycle), as desired.

The proposed protocol was explored using sodium ion-selective electrodes containing an aqueous inner solution. To evaluate the system, a range of potential increments from the open circuit potential were applied by a potentiostat to a solution containing 135 mM NaCl. The chosen range of 2 mV approximately reflects the potentiometric measuring range for the detection of sodium ions in physiological samples. The potential increments result in appropriate current transients (Fig. S4.3, top) and corresponding integrated charge values shown in Fig. S4.3, bottom. Figure 4.1 shows the observed slope of 10.3 ± 0.37 nC mV^{-1}, which agrees with the expected value of 10.0 nC mV^{-1} for the chosen capacitive element (10 µF). Figure S4.3 gives repeated charge-time integrations obtained for a fixed applied potential increment of 1.2 mV.

The measurement uncertainty is calculated as an average standard deviation of 0.368 nC (n = 11), translating into a precision of 0.035 mV or 0.14 mM (ca. 0.14% precision of concentration uncertainty) in direct potentiometry.

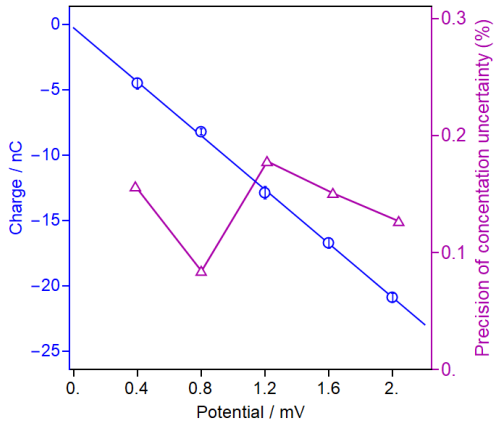

Figure 4.1. Capacitive readout upon applying incremental potential values of 0.4-2.0 mV to a cell containing a reference solution of 135 mM NaCl. Left axis: Correlation of integrated charge with applied potential (blue circles) with the linear regression (blue solid line) of Q (nC) = 0.23 – 10.3×E (mV), R^2 = 0.999. Right axis: Purple triangles give the precision of concentration uncertainty calculated from the error bars of the charge values shown

The capacitive readout using the electronic discharging system introduced here was subsequently applied to the measurement of NaCl solutions in the concentration range of 135 mM-145 mM, which reflects the normal sodium range in blood serum, at concentration increments of 2.0 mM. An initial experiment was carried out with variable NaCl sample concentrations while using 135 mM NaCl as a reference solution. The sample solution was transferred to the detection cell by flow, which was then stopped for measurement. Figure 4.2A and S4.4 illustrate the observed current spikes and integrated charge over time of NaCl solutions at varying concentrations (n = 5 for each concentration). Since the reference potential is a stored value and the capacitor is discharged after each reading by the electronic circuit, consecutive readings on the same sample and on different sample solutions can be measured without repeatedly returning to the reference solution. This improves sample frequency relative to previous work [25]: shown here are 5 readings each for 5 samples during a period of 33 min.

Figure 4.2B shows an overlay of magnified current spikes recorded at different levels of sodium concentration. A higher sodium concentration in solution causes a larger potential difference between sample and reference potential, resulting in a larger current spike (ohm's law) and integrated charge.

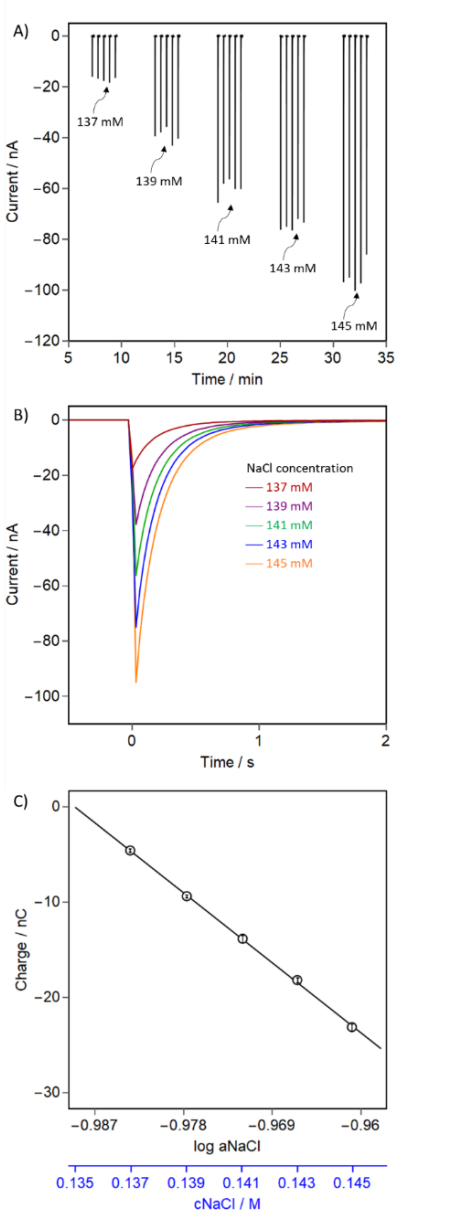

Figure 4.2. Constant-potential coulometric measurement of NaCl standard solutions of different concentrations at 2 mM increments, using 135 mM NaCl as reference solution. The experiment was performed with a Na^+-ISE with a 10 µF capacitor placed in series, using the automatic measurement system with electronic components. (A) Repeatability of the 5 consecutive current-time traces for each NaCl sample, ranging in concentrations from 137 mM to 145 mM. (B) Overlay of the current-time transients shown in (A). (C) Linear dependence of charge vs log a_{NaCl} (upper black x-axis), corresponding to the sodium concentrations on the blue x-axis.

The corresponding integrated charge-time information is shown in Fig. S4.4. A linear correlation of charge vs logarithmic sodium activity with the regression equation of Q (C) = $-80.5\times10^{-8} - 81.4\times10^{-8}\times\log a_{NaCl}$ is given in Fig. 4.2C. The value is super-Nernstian (theoretical: 59.2×10^{-8} C/decade)[63]. This is explained by a

flow-induced potential drift, which may have a significant impact on the recorded electrode slope because of the very narrow potential window of about 2 mV. However, the reproducibility of measured data is not affected as the influence of the drift remained consistent for all sample measurements. An apparently super-Nernstian slope of 75.03 mV was also obtained when measuring by direct potentiometric as shown in Fig. S4.5C, suggesting that this is not connected to the novel readout protocol. The narrow measuring range allows one also to represent the calibration curve linearly (see blue x-axis on Fig. 4.2C), corresponding to the fitting equation of $Q\ (C) = 0.31\times10^{-6} - 2.32\times10^{-6}\times c_{NaCl}$. The precision obtained from capacitive readout is found as 0.11 mM NaCl (average standard deviation, n = 5), which is similar to that observed by potential control only (see above). Direct potentiometry was carried out as a comparative method for the same range of NaCl by flow analysis as given in Fig. S4.5A. The calibration of electromotive force (EMF) vs logarithmic of NaCl activity (and NaCl concentration) are shown in Figure S4.5B and C. The precision from potentiometry is found to be 0.52 mM (n = 5), which is five times worse than the measurement using the capacitive readout method.

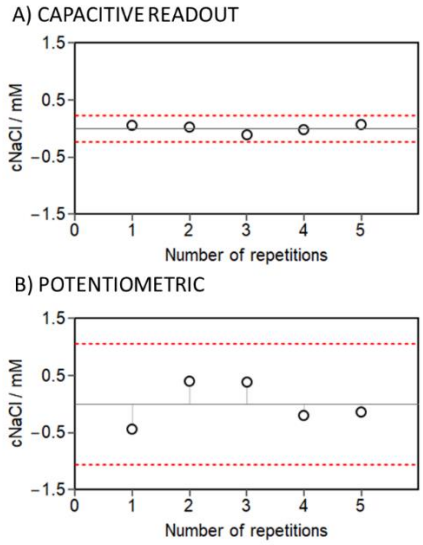

Figure 4.3. Residual plots of (A) capacitive readout compared with (B) direct potentiometry at 141 mM NaCl. Circles are the variations of the observed sodium concentrations from the mean value (black solid line). Red dashed lines are 2SD for each technique.

Figures 4.3 and S4.6 give the residuals for the capacitive and potentiometric readouts given as the deviations of the measured concentration from the mean value. The red dashed line is double the average standard deviation (2SD) of each technique. The residual plot for the capacitive readout shows that the errors

distribute symmetrically and close to the zero line (Fig. 4.3A). It indicates that the proposed method gives improved precision that allows one to diminish the uncertainty of sodium activity measurements.

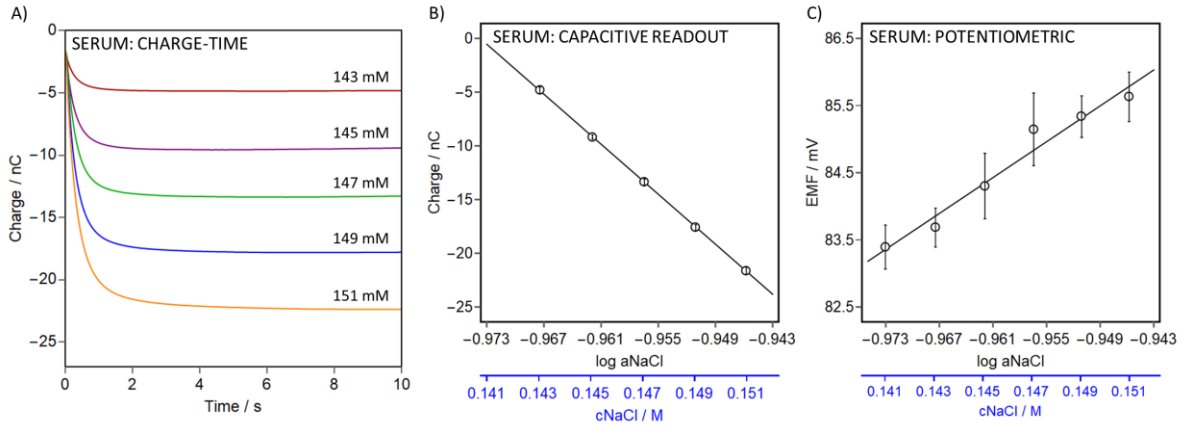

Figure 4.4. Sodium measurements in pooled serum obtained by capacitive readout and direct potentiometry. (A) Overlay of integrated charge vs time traces measured by capacitive readout using Na^+-ISE and 10 µF capacitor for 2 mM NaCl concentration increments, as indicated, where unmodified serum served as the reference solution. (B) linear dependence of charge vs logarithmic sodium activity with R^2 = 1.000. (C) Linear regression of EMF vs logarithmic sodium activity recorded by direct potentiometry for the same concentration range with R^2 = 0.964. The lower x-axis (blue) shows the corresponding sodium concentrations for information.

The polymeric-membrane based sodium-selective electrode was subsequently used to measure sodium concentration in pooled human serum by the proposed method. Calibration curves were obtained by standard addition of NaCl into serum sample at increments of 2 mM while the observed potential for unspiked serum was used as the reference value. Figure 4.4A shows an overlay of overall integrated charge recorded at different levels of sodium in the serum sample. The currents integrated for the visual period of the transient (2 s) and a further 10 s are found to be different by just 1.8% (0.3 nC). This response time is attractive for practical applications. A linear regression of charge as a function of logarithmic sodium activity with Q (C) = $-75.5\times10^{-8} - 77.6\times10^{-8}\times\log a_{NaCl}$ was obtained. The charge vs concentration relationship is given by the second x-axis, using a fitting equation of Q (C) = $0.30\times10^{-6} - 2.10\times10^{-6}\times c_{NaCl}$, giving a precision of 0.13 mM NaCl (standard deviation; n = 3, see Fig. 4.4B). The relationship between current-time and charge-time are shown in Fig. S4.7. Direct potentiometry was used as a comparative method for serum sodium as well. It was found that the measured potential tended to deviate from linearity (EMF (mV) =170 + 89.0×log a_{NaCl}) as illustrated in Fig. 4.4C. As the NaCl concentration range of 141 mM-151 mM in serum provides a potential difference of about 2 mV, the observed potential was found to fluctuate and the changes were difficult to distinguish as seen in Figure S4.8. For this reason, the standard

deviations were found to be larger than for the capacitive readout method (Fig. 4.4B and C). The precision for direct potentiometry (1.60 mM) was an order of magnitude inferior compared to the proposed method. The results indicate that the capacitive readout with the incorporated automated switching protocol through electronic components can be used to measure the concentration of sodium in the relevant concentration range of clinical samples.

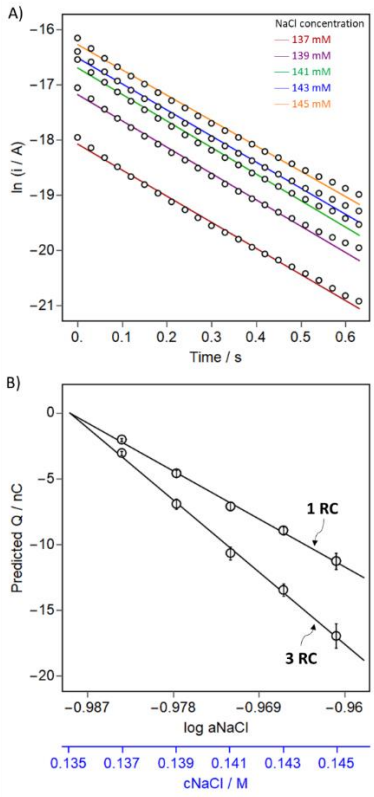

Figure 4.5. Predicted charge from fitting to the charging current equation. (A) Plot between the natural logarithm of the current vs time for a standard solution concentration range from 137 mM to 145 mM, where 135 mM NaCl was used as reference solution (data shown in Figure 4.2A). Solid lines are linear fits for ln I vs time. (B) Linear correlation of predicted charge vs. log a_{NaCl} with regressions of Q (C) = $-41.9\times10^{-8} - 42.4\times10^{-8}\times\log a_{NaCl}$ and Q (C) = $-63.0\times10^{-8} - 63.8\times10^{-8}\times\log a_{NaCl}$ for 1 RC and 3 RC interval times, respectively. Lower blue x-axis shows the corresponding sodium concentrations.

The experiments described above involve the integration of each current transient until a near-zero baseline is reached, which takes on the order of 10 s (Fig. 4.2). This time could be considerably shortened if the current transient is reliably described by a circuit containing a capacitor and resistance in series ($I = I_0\, e^{-t/RC}$). In that case, a simple extrapolation to longer times would allow one to detect the charge in a much

shorter time. To evaluate this, the logarithmic current over time is shown in Fig. 4.5A as solid line. The data suggest that the logarithmic current changes linearly with time. By correlating the slope of this fitted line to a single time constant (RC), the charge was determined within a plotting range of 1 RC (0.22 s), 3 RC (0.66 s) where the capacitor accumulates ~ 63%, 95% of the final charge as follows:

$$Q(t) = C\frac{s}{z}log\left[\frac{a_{initial}}{a_{final}}\right]\left(1 - e^{-\frac{t}{RC}}\right) \quad (1)$$

$$Q(t) = C(RI_0)\left(1 - e^{-\frac{t}{RC}}\right) \quad (2)$$

$$Q(t) = slope\ I_0\ \left(1 - e^{-\frac{t}{RC}}\right) \quad (3)$$

where the slope and I_0 was obtained from Fig. 4.5A, s is the Nernst slope and z is the charge of the analyte ion. The linearization of the predicted charge vs logarithmic sodium activity resulted in near-Nernstian slopes of 67.08 mV and 67.14 mV for RC and 3 RC time intervals, respectively, and a precision of 0.24 mM (see Fig. 4.5B). The charge predicted at infinite time interval was found merely 5% greater than that of 3 RC. Moreover, the slope and the precision of infinite time interval is about the same as RC and 3RC intervals. While this approach appears to be promising, it goes at the expense of precision as the value is worse than that obtained from the full integration method (0.11 mM NaCl, Fig. 4.2C), which includes additional charge increments at longer times. Still, the method may be attractive for rapid measurements where waiting for an equilibrium state is not desired. In that case the acquisition time for each signal can be shortened from 10 s to just 0.22 s. Note, however, that data acquisition time is not equal to sensor response time and the two should not be confounded. In particular, the flow system used here for switching sample solutions limits the chronoamperometric sample throughput (see 2.5 Chronoamperometric Measurements) and may need to be optimized to further shorten turnover time.

4.4 Supporting information

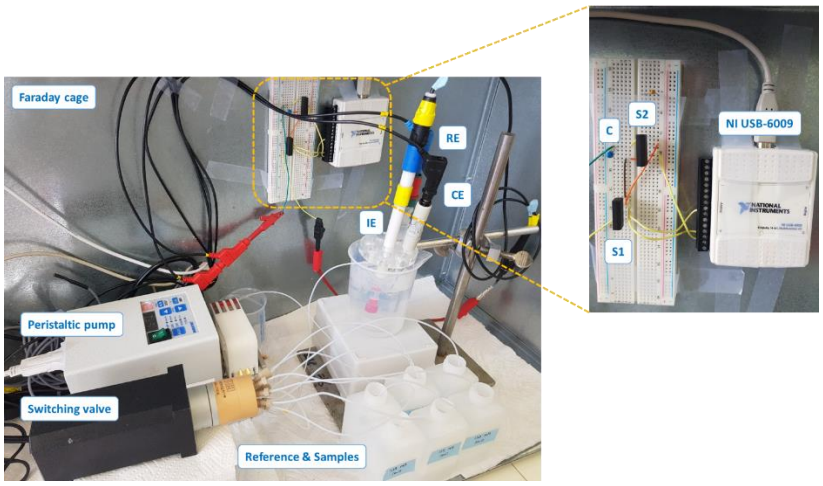

Figure S4.1. Photograph of electronic control for constant-potential capacitive readout. All devices were placed in a Faraday cage, including the peristaltic pump, switching valve, NI USB-6009: National Instrument USB-6009; C: capacitor; S1: reed relay switch 1; S2: reed relay switch 2; IE: indicator electrode; RE: reference electrode; CE: counter electrode. The sample and reference solutions were transferred by an automated flow system.

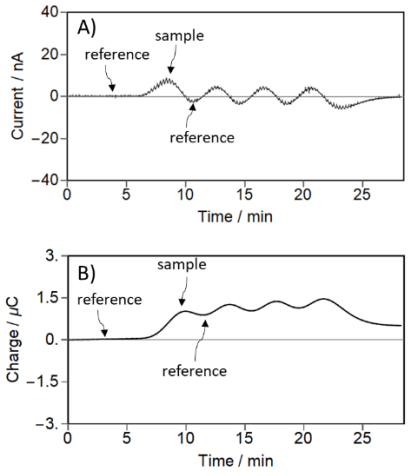

Figure S4.2. Capacitive readout of pH change using a continuous flow without an air-gap dividing the two solutions. The experiment was performed by placing a hydrogen ion-selective electrode in series with a 100 µF capacitor. Tris-buffer in 0.1 M NaCl background solution was used for monitoring pH change between reference solution (pH 7.0) and sample solution (pH 8.0). A) chronoamperometric record of current over time. B) Integrated charge accumulation over time.

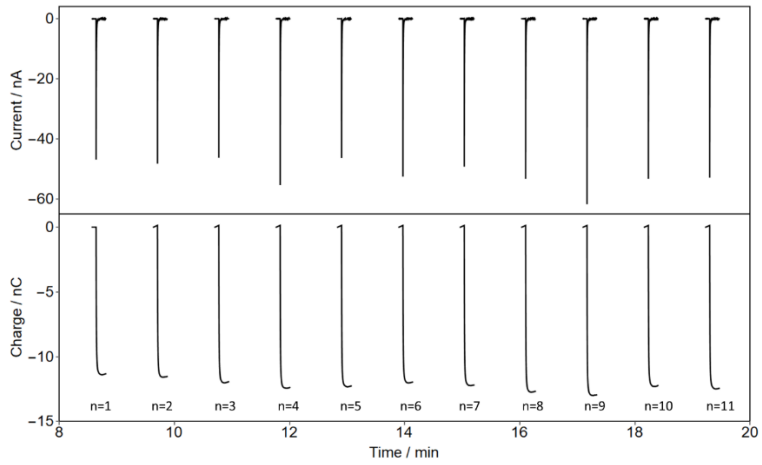

Figure S4.3. Reproducibly study carried out by Na^+-selective electrode connected in series with a 10 µF capacitor in a 135 mM NaCl reference solution. Constant-potential coulometry was performed by applying a fixed potential to the reference solution for 11 repetitions. Top) A chronoamperometric record of current-time obtained by applying constant potential of 1.2 mV to the cell. Bottom) Charge integration over time for the data shown in the top graph.

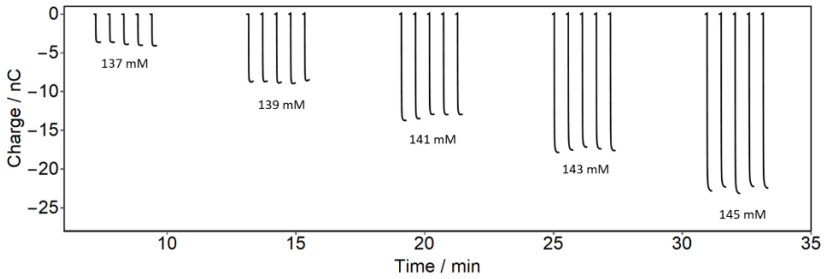

Figure S4.4. Integrated charge–time information obtained by the constant-potential coulometric measurement of NaCl standard solution at different concentrations using a 2 mM increment, where 135 mM NaCl was used as reference solution (Figure 4.2A). The experiment was performed by Na^+-ISE with a 10 µF capacitor placed in series. The automatic measurement system was controlled by electronic components.

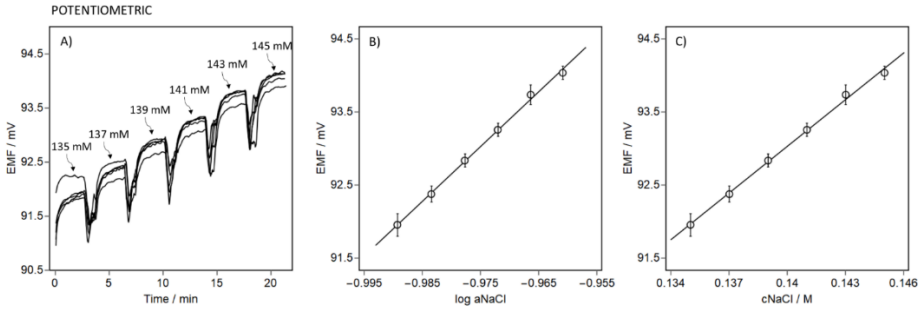

Figure S4.5. A) Direct potentiometric readout of EMF vs time of varying concentrations of NaCl (135 mM to 145 mM) with an increment of 2.0 mM using a Na^+-ISE (n = 5). The measurement was performed by the same automatic

flow system. B) Linear correlation of EMF vs log a_{NaCl} with EMF (mV) = 166.2 + 75.03×log a_{NaCl} and R^2 = 0.9984. C) Plot of EMF vs concentration of NaCl with fitting equation of EMF (mV) = 63.2 + 212.97×c_{NaCl} and R^2 = 0.998.

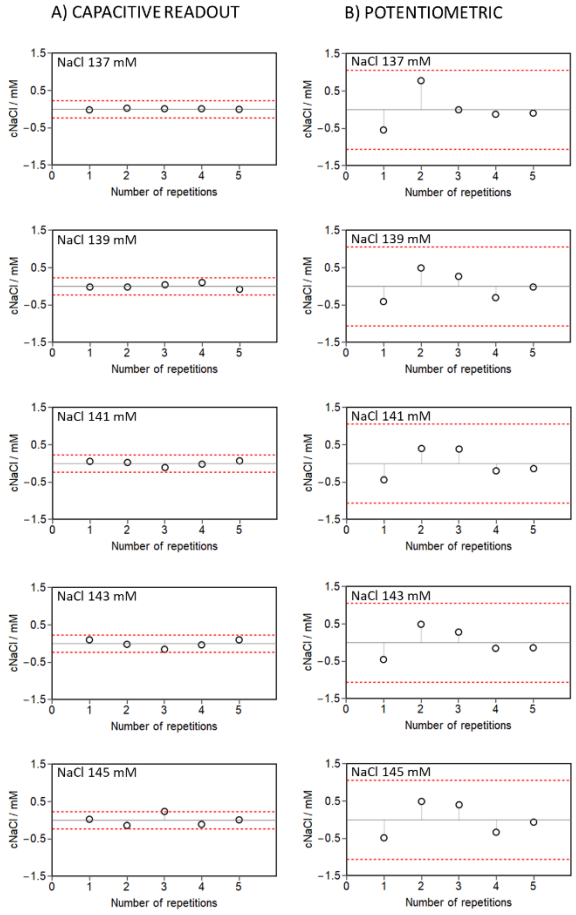

Figure S4.6. Residual plot of A) capacitive readout and B) potentiometric readout used for sodium measurements ranging from 137 mM to 145 mM. Shown are the deviation of the observed concentrations from the mean value (black solid line). Red dashed lines indicate twice the standard deviation (2SD) for each technique.

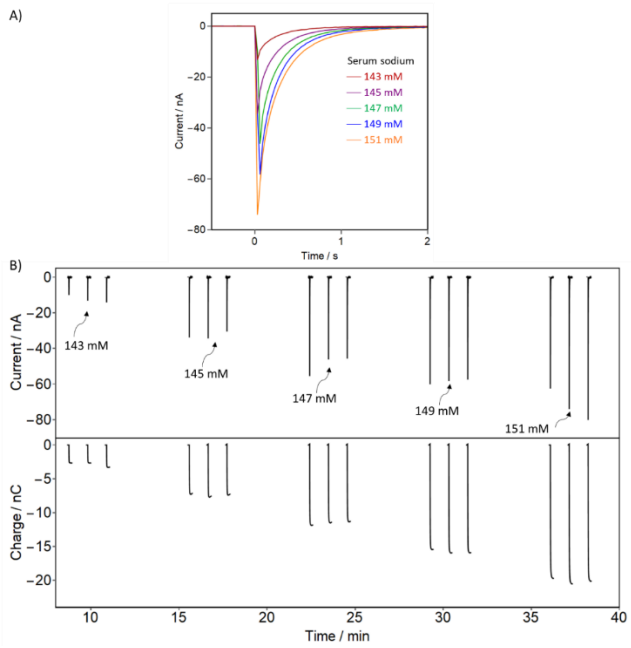

Figure S4.7. Results of capacitive readout of serum sodium in the range of of 143 to 151 mM NaCl at 2.0 mM increments where unspiked serum (141 mM) served as the reference solution. Na^+-ISE controlled by electronic circuit and connected in series with a 10 µF capacitor was used to monitor the concentration changes. A) Overlay of current-time traces at different concentration of serum sodium. B, top) Complete chronoamperometric raw data with n = 3. B; bottom) Integrated total charge over time (10 s) for the data shown in B, top.

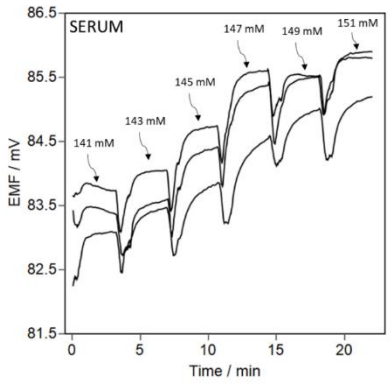

Figure S4.8. Direct potentiometry of serum sodium with a sodium-selective membrane electrode. Measured EMF over time obtained from introducing different concentrations of serum sodium (141 mM – 151 mM) to the indicator electrode by the same automatic flow system used throughout the study.

Chapter 5: Development of portable capacitive readout device and computer simulation of current-polarized ion-selective membranes

5.1 Understanding membrane polarization for development of portable constant-potential coulometric device

Conventional ion-selective electrodes (ISEs) are mainly used in zero-current potentiometry for a wide range of applications, particularly environmental and clinical analysis. The sensing membrane of ISEs is usually made of poly(vinyl chloride) (PVC) in which dioctyl sebacate (DOS) or 2-nitrophenyl octylether (o-NPOE) (1:2 wt ratio) serves as the plasticizer[18]. An ion exchanger (lipophilic anions or lipophilic cations) and a selective complexing agent (ionophore) are added into the membrane to allow ion-exchanger properties of the membrane such that the concentration of interest ions in membrane phase must remain constant during an experiment[23]. Prior to use, such membranes are conditioned in primary ion for 10-20 h to achieve a steady state[135]. In traditional ISEs, an insoluble ion-selective membrane (ISM) separates the inner filling solution and aqueous sample. Its potential difference is measured against a reference electrode. Since the ion-transfer reactions at the membrane|sample interface are usually very fast, the thermodynamic control of phase-boundary potential is sufficient to described electromotive behavior of the sample composition. Thus, the majority of theoretical models of ISEs have focused on steady-state approaches.[136-138]. However, a number of attractive methods in order to enhance ISEs performance have been reported either under controlled current or potential conditions[139]. Lindner and researchers introduced a method to achieve lower detection limit by applying relatively small galvanostatic current in order to gradually compensate ion flux across a perm-selective PVC[140]. Pulstrodes based on non-equilibrium measurement by imposing current pulse to forces ions to extract into the membrane in order to adjust concentration of primary ions in phase boundary region. The transient potential is recorded as a signal readout[141]. More recently, a novel technique based on constant-potential coulometry of solid-contact ISEs based conducting polymers (CPs) was reported[57-59]. The CP is placed between the metallic surface and the ISM and serveds as redox-capacitor. A constant potential is applied during the entire measurement whilst the concentration of the primary ions is altered, resulting in a transient current. Since the oxidation/reduction of CPs may be limited by charge transport, our group presented the use of commercially available electronic capacitors instead of CPs on a method so-called constant-potential capacitive readout[25]. Hence, ideal capacitive properties have been confirmed and it can be easily altered to amplify the current signal, making it optimally suitable for each application. Coulometric readout is known to improve sensitivity by producing a current signal that is easier to identify than that of direct potentiometric measurement[25, 60]. This approach has also been extended to the

establishment of the CP solid-contact ISE placed in series with a capacitor based on Kirchhoff's circuit laws[111]. Capacitive readout has been accomplished for ultrahigh-sensitive measurement of pH in modified seawater samples and measurement of sodium in serum using solid-contact ISEs in series with a capacitor[25, 111]. Additionally, an electronic circuit was modified in order to automatically control measurement procedure of capacitive readout[67]. Due to the equipment's size, however, it is not yet suitable for on-field analysis. In this work, we describe for the first time a portable constant-potential coulometric device by inegrating a small potentiostat and electronic circuit. A range of capacitors of interest was placed inside the device. This approach aims for real-time monitoring, for instance of small pH variations in seawater.

By implementating non-zero current techniques as mentioned above it is evident that the current flow alters the concentration profile of all mobile ionic species in the membrane[139, 142]. Computer simulations, therefore, may be advantageous to acquire a better understanding of the response mechanisms and dynamic phenomena of ISEs. There is a series of theoretical descriptions available for such dynamic potentiometry. Dynamic evaluation of concentration profiles under zero-current condition have been developed using the Nernst-Planck-Poisson equations[143, 144] or the phase boundary model[145, 146]. In addition, digital solutions were presented to study the electrical behavior of membranes based on liquid ion-exchangers and extended to ionophore membranes with mobile ion-exchanger sites[147]. Buck and Berube explored time-dependent models of electron hopping in the ISMs using the theta function[148]. Mathematical models to describe the effects of constant current have been investigated by Lindner's group and provide information on concentration polarization in the membrane in space and time[149] as well as for large-current chronopotentiometry of ionophore-based ion-selective membranes[150]. In chronoamperometry, a classical model has been obtained by considering a modified Cottrellian term[151].

For the theoretical description of constant-potential coulometry, the transient current has been described in terms of the RC time constant (or τ) involving resistance (R) and capacitance (C) of the electrochemical cell. This approach was further studied by Mikhelson's group where concentration polarization is considered so that a Cottrellian term was added into the charging equation[64]. However, there is no mathematical model available for explaining the phenomena of ion transport inside ISMs during and after a passage of exponentially transient current. Consequently, a knowledge of concentration and potential profiles in the space and time domains would be helpful for the development of the measurement procedure for portable capacitive readout device. A full understanding of the associated mechanism may allow us to enhance performances of the approach in terms of the resulting sensitivity, reproducibly and precision.

Here, we developed a new portable device based on the constant-potential coulometric principle where a potentiometric pH probe is placed in series with a commercial capacitor for seawater measurement. The computer simulation based on Fick's second law describes how a non-constant current gives rise to concentration polarization and affects the phase boundary potential of the ISE. We show that a regeneration of membrane is required in order to acquire better precision. A modified RC charging current equation considering membrane polarization over time is reported that also includes electrical migration effects.

5.2 Experimental and preparation for capacitive readout method

Materials and Reagents. Sodium chloride (NaCl), acetic acid, phosphoric acid, boric acid, hydrogen ionophore I, high molecular weight poly(vinyl chloride) (PVC), Bis(2-ethylhexyl) sebacate (DOS), 2-nitrophenyl octyl ether (o-NPOE), sodium tetrakis[3,5-bis(trifluoromethyl)phenyl]borate (NaTFPB), tetrakis(4-chlorophenyl)borate tetradodecylammonium salt (ETH 500), and tetrahydrofuran (THF) were purchased from Sigma-Aldrich. Chloroform (analytical grade), 1 M sodium hydroxide (NaOH) volumetric solution and 1 M hydrochloric acid (HCl) volumetric solution was purchased from Fisher Scientific. Aqueous solutions were prepared by dissolving the respective salts in deionized water (>18 MΩ cm).

Preparation of the electrodes. A PVC based ion-selective membrane was used for pH measurements, which was composed of 15 mmol kg^{-1} hydrogen ionophore I, 5 mmol kg^{-1} NaTFPB ion-exchanger, 10 wt%, 5 wt% or 2.5 wt% of ETH 500, The rest weight is plasticized polymer with 1:2 ratio of o-NPOE or DOS and PVC (total mass of 200 mg). The cocktail was dissolved in 2.0 mL of THF and poured into glass ring (22 mm ID) affixed onto a glass slide. The solution was allowed to evaporate overnight. This initial membrane was cut with a hole-puncher into small pieces of 8 mm diameter and mounted into Ostec electrode bodies. The electrodes were conditioned in inner filling solution of 10 mM universal buffer and 100 mM NaCl overnight.

Sample preparation A mixed solution of acetic acid, phosphoric acid, and boric acid was dissolved in 10 mM NaCl background electrolyte to obtain the universal buffer at 100 mM final concentration. Seawater from the Mediterranean Sea (Italy) with a salinity of 38 parts per thousand was used as sample solution. The seawater sample was prepared in 100 mM Tris-HCl buffer to maintain the pH at 7.9 and used as reference solution. The desired pH was adjusted by addition of 1 M NaOH or 1 M HCl solution.

Electrochemical Measurements. A double junction Ag/AgCl/3 M KCl/1 M LiOAc electrode (Metrohm, Switzerland) and a platinum rod (Metrohm, Switzerland) were used in a three-electrode cell for all

experiments. A PGSTAT302N Autolab (Metrohm Autolab B.V., Switzerland) controlled by Nova 2.1.4 software was used to perform chronoamperometry, chronopotentiomety, and electrochemical impedance spectroscopy (EIS). Chronoamperometry of a hydrogen-selective electrode (H^+-ISE) connected in series with a commercially available capacitor (1 µF to 220 µF) was used as a standard method in order to evaluate the new portable potentiostat. The procedure was reported elsewhere (publication III). Chronopotentiometry was used to study current perturbation of H^+-ISE without a capacitor in series. The potential was recorded before, during, and after applied current range from 1 nA to 1000 nA. EIS experiments were used to explore H^+-ISEs containing different plasticizers and concentrations of ETH 500 without capacitor in series. Impedance spectra were recorded at OCP in 10 mM universal buffer and 100 mM NaCl with an ac excitation amplitude of 10 mV. A frequency range of 100 kHz – 0.1 Hz was used.

Fabrication of a portable potentiostat A portable potentiostat configured for performing coulometric measurements is illustrated in Fig. 5.1. It is called PotentioCap. The dimensions of the box is 18.5 cm width × 10.7 cm length × 3.6 cm height and its weight is 370 g. This instrument is based on a small commercial potentiostat called EmStat Pico module (PalmSens BV, The Netherlands) with high speed mode. The Emstat is a complete potentiostat in a module. Its main characteristic is its impressive integration. It includes a complete programmable measurement system in a very small size that is 30.5 mm width × 18 mm length × 2.6 mm height. This permits us to fit all needed circuits in a small enclosure. PotentioCap contains tantalum type capacitors (22 µF, 47 µF, 100 µF, 220 µF) coupled with relays that are electric switches operated by a signal in one circuit to control another circuit. The control is through an insulated USB interface connected to a computer using a standard serial port. Three electrodes channels including working electrode, reference electrode, and counter electrode of the potentiostat are available on standard BNC (Bayonet Neill–Concelman) connectors. A custom-developed LabView 2010 software is used to operate the measurement. Figure 5.1A shows the top view of the box, which indicate the internal states of the instrument. The back side view (Fig. 5.1B) shows the position of the USB connector. The front side view shows the connections for the three electrode cell (Fig. 5.1C). The electronic circuit to implement the automated system is illustrated in Fig. 5.1D. The instrument includes three main parts: i) The isolation part that galvanically isolates the instrument. ii) The switches part is a set of relays that reorganize the signal path. iii) The potentiometer part is the measurement part. The 'brain' of the PotentioCap is the Emstat module that controls every part of the device.

For coulometric measurements, the open circuit potential (OCP) of the sensing electrode (vs reference electrode) is determined and subsequently enforced unto the cell by the potentiostat during the chronoamperometric measurements in universal buffer. Transient currents were recorded while the pH was

alternated by consecutively adding NaOH for the basic pH range. The current was then integrated to obtain charge versus pH information.

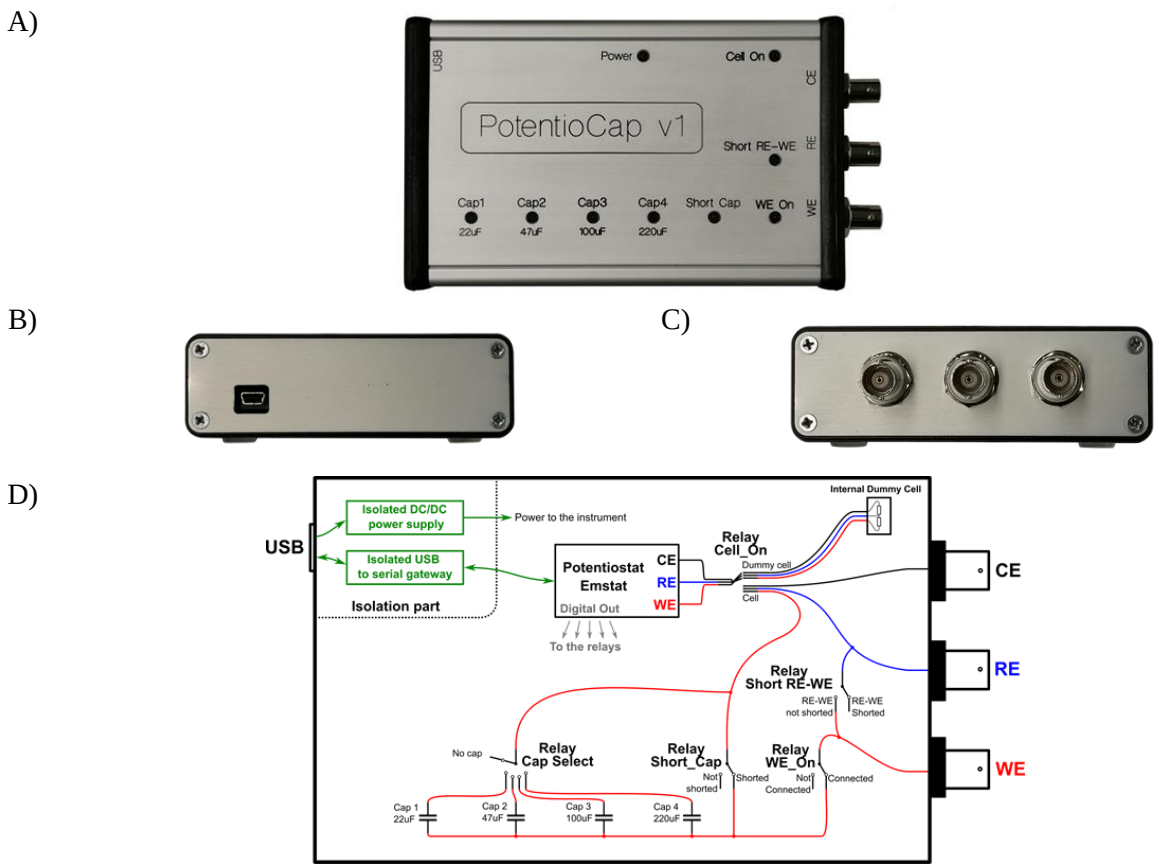

Figure 5.1. Configuration of PotentioCap: (A) the top view, (B) the back side view, (C) the front side view, and (D) the electronic circuit.

5.3 Results and discussion

We use here a hydrogen-selective based PVC polymeric membrane as sensing electrode. The H-ISEs is prepared as seen in the Electrode preparation section. Two types of plasticizers including PCV/DOS and PVC/NPOE were added with the lipophilic electrolyte ETH 500 at 10 wt%, 5 wt%, and 2.5 wt% relative to total membrane mass. Those H-ISEs were characterized by EIS in 10 mM universal buffer pH 7.0 and 100 mM NaCl as shown in Fig. S5.1. The resistance of PVC/NPOE (Fig. S5.1A) was found to be significant smaller than that of PVC/DOS (Fig. S5.1B) owing to the lower lipophilicity of NPOE. According to Ohm's law, a smaller resistance leads to a higher current, which may be an advantage for a better signal-to-noise ratio of chronoamperometric measurements. ETH 500 was added to further reduce the resistance of the

membrane. EIS shows that a higher percentage of ETH 500 give a lower resistance for both of PVC/NPOE and PVC/DOS, as expected. Coulometric readout involves current (electric charge) passing between a H-ISE and a counter electrode. Thus, chronopotentiometry was used to study the potential change of the H-ISM during passage of current and described in term of potential stability. Figure S5.2 illustrated the potential changes of the H-ISEs in universal buffer: i) OCP recorded before perturbation for 1 min (black line), ii) potential drift (iR drop) recorded during current perturbation for 2 s (green line), and iii) OCP recorded immediately after current perturbation for 1 min (yellow line). As described by Ohm's law, the potential is proportional to resistance, which agrees with the chronopotentiogram where iR drop of PVC/DOS (Fig. S5.2B) is greater than PVC/NPOE (Fig. S5.2A). Next, we focused on the potential stability of the H-ISEs based on PVC/NPOE and PVC/DOS containing different amounts of ETH 500. The potential rising sharply over the time indicates the effects of current on concentration polarization of ionic species in the membrane. Figure S5.3 shows chronopotentiometric measurements of potential drift while currents ranging from 1 to 1000 nA were applied for 2 s. The slope of potential over time for PVC/NPOE and PVC/DOS are plotted in Fig. 5.2. Larger current perturbations result in greater potential drifts. However, the H-ISEs prepared with PVC/NPOE gave more stable potentials than with PVC/DOS. The potential of PCV/NPOE is found to drift less with a lower amount of ETH 500 but this was not the case for PVC/DOS. From the experimental data, hydrogen-selective membrane based PVC/NOPE plasticizer containing 2.5 wt% ETH 500 provides best potential stability. This optimized H-ISE was employed for further experiments.

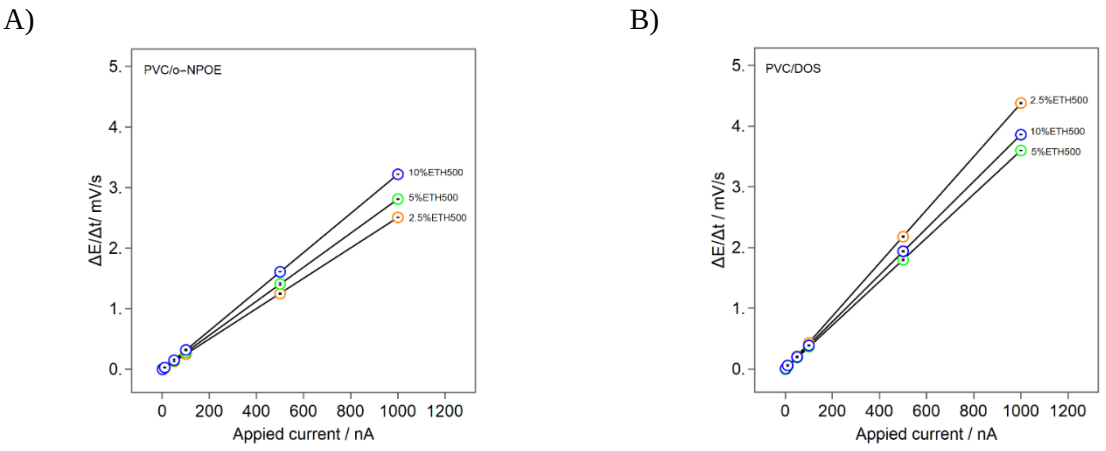

Figure 5.2. Slope of potential drift over time recored by chronopotentiometry when various current is appled to H-ISEs based (A) PVC/NPOE and (B) PVC/DOS with 2.5 wt% (orange circle), 5 wt% (green circle), and 10 wt% (blue) of ETH 500.

After current perturbation, the membranes were left at open circuit to allow the potential to regenerate for 1 min. The difference of OCP before and after applying current is shown in Fig. 5.3. It is clearly seen for both PVC/NPOE and PVC/DOS that the potential deviations between regenerating potential and initial OCP is larger than about 0.1 mV where a current over 100 nA (or charge over 0.2 µC) is applied. The H-ISE with 2.5 wt% ETH 500 is shown to give a smaller potential deviation. This result allows us to choose a proper capacitance of the capacitor in series with the H-ISE that is optimized for each application. Although the larger capacitance gives better sensitivity it also requires more charge pass across the membrane, leading to larger changes of the phase boundary potential.

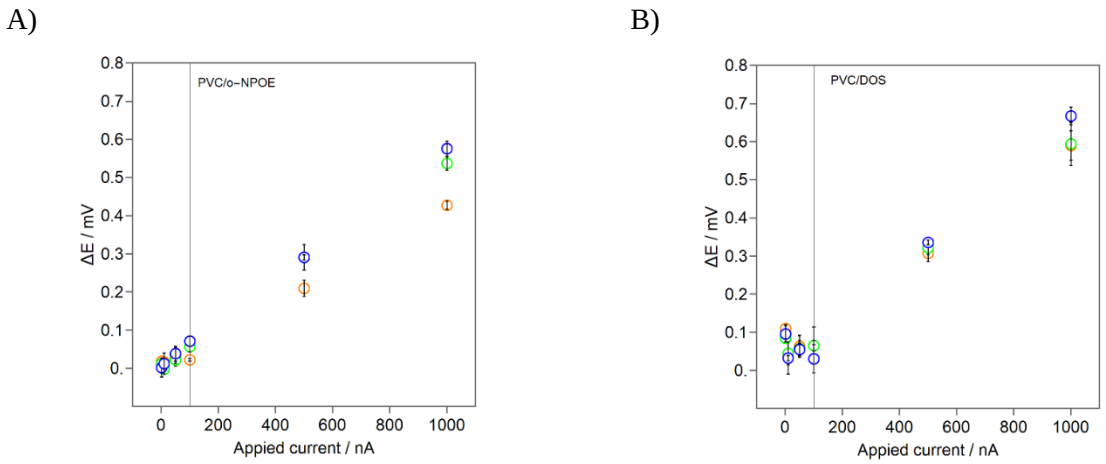

Figure 5.3. Potential deviations between before and after current perturbation of H-ISE with (A) PVC/NPOE and (B) PVC/DOS plasticizer containing 2.5 wt% (orange circle), 5 wt% (greeen circle), and 10 wt% of ETH500.

Constant-potential capacitive readout using optimized electrode and capacitance was tested by the new portable device, the so-called PotentioCap. The circuit was electronically controlled as mention in Chapter 4. The H-ISE is placed in series with a capacitor of 47 µF in order to improve sensitivity. The OCP of the H-ISE against a commercial Ag/AgCl reference electrode was measured in universal buffer pH 7.90 as a reference potential and stored by the device. The pH of the universal buffer was changed in increments of 0.01 pH units by the addition of NaOH. The reference potential was sequentially applied to the cell. Transient currents were then recorded with an interval time of 5 ms. The current was integrated over time to obtain the charge-time information. The capacitor was electronically discharged prior to the next measurement. The obtained results were evaluated by using the Autolab as a potentiostat coupled with the electronic control for capacitive readout as shown in Fig. 5.4. Both current and integrated charge signals obtained from the PotentioCap (Fig. 5.4 solid line) are found to be comparable to the ones obtained from the Autolab (Fig. 5.4 dashed line). This may imply that potable PotentioCap can be used instead of Autolab, which is better suited for on-site analysis.

A) Current vs time

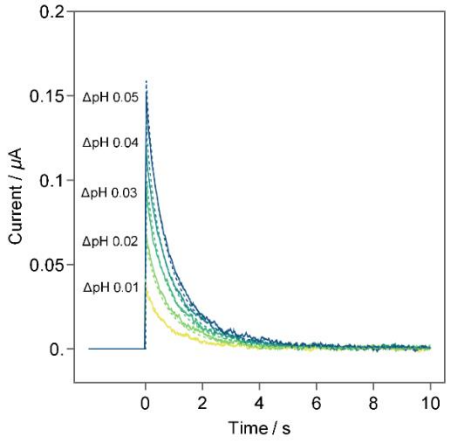

B) Charge vs time

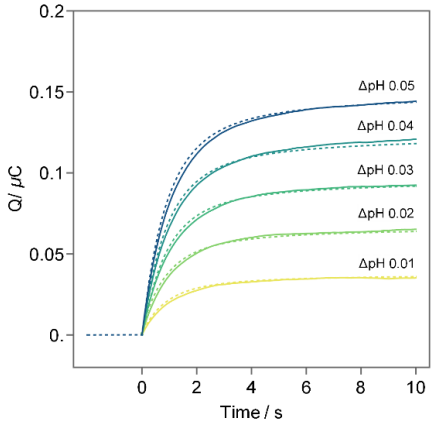

Figure 5.4. Chronoaperometric measurements of H-ISE in series with a 47 µF capacitor. (A) Current transient and (B) integrated charge of 0.01 - 0.05 pH units obtained from Emstat (solid line) vs Autolab (dashed line).

A) PotentioCap

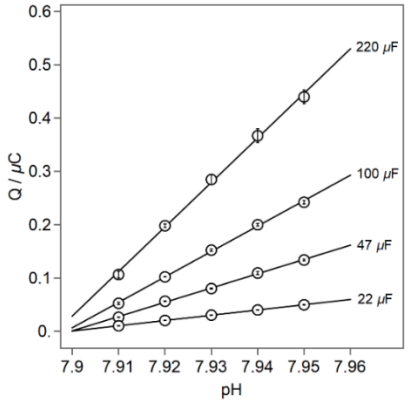

B) Autolab

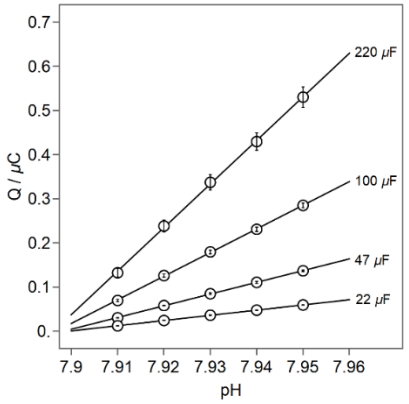

Figure 5.5. Calibration curves of charge vs pH with difference capacitors of 22-220 µF obtained from A) PotentioCap and B) Autolab.

The corresponding calibration curves of integrated charge against pH are illustrated in Fig. 5.5. As expected, an increase of the capacitance value enhances the sensitivity of the pH measurement, which was observed for both PotentioCap and Autolab. A linear correlation of charge vs pH is observed by using capacitors ranging from 22-100 µF. However, the obtained charges deviated from linearity and the standard deviations (n = 3) were substantially greater when a 220 µF capacitor was used. The results are consistent with chonopotentiometric measurements in which charge flows across the membrane of more than 0.2 µC resulted in a significant deviation of the membrane potential. As a consequence, a H-ISE connected in series with a 47 µF capacitor is found to provide sufficient sensitivity and reproducibility for pH measurement with an increment of 0.01 pH units. The slope of using the capacitor of 47 uF in series with H-ISE obtained

from the PotentioCap is 2.68 μC/decade, which is comparable to one from Autolab with 2.65 μC/decade. The observed slopes are near the theoretical value of 2.78 μC/decade, which suggests that near-Nernstian behavior (59.2 mV) is achieved.

Subsequently, the PotentioCap device was tested with actual seawater samples without filtration. Seawater was collected from Mediterranean Sea (Italy) with a salinity of 38 ppt. The pH of seawater was stabilized in 10 mM Tris buffer at pH 7.90. As illustrated in Fig. 5.6, a linear relationship between integrated charge and pH change is obtained from PotentioCap (black solid line) with a linear equation of $Q\,(\mu C) = 2.49\Delta pH - 0.002$, which agrees well with the linear curve obserbed from Autolab (blue dashed line: $Q\,(\mu C) = 2.49\Delta pH + 0.003$). PotentioCap and Autolabe give precisions of 0.6 mpH and 0.5 mpH, respectively, which are better than a conventional pH glass electrode (0.02 pH precision). On-site saltwater measurement with a portable capacitive reading device has been found to be practicable. However, in order to achieve the best performance for this approach, the measuring procedure still needs to be optimized.

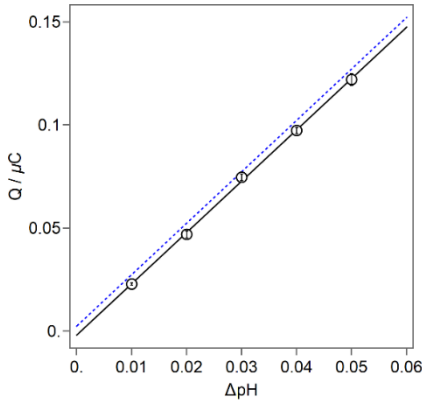

Figure 5.6. Calibration curves between charge and pH change of stabilized seawater obtained from PotentioCap (black solid line) comparing with Autolab (blue dashed line).

Computational simulation of the ion-selective membrane is important to understand how concentration of ion species polarize in the membrane. In order to evaluate the mathematical model, the simulation was firstly carried out for a controlled current experiment. When a current i is applied across the ion-selective membrane, an ion flux J will occur. Based on the Nernst Planck equation in absence of electrical migration and convective effects at the interface, the relationship between this flux and the concentration gradient will be governed with Fick's first law:

$$i = z_j F A J_j(t) = -nFAD_j \frac{(c_{j,n+1}(t) - c_{j,n}(t))}{\delta} \qquad 5.1$$

where D and δ are the diffusion coefficient and the diffusion-layer thickness of ion J with charge z_j in the membrane phase, $c_{j,n+1}(t)$ and $c_{j,n}(t)$ are the time-dependent concentrations at membrane phase of species j from position n to position $n+1$. The first element near membrane surface is the position $n=0$, while F is the Faraday constant and A is the membrane surface area. Concentration changes with time are described by diffusion as:

$$c_{j,n}(t+\Delta t) = c_{j,n}(t) + \left\{c_{j,n-1} - 2c_{j,n} + c_{j,n+1}\right\}\frac{D_j \Delta t}{\delta^2} \qquad 5.2$$

In case of electrical migration and diffusion are considered, eq. 5.2 is modified to:

$$c_{j,n}(t+\Delta t) = c_{j,n}(t) + \frac{D_j \Delta t}{\delta^2}\left\{c_{j,n-1} - 2c_{j,n} + c_{j,n+1} + \left(c_{j,n-1} - c_{j,n+1}\right)\frac{z_j F}{2RT}\Delta\phi\right\} \qquad 5.3$$

where Δt is the time increment chosen in the simulation and $\Delta\phi$ electrochemical potential. The term F/RT is 28.92 mV at 298 K. Subsequently, the membrane potential of the membrane exhibiting the concentration polarization is determined. The membrane potential normally depends on the phase boundary potentials at both sides of the membrane. If the phase boundary at the inner side is symbolized by a prime (‘), the membrane potential is given as:

$$E_M = \frac{RT}{z_j F} ln \frac{a_{j^{z_j}}^{aq}}{a_{j^{z_j}}^{m}} \frac{a_{j^{z_j}}^{m\prime}}{a_{j^{z_j}}^{aq\prime}} \qquad 5.4$$

Here, we assume that the hydrogen ion activity in sample solution is constant due to its buffering property, thus $a_{j^{z_j}}^{aq} = a_{j^{z_j}}^{aq\prime}$. For simplicity membrane activity coefficients are set to unity so that $a_{j^{z_j}}^{m} \cong c_{j^{z_j}}^{m}$. If the ion j extracting into the membrane containing excess amount of ionophore L, it may from complex jL with an assistance of ion-exchanger R. To solve free membrane concentration of j denoted as c_j^m for calculation of eq. 5.4, the complex formation according to eq. 5.5 is used.

$$c_j^m = \frac{c_R^m}{\beta_{jL} c_L^m} \qquad 5.5$$

Figure 5.7 depicted the computational simulations of potential drift (top) and concentration polarization in the membrane (bottom) of chronopotentiometry of H-ISE in universal buffer pH 7.14. The following parameters were used for the simulations: $z_j = 1$, $\Delta t = 1$ ms, i = 100 nA, A = 0.2 cm^2, , $D_{org} = 10^{-12}$ m^2 s^{-1}, δ

= 150 µm, and $a_J(aq) = 10^{-7.14}$, L = 15 mM, $\log\beta_H = 12.6$. Figure 5.7 (top) shows the magnitude of the over potential including the iR drop of 1.3 mV while 100 nA current is applied for 2 s. After current perturbation, the response potential drops to near the OCP. The proposed mathematical model correlates well with the experimental results under the same conditions. The passage 0.2 µC of charge across the membrane causes ~1% change in membrane concentration, which reduce to ~0.2% after left to regenerate at zero-current for 1 min (see Fig. 5.7 bottom). The outcome demonstrates that the suggested mathematical model is reliable and may be adapted for controlled potential experiments.

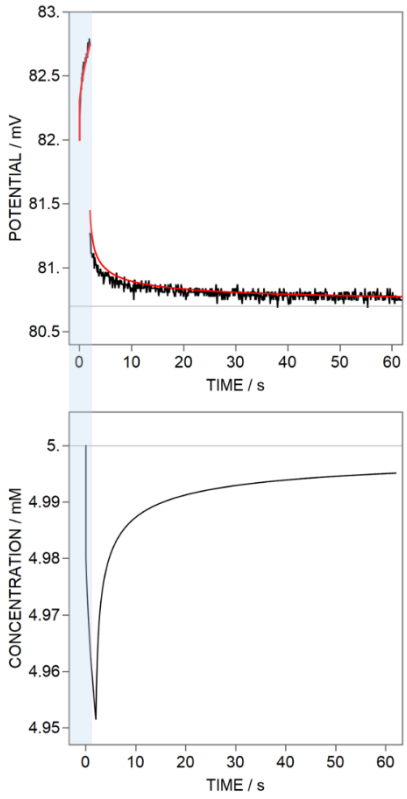

Figure 5.7. Simulation of membrane potential (top: red solid line) and concentration (bottom) over time during current perturbation and fitting with an experimental result (top: black solid line). The horizontal lines identical original OCP (top) and original primary ion concentration in the membrane (bottom). The blue line is when current 100 nA is applied for 2 s.

The first prototype of PotentioCap relies on the electronic circuit presented in Chapter 4. The measurement procedure consists of six parts: i) disconnecting of the sensing electrode to introduce reference solution, ii) making the connection for measurement and storing the value of the OCP of the reference solution by the potentiostat, iii) changing to the sample solution while the electrode connection is broken, iv) applying the

reference potential to the cell, v) immediately recording the transient current once the connection is made, and vi) electronic discharging the capacitor prior to next measurement. Step iii to vi are repeated for each sample as needed in order to determine standard deviations. The demonstration of using the portable PotentioCap for pH measurement is shown in Fig. 5.4-5.6. It is critical to understand the phenomena of ion diffusion in the selective membrane during the entire experimental processes in order to optimize the measuring protocol.

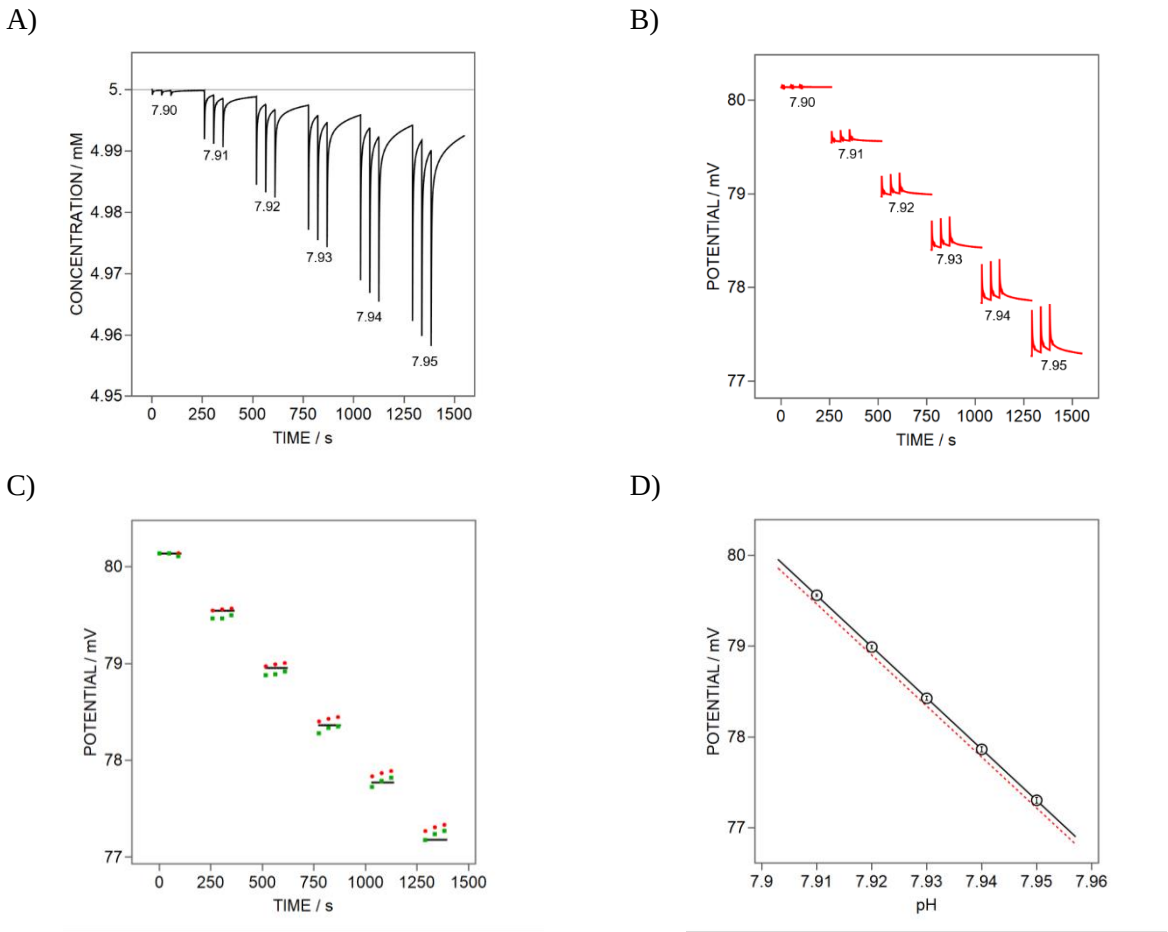

Figure 5.8. Numerial simulation of (A) concentration polarization and (B) potential response during constant-potential coulometric measurement. Black horizontal line in (A) indicate initial concentration in the membrane. (C) Simulated open circuit potential (OCP) (red circle) comparing with OCP obtained from experimental result and theoretical prediction based on Nernst eqation (black solid line) and (D) Calubration curves of potential vs pH obtain form simulation (black solid line) and experimetal (red dashed line).

Here, we used the mathematical model described above to predict the membrane concentration and potential as illustrated in Fig. 5.8. The computational simulation mimics the real experimental procedure when an exponential current (RC current) is generated by the controlled constant potential. Figure 5.8A shows how

the transient current (charge flow) influences the concentration gradient at the H-ISM interface for the measurement with three repetitions of a 0.01 pH increment. In between each sample, the membrane was regenerated under zero current for 2 min. It is clear that the membrane concentration at the interface does not reach initial concentration (5mM hydrogen ion complexes) despite the regeneration. The membrane concentration at the interface decreases by ~1% at the end of the measurement. The phase boundary potential as a result of concentration gradients in the ISM is depicted in Fig. 5.8B. The OCP of each pH sample solution was determined before recording current as illustrated in Fig.5.8C. In comparison to calculated potential response (red circle), the OCP acquired from the experiment (green rectangular) exhibit the same tendency of potential drift. The Nernst equation is used to predict theoretical value of potential change over time (Fig. 5.8C black solid line). The potential raises upward as a result of anodic current perturbation compared to zero current potentiometry. Consequently, linear relationships between potential and pH obtained from both of experimental and simulation are sub-Nernstian with a slope of 56.1 mV/decade and 56.4 mV/decade, respectively (Fig. 5.8D).

Note that the slope of charge over pH change is equal to the Nernst slope multiplied by the capacitance value (slope = $s_{Nernst}C$). If s_{Nernst} was 56.4 mV, the calculated slope of $\Delta Q/\Delta pH$ is 2.65 μC/decade when a 47 μF capacitor was employed. The result correlates well with the slope of charge vs pH obtained in Fig. 5.5 ($\Delta Q/\Delta pH$ = 2.65 μC/decade). The standard deviation (n=3) obtained from simulation was 0.022 mV or 1.034 nC, which is converted to a precision of 0.39 mpH. The numerical simulation demonstrates that concentration polarization, which causes a fluctuation in membrane potential, results in a slope of the capacitive readout approach that falls short of the theoretical expectation.

As acknowledgment earlier, the sensitivity of the constant-potential capacitive readout directly relates to the phase boundary potential. The imposed potential difference between reference solution and sample solution results in a finite required charge to reach the new charge state of the capacitor. In order to obtain minimal potential drifts, ISM regeneration by a non-zero current technique should be considered. This approach has been carried out for ultrasensitive pH measurement (see Chapter 2). The reference solution is introduced to the detection cell after each sample measurement in order to discharge the capacitor. In consequence, the ISM is also forced to be regenerated by applying the initial OCP of the reference solution for a certain time, which causes a transient current in the opposite direction until it reaches the new equilibrium state. As a result, a precision (standard deviation) of 28 μpH and 67 μpH was obtained for pH measurement in standard solution and stabilized seawater, respectively. This approach, however, required the flow of reference solution after each sample analysis, which causes a long measurement time. Also, an air gap was needed in between the reference solution and the sample solution to minimize dispersion, which

may lower the current signal-to-noise ratio. In this work, we suggest to regenerate the ISM by a controlled constant potential. The phenomena of concentration gradients and potential regeneration in the ISM was studied by computational simulation.

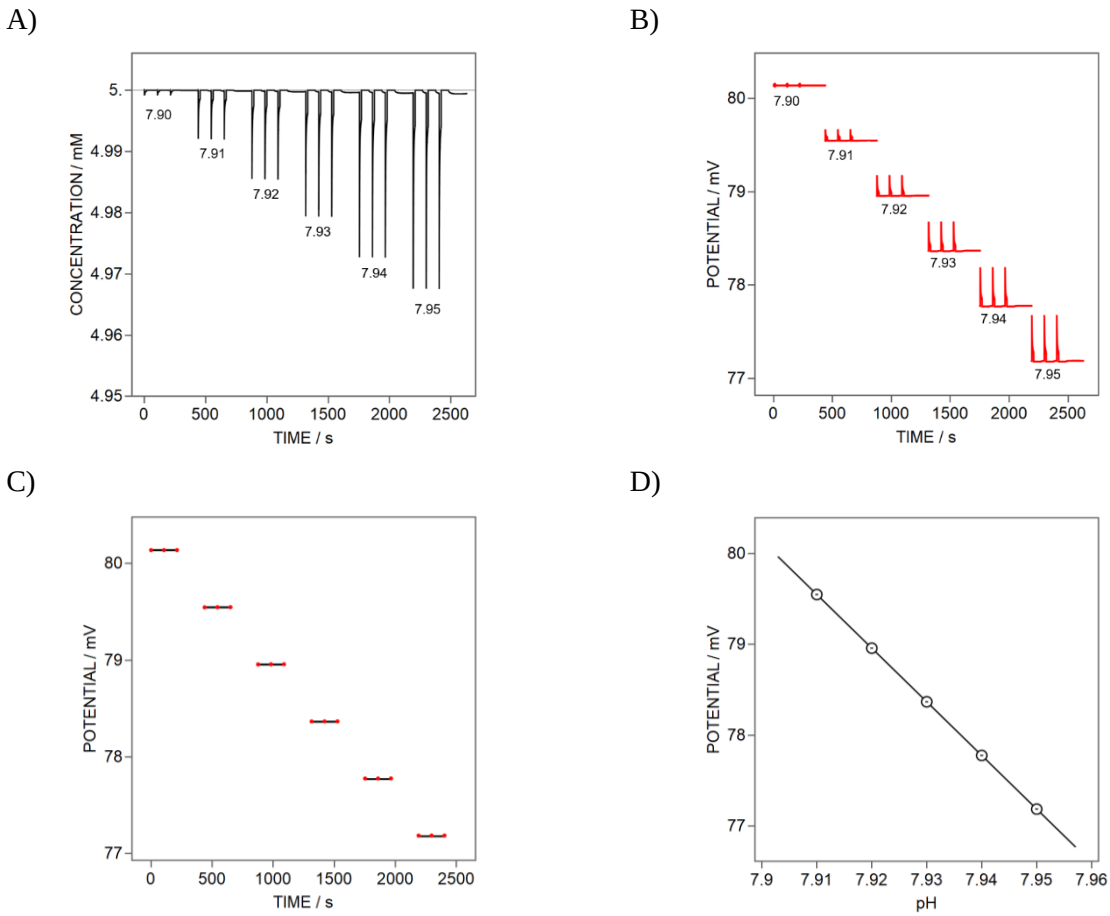

Figure 5.9. Calculated responses of (A) concentration polarization and (B) potential drift when the membrane is regenerated by controlling potental after constant-potential coulometric measurement. Black horizontal line in A) indicate initial concentration in the membrane. (C) Simulated open circuit potential (OCP) (red circle) in comparision of theoretical calculation based on Nernst eqation (black solid line) and (D) Calibration curve of potential vs pH obtain form simulation.

The same measurement procedure for capacitive readout is modified by recording the OCP of the sample solution and enforcing the same OCP after each current measurement. Introduction of the reference solution to the cell, therefore, is no longer required. As a consequence of that method, the phase boundary potentials are forced again to their initial values, which minimizes potential drift for next measurement (Fig. 5.9B). As a result of the controlled potential, the membrane concentration approaches the original concentration (Fig. 5.9A). Figure 5.9C confirms that the simulated OCP (red circles) is close to the theoretical prediction

calculated from the Nernst equation (black solid line). A linear correlation between potential and pH is obtained with a slope of 59.0 mV (59.2 mV for Nernst). It means that membrane regeneration by applying a constant OCP dramatically reduces the potential deviation from theoretical behavior. Precision of coulometric readout is predicted form standard deviation (n=3) obtained from the simulation of 0.592 µV or 27.8 pC. The precision is found to be excellent, to 10 µpH, which is comparable to the one obtained for ultrasensitive pH measurement in Chapter 2. This information may be useful in designing a new measurement procedure for the future generation of PotentioCap.

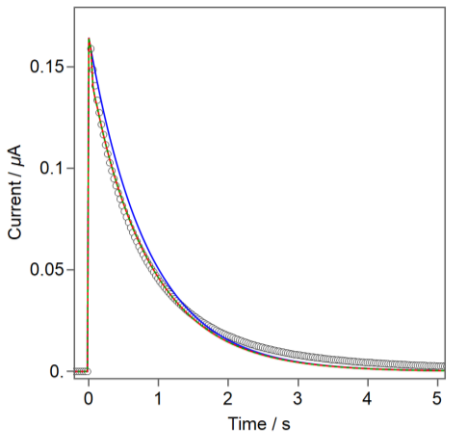

Figure 5.10. Numerical simulation of transient current by considering membrane potential change by time (read solid line) in comparison with constant potential (blue solid line). Green dashed line is when electronic migration is considered for membrane concentration and potential. Circle indicate transient current obtained from experimental result of 0.05 pH change.

As described previously, the phase boundary potential changes with time. The simulation of transient current using a constant potential in the general RC charging current equation as eq. 5.6 may not be sufficiently accurate. We presented for the first time a mathematic model where ion flux is taken in to account to predict the current spike of capacitive readout method. Thus, eq. 5.7 is employed when the potential change depends on time, which is the result of a previous current transient flowing through the ISM in a previous measurement interval. Current and potential are calculated simultaneously from eq.5.1 and eq.5.4 while the concentration gradient occurs. Resistance and capacitance of the cell were chosen as 18 kΩ and 47 µF, respectively

$$i = \frac{E}{R_{cell}} e^{-t/R_{cell}C} \qquad 5.6$$

$$i_{n=0}(t) = \frac{E_{n=0}(t)}{R_{cell}} e^{-t/R_{cell}C} \quad 5.7$$

Figure 5.10 depicts the calculated current responses (red solid line) that are compared to experimental results (circles) observed from pH measurement with a 0.05 pH unit change using an H-ISE. Additionally, the transient current was also evaluated classically by using a constant potential as shown in Fig. 5.10 (blue solid line). The current decay from the drifting potential is sharper than that of the constant potential. At longer times, the current reaches zero baseline faster than one from the experimental data. This may be due to the accumulating concentration gradient in the ISM caused by previous sample measurements. This model could be useful for predicting current transients so that reaching an equilibrium state may not always be required. Mass transport considering diffusion as well as electric migration was also considered by using eq. 5.3 Normally, the effects of migration is normally quite small when concentration gradients are important. Indeed, the simulated transient current computed by considering electrical migration (green dashed line) shows no difference when compared to only diffusion processes (red solid line). This would suggest that migration effects have no significant importance to the current decay.

5.4 Supporting information

A) PVC/NPOE

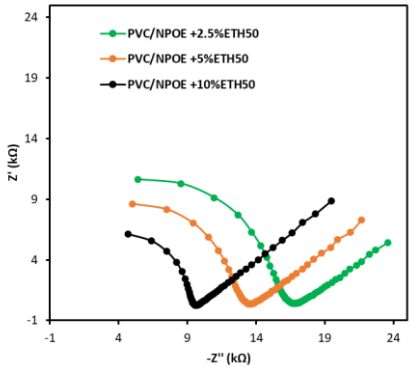

B) PVC/DOS

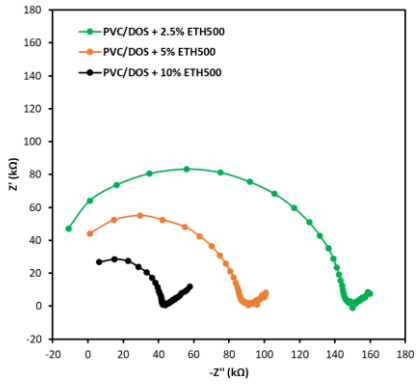

Figure S5.1 Impedance study of hydrogen-selective membranes preparing with different plasticizers of (A) PVC/NPOE and (B) PVC/DOS. The ETH500 were added into the membrane with 2.5 wt%, 5 wt%, and 10 wt%.

A) PVC/NPOE B) PVC/DOS

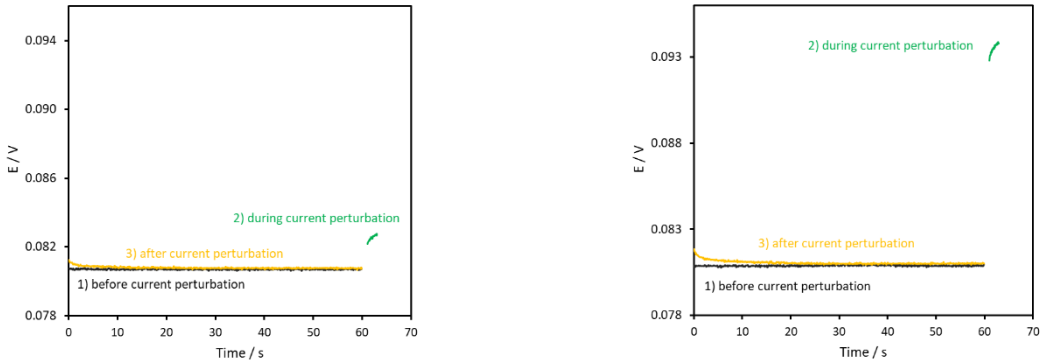

Figure S5.2 Chronopotentiometric measurement of hydrogen-selective electrodes containing 2.5 wt% of plasticizers (A) PVC/NPOE and (B) PVC/DOS. Potentials were recorded before current perturbation (black line), during current perturbation of 100 nA for 2 s (or 0.2 µC; green line), and after current perturbation (yellow line).

A) PVC/DOS +2.5% ETH500 B) PVC/DOS +5% ETH500 C) PVC/DOS +10% ETH500

D) PVC/NPOE +2.5% ETH500 E) PVC/NPOE +5% ETH500 F) PVC/NPOE +10% ETH500

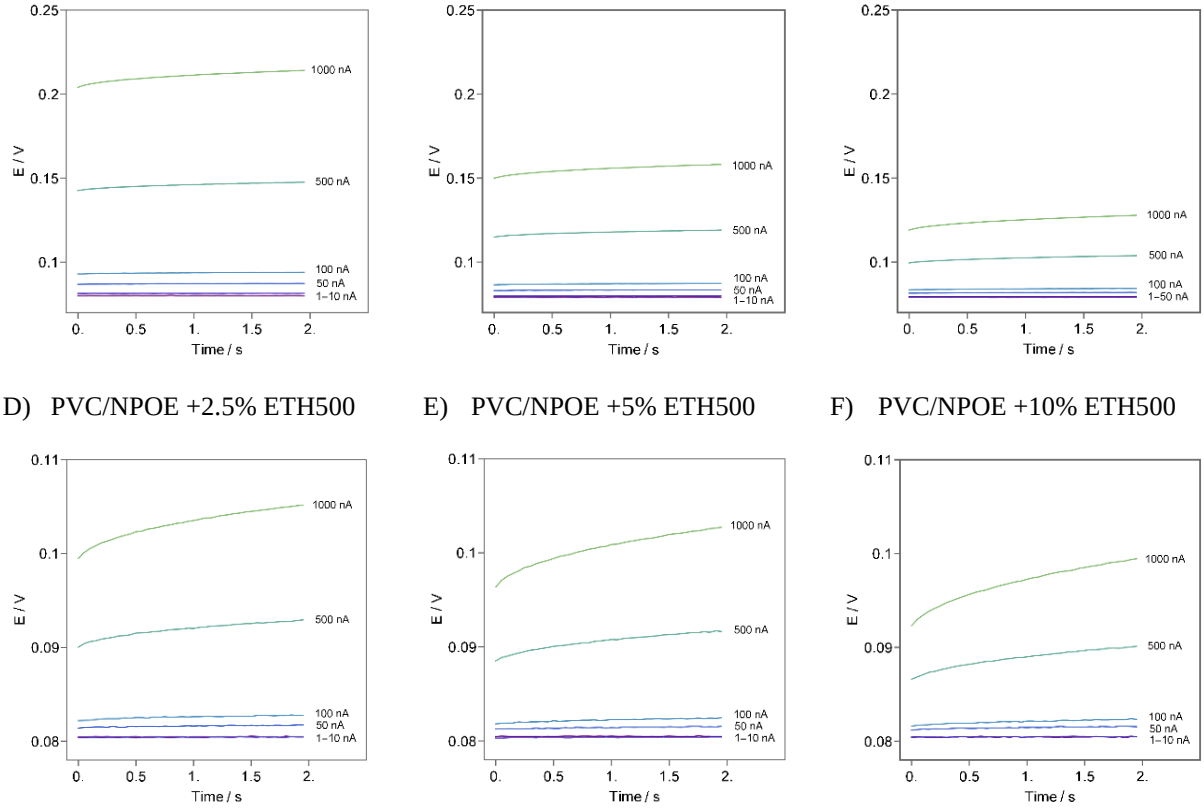

Figure S5.3. Chronopotentiometric recorded of potential drift during current perturbation ranging from 1-1000 nA for 2 s (0.02-2 µC) with membranes containing various amount of ETH500 and different plasticizers as labeled in the Figure.

Conclusions

The main goals of this thesis is to develop a sensor that enhance sensitivity of the signal readout with very high precision and make it convincing for real world analysis. Direct potentiometry has been in use for over a century for the determination of pH. While it remains the gold standard, it does not provide the precision required to assess very small pH changes in important applications such as ocean acidification. In chapter 2, we have shown that potentiometric pH probes can be made orders of magnitude more sensitive by imposing a potential change at the pH electrode over an electronic capacitive element placed in series while maintaining a constant cell potential. The resulting current transient required to charge the capacitor with the same potential amplitude (of opposite sign) is much easier to identify and isolate than a potential-time trace. The precision of this technique is found to be extraordinary, corresponding to just a few microvolts or dozens of micro-pH units and may serve as a basis for applications where very small concentration changes need to be reliably quantified, as in ocean acidification. We note that this advance concerns the underlying measurement principle only. Care must be taken to avoid systematic errors originating from sample manipulation steps, especially re-equilibration with atmospheric CO_2.

Chapter 3 exhibits accomplishment of solid-contact ion-selective electrodes (SC-ISEs) for capacitive readout. SC-ISEs containing capacitive (f-SWCNTs) or redox (POT) solid-contact materials give sluggish, nonideal current transients that make it difficult to apply this attractive readout principle. This behavior suggests that solid-contact materials act as pseudocapacitors that are difficult to describe as a circuit element. On the other hand, constant potential capacitive readout of ion-selective electrodes with aqueous inner solution using a commercially available capacitor were recently reported to give ultrahigh sensitivity, with pH measurement as example. However, it was unclear to what extent this approach could be applied to solid-contact ISEs exhibiting a capacitive transducing layer. Kirchhoff's law for two capacitors connected in series (SC in series with electronic capacitor) suggests that the capacitance for the cell should be dominated by the smallest capacitor. This was found to be confirmed, giving evidence that the desirable capacitive behavior can be imposed by an added electronic capacitor. Still, the accumulation of charge at the electronic capacitor may become limited by the ion-to-electron transducing process at the SC-ISE electrode. For this reason, a larger thickness of transducing material should be preferred. With the f-SWCNT material used here, drop-casting of six layers is sufficient to allow the charging of the added capacitor up to 100 μF. In the case of a single layer of drop-cast POT, a smaller range of added capacitor is acceptable, from 1 to 4.7 μF. This suggests that POT-SC-ISEs may be suitable for applications that do not require the highest possible sensitivity, because higher added capacitances give larger signals. In all cases,

the charge obtained from experiment gave good agreement with theoretical predictions. Electrochemical impedance data confirmed that the diffusion dependence of SC-ISE can be overcome to give pure capacitive behavior. Therefore, the long measurement time and current drifts as major drawbacks of coulometric readout has been overcome to give response times on the order of a few seconds with rapidly decaying current transients. The results obtained here are promising for further development of this class of sensors for applications that require very high sensitivity.

The concept of constant potential capacitive readout of ion-selective membranes has been introduced to improve their sensitivity and precision. The main drawbacks of the coulometric technique are associated with longer measurement times, baseline current drifts and complicated fluidic handling that may not be suitable for routine measurement such as clinical or environmental applications. We have introduced in Chapter 4 a new methodology for the automatic capacitive readout using potentiometric probes for sodium measurement. The automated switching protocol with the help of an electronic circuit to control the charging and discharging events of the electronic capacitor helps one to achieve rapid measurements with improved precision. Here, the use of an external electronic capacitor for coulometric measurements is crucially important as it becomes easy to control its properties by adequate electronics when compared to a chemically induced solid-state capacitive layer. Since the chemical discharging of the capacitor by exposure to a reference solution is no longer necessary (see Chapter 2), the associated fluidics are much simplified while ensuring that the remaining charge in the capacitor is eliminated. The reference potential is recorded and stored by the potentiostat just once before starting the measurement, allowing one to perform multiple consecutive measurements on the same sample. The precision of this method is found to be much improved than direct potentiometry with the same setup, suggesting that the technique is attractive for applications that require high precision, as in clinical diagnostics. Despite these advances it must be kept in mind that any potential drifts translate into a stored reference potential that no longer reflects the true value, which may be a source of systematic errors. This protocol therefore requires ion-selective membranes and current amplitudes that minimize such drifts.

The last Chapter 5 integrates all the knowledge obtained earlier to develop a portable capacitive readout device aiming for on-site measurements. The capacitive readout method was accomplished in laboratory using a regular potentiostat coupled with an external electronic system. This system, however, is not practicable for portability. Here we presented a miniaturized PotentioCap which consists of a small potentiostat and an electronic circuit including a range of capacitor (22-220 µF). All components are placed in a small, lightweight box. The measurement protocol is designed and controlled by LabView software. The PotentioCap was tested and evaluated with the regular capacitive readout using H-ISE in series with a

capacitor for pH measurements in standard solution and stabilized seawater. The linear relationship between charge and pH agreed well with one obtained by a benchtop device and external circuit. Our proposed device has shown a potential for replacing laboratory devices, making it promising for real world analysis. Measurement protocols e.g. chronoamperometry and discharging the capacitor require further optimization to improve its performance. Numerical simulation was performed for the time- and space dependent concentrations and associated potentials inside an ion-selective membrane during capacitive readout. The mathematical model based on Nernst-Planck equation was employed to realize concentration profile during an exponentially decaying current transient. Concentration gradients in the membrane cause a phase boundary potential drift and result in lower reproducibility and precision. Hence, we suggest here to regenerate the membrane concentrations by applying an open circuit potential of the sample solution for 1 min prior next measurement. Consequently, the calculated precision for capacitive readout (10 µpH) is found to be ten times better than without regeneration. The approach agrees well with the ultrasensitive pH measurement described in Chapter 2 with precision in the tens of micropH units. The portable PotentioCap and optimized protocol provide the possibility of being powerful analytical tools for on-field analysis in the future, e.g. in clinical and environmental measurements. However, the robustness of the sensing probe is a crucial aspect and therefore the development of ideal nonpolarizable electrodes may be important for further development of the capacitive readout principle.

References

1. Janata, J., Centennial retrospective on chemical sensors. *Anal. Chem.* **2001,** *73* (5), 150A-153A.
2. Zhu, C.; Yang, G.; Li, H.; Du, D.; Lin, Y., Electrochemical Sensors and Biosensors Based on Nanomaterials and Nanostructures. *Anal. Chem.* **2015,** *87* (1), 230-249.
3. Bakker, E.; Telting-Diaz, M., Electrochemical Sensors. *Anal. Chem.* **2002,** *74* (12), 2781-2800.
4. Bakker, E., Enhancing ion-selective polymeric membrane electrodes by instrumental control. *TrAC, Trends Anal. Chem.* **2014,** *53*, 98-105.
5. Windmiller, J. R.; Wang, J., Wearable Electrochemical Sensors and Biosensors: A Review. *Electroanalysis* **2013,** *25* (1), 29-46.
6. Stradiotto, N. R.; Yamanaka, H.; Zanoni, M. V. B., Electrochemical sensors: a powerful tool in analytical chemistry. *J. Braz. Chem. Soc* **2003,** *14*, 159-173.
7. Cremer, M., *Z. Biologie* **1906,** *47*, 562.
8. Haber, F.; Hlemensiewicz, Z., Über elektrische Phasengrenzkräfte. *Z. Phys. Chem.* **1909,** *67U* (1), 385-431.
9. Harrision, S., Golden Future: the First Fifty Years of Beckman Instruments. *Claremont University Center, CA* **1985**.
10. Lindner, E.; Tóth, K., To the Memory of Ernő Pungor: A Subjective View on the History of Ion-Selective Electrodes. *Electroanalysis* **2009,** *21* (17-18), 1887-1894.
11. Ross, J. W., Calcium-selective electrode with liquid ion exchanger. *Science* **1967,** *156* (3780), 1378-1379.
12. Simon, W., *Swiss Pat. 479870* **1969**.
13. Frant, M.-S.; Ross Jr, J., Potassium ion specific electrode with high selectivity for potassium over sodium. *Science* **1970,** *167* (3920), 987-988.
14. Meyerhoff, M. E., New in vitro analytical approaches for clinical chemistry measurements in critical care. *Clin. Chem.* **1990,** *36* (8), 1567-1572.
15. Ma, S. C.; Yang, V. C.; Meyerhoff, M. E., Heparin-responsive electrochemical sensor: a preliminary study. *Anal. Chem.* **1992,** *64* (6), 694-697.
16. Winkler, S.; Rieger, L.; Saracevic, E.; Pressl, A.; Gruber, G., Application of ion-sensitive sensors in water quality monitoring. *Water Sci. Technol.* **2004,** *50* (11), 105-114.
17. Lewenstam, A.; Maj-Zurawska, M.; Hulanicki, A., Application of ion-selective electrodes in clinical analysis. *Electroanalysis* **1991,** *3*, 727-734.

18. Bakker, E.; Bühlmann, P.; Pretsch, E., Carrier-Based Ion-Selective Electrodes and Bulk Optodes. 1. General Characteristics. *Chem. Rev.* **1997,** *97* (8), 3083-3132.
19. Guggenheim, E. A., The conceptions of electrical potential difference between two phases and the individual activities of ions. *J. Phys. Chem* **2002,** *33* (6), 842-849.
20. Guggenheim, E., On the conception of electrical potential difference between two phases. II. *The J. Phys. Chem* **2002,** *34* (7), 1540-1543.
21. Meyerhoff, M. E.; Opdycke, W. N., Ion-Selective Electrodes. *Advances in Clinical Chemistry*, Spiegel, H. E., Ed. Elsevier: 1986; Vol. 25, pp 1-47.
22. Bakker, E.; Nägele, M.; Schaller, U.; Pretsch, E., Applicability of the phase boundary potential model to the mechanistic understanding of solvent polymeric membrane-based ion-selective electrodes. *Electroanalysis* **1995,** *7* (9), 817-822.
23. Bühlmann, P.; Pretsch, E.; Bakker, E., Carrier-Based Ion-Selective Electrodes and Bulk Optodes. 2. Ionophores for Potentiometric and Optical Sensors. *Chem. Rev.* **1998,** *98* (4), 1593-1688.
24. Zook, J. M.; Langmaier, J.; Lindner, E., Current-polarized ion-selective membranes: The influence of plasticizer and lipophilic background electrolyte on concentration profiles, resistance, and voltage transients. *Sens. Actuators B Chem.* **2009,** *136* (2), 410-418.
25. Kraikaew, P.; Jeanneret, S.; Soda, Y.; Cherubini, T.; Bakker, E., Ultrasensitive Seawater pH Measurement by Capacitive Readout of Potentiometric Sensors. *ACS Sensors* **2020,** *5* (3), 650-654.
26. Cuartero, M.; Pankratova, N.; Cherubini, T.; Crespo, G. A.; Massa, F.; Confalonieri, F.; Bakker, E., In Situ Detection of Species Relevant to the Carbon Cycle in Seawater with Submersible Potentiometric Probes. *Environ. Sci. Technol. Lett.* **2017,** *4* (10), 410-415.
27. Long, R.; Bakker, E., Optical determination of ionophore diffusion coefficients in plasticized poly(vinyl chloride) sensing films. *Anal. Chim. Acta* **2004,** *511* (1), 91-95.
28. Morf, W. E., The principles of ion-selective electrodes and of membrane transport. *New York : Elsevier* **1981**.
29. Bühlmann, P.; Chen, L. D., Ion-selective electrodes with ionophore-doped sensing membranes. *Supramolecular Chemistry: From Molecules to Nanomaterials* **2012,** *5*, 2539.
30. Bakker, E.; Pretsch, E.; Bühlmann, P., Selectivity of Potentiometric Ion Sensors. *Anal. Chem.* **2000,** *72* (6), 1127-1133.
31. Buck, R. P.; Lindner, E., Recommendations for nomenclature of ionselective electrodes (IUPAC Recommendations 1994). *Pure Appl. Chem.* **1994,** *66* (12), 2527-2536.
32. Ceresa, A.; Radu, A.; Peper, S.; Bakker, E.; Pretsch, E., Rational Design of Potentiometric Trace Level Ion Sensors. A Ag+-Selective Electrode with a 100 ppt Detection Limit. *Anal. Chem.* **2002,** *74* (16), 4027-4036.

33. Fibbioli, M.; Morf, W. E.; Badertscher, M.; de Rooij, N. F.; Pretsch, E., Potential Drifts of Solid-Contacted Ion-Selective Electrodes Due to Zero-Current Ion Fluxes Through the Sensor Membrane. *Electroanalysis* **2000,** *12* (16), 1286-1292.
34. De Marco, R.; Veder, J.-P.; Clarke, G.; Nelson, A.; Prince, K.; Pretsch, E.; Bakker, E., Evidence of a water layer in solid-contact polymeric ion sensors. *PCCP* **2008,** *10* (1), 73-76.
35. Cattrall, R. W.; Hamilton, I. C., Coated-Wire Ion-Selective Electrodes. *Ion-Selective Electrode Reviews*, Thomas, J. D. R., Ed. Elsevier: 1984; Vol. 6, pp 125-172.
36. Cadogan, A.; Gao, Z.; Lewenstam, A.; Ivaska, A.; Diamond, D., All-solid-state sodium-selective electrode based on a calixarene ionophore in a poly(vinyl chloride) membrane with a polypyrrole solid contact. *Anal. Chem.* **1992,** *64* (21), 2496-2501.
37. Bobacka, J.; McCarrick, M.; Lewenstam, A.; Ivaska, A., All solid-state poly(vinyl chloride) membrane ion-selective electrodes with poly(3-octylthiophene) solid internal contact. *Analyst* **1994,** *119* (9), 1985-1991.
38. Michalska, A.; Hulanicki, A.; Lewenstam, A., All-Solid-State Potentiometric Sensors for Potassium and Sodium Based on Poly(pyrrole) Solid Contact. *Microchem. J.* **1997,** *57* (1), 59-64.
39. Michalska, A.; Konopka, A.; Maj-Zurawska, M., All-Solid-State Calcium Solvent Polymeric Membrane Electrode for Low-Level Concentration Measurements. *Anal. Chem.* **2003,** *75* (1), 141-144.
40. Bobacka, J., Potential Stability of All-Solid-State Ion-Selective Electrodes Using Conducting Polymers as Ion-to-Electron Transducers. *Anal. Chem.* **1999,** *71* (21), 4932-4937.
41. Bobacka, J., Conducting Polymer-Based Solid-State Ion-Selective Electrodes. *Electroanalysis* **2006,** *18* (1), 7-18.
42. Crespo, G. A.; Macho, S.; Rius, F. X., Ion-Selective Electrodes Using Carbon Nanotubes as Ion-to-Electron Transducers. *Anal. Chem.* **2008,** *80* (4), 1316-1322.
43. Pławińska, Ż.; Michalska, A.; Maksymiuk, K., Optimization of capacitance of conducting polymer solid contact in ion-selective electrodes. *Electrochim. Acta* **2016,** *187*, 397-405.
44. Guzinski, M.; Jarvis, J. M.; D'Orazio, P.; Izadyar, A.; Pendley, B. D.; Lindner, E., Solid-Contact pH Sensor without CO2 Interference with a Superhydrophobic PEDOT-C14 as Solid Contact: The Ultimate "Water Layer" Test. *Anal. Chem.* **2017,** *89* (16), 8468-8475.
45. Jarvis, J. M.; Guzinski, M.; Pendley, B. D.; Lindner, E., Poly(3-octylthiophene) as solid contact for ion-selective electrodes: contradictions and possibilities. *J. Solid State Electrochem.* **2016,** *20* (11), 3033-3041.

46. Kim, Y.; Amemiya, S., Stripping Analysis of Nanomolar Perchlorate in Drinking Water with a Voltammetric Ion-Selective Electrode Based on Thin-Layer Liquid Membrane. *Anal. Chem.* **2008,** *80* (15), 6056-6065.
47. Si, P.; Bakker, E., Thin layer electrochemical extraction of non-redoxactive cations with an anion-exchanging conducting polymer overlaid with a selective membrane. *Chem. Commun.* **2009,** (35), 5260-5262.
48. Cuartero, M.; Bishop, J.; Walker, R.; Acres, R. G.; Bakker, E.; De Marco, R.; Crespo, G. A., Evidence of double layer/capacitive charging in carbon nanomaterial-based solid contact polymeric ion-selective electrodes. *Chem. Commun.* **2016,** *52* (62), 9703-9706.
49. Yuan, D.; Anthis, A. H. C.; Ghahraman Afshar, M.; Pankratova, N.; Cuartero, M.; Crespo, G. A.; Bakker, E., All-Solid-State Potentiometric Sensors with a Multiwalled Carbon Nanotube Inner Transducing Layer for Anion Detection in Environmental Samples. *Anal. Chem.* **2015,** *87* (17), 8640-8645.
50. Lindfors, T., Light sensitivity and potential stability of electrically conducting polymers commonly used in solid contact ion-selective electrodes. *J. Solid State Electrochem.* **2009,** *13* (1), 77-89.
51. Lindner, E.; Gyurcsányi, R. E., Quality control criteria for solid-contact, solvent polymeric membrane ion-selective electrodes. *J. Solid State Electrochem.* **2009,** *13* (1), 51-68.
52. Vanamo, U.; Bobacka, J., Instrument-Free Control of the Standard Potential of Potentiometric Solid-Contact Ion-Selective Electrodes by Short-Circuiting with a Conventional Reference Electrode. *Anal. Chem.* **2014,** *86* (21), 10540-10545.
53. Vanamo, U.; Bobacka, J., Electrochemical control of the standard potential of solid-contact ion-selective electrodes having a conducting polymer as ion-to-electron transducer. *Electrochim. Acta* **2014,** *122*, 316-321.
54. Grygolowicz-Pawlak, E.; Bakker, E., Thin Layer Coulometry with Ionophore Based Ion-Selective Membranes. *Anal. Chem.* **2010,** *82* (11), 4537-4542.
55. Dorokhin, D.; Crespo, G. A.; Afshar, M. G.; Bakker, E., A low-cost thin layer coulometric microfluidic device based on an ion-selective membrane for calcium determination. *Analyst* **2014,** *139* (1), 48-51.
56. Peshkova, M. A.; Sokalski, T.; Mikhelson, K. N.; Lewenstam, A., Obtaining Nernstian Response of a Ca2+-Selective Electrode in a Broad Concentration Range by Tuned Galvanostatic Polarization. *Anal. Chem.* **2008,** *80* (23), 9181-9187.
57. Hupa, E.; Vanamo, U.; Bobacka, J., Novel Ion-to-Electron Transduction Principle for Solid-Contact ISEs. *Electroanalysis* **2015,** *27* (3), 591-594.

58. Vanamo, U.; Hupa, E.; Yrjänä, V.; Bobacka, J., New Signal Readout Principle for Solid-Contact Ion-Selective Electrodes. *Anal. Chem.* **2016,** *88* (8), 4369-4374.
59. Han, T.; Vanamo, U.; Bobacka, J., Influence of Electrode Geometry on the Response of Solid-Contact Ion-Selective Electrodes when Utilizing a New Coulometric Signal Readout Method. *ChemElectroChem* **2016,** *3* (12), 2071-2077.
60. Han, T.; Mattinen, U.; Bobacka, J., Improving the Sensitivity of Solid-Contact Ion-Selective Electrodes by Using Coulometric Signal Transduction. *ACS Sensors* **2019,** *4* (4), 900-906.
61. Han, T.; Mousavi, Z.; Mattinen, U.; Bobacka, J., Coulometric response characteristics of solid contact ion-selective electrodes for divalent cations. *J. Solid State Electrochem.* **2020**.
62. Han, T.; Mattinen, U.; Mousavi, Z.; Bobacka, J., Coulometric response of solid-contact anion-sensitive electrodes. *Electrochim. Acta* **2021,** *367*, 137566.
63. Jarolímová, Z.; Han, T.; Mattinen, U.; Bobacka, J.; Bakker, E., Capacitive Model for Coulometric Readout of Ion-Selective Electrodes. *Anal. Chem.* **2018,** *90* (14), 8700-8707.
64. Kondratyeva, Y. O.; Tolstopjatova, E. G.; Kirsanov, D. O.; Mikhelson, K. N., Chronoamperometric and coulometric analysis with ionophore-based ion-selective electrodes: A modified theory and the potassium ion assay in serum samples. *Sens. Actuators B Chem.* **2020,** *310*, 127894.
65. Charles K. Alexander, M. N. O. S., Fundamentals of Electric Circuits. *New York, McGraw-Hill fifth edition*.
66. RC Charging Circuit. *https://www.electronics-tutorials.ws/rc/rc_1.html*.
67. Kraikaew, P.; Sailapu, S. K.; Bakker, E., Electronic control of constant potential capacitive readout of ion-selective electrodes for high precision sensing. *Sens. Actuators B Chem.* **2021,** *344*, 130282.
68. Allen J. Bard, L. R. F., Electrochemical Methods, Fundamentals and Applications. *John Wiley & Sons* **2001**.
69. Rubinson, J. F.; Kayinamura, Y. P., Charge transport in conducting polymers: insights from impedance spectroscopy. *Chem. Soc. Rev.* **2009,** *38* (12), 3339-3347.
70. Mei, B.-A.; Munteshari, O.; Lau, J.; Dunn, B.; Pilon, L., Physical Interpretations of Nyquist Plots for EDLC Electrodes and Devices. *J. Phys. Chem. C* **2018,** *122* (1), 194-206.
71. Wang, X.-d.; Meier, R. J.; Wolfbeis, O. S., Fluorescent pH-Sensitive Nanoparticles in an Agarose Matrix for Imaging of Bacterial Growth and Metabolism. *Angew. Chem. Int. Ed.* **2013,** *52* (1), 406-409.
72. Kim, J.; Campbell, A. S.; de Ávila, B. E.-F.; Wang, J., Wearable biosensors for healthcare monitoring. *Nat. Biotechnol.* **2019,** *37* (4), 389-406.

73. Nakata, S.; Shiomi, M.; Fujita, Y.; Arie, T.; Akita, S.; Takei, K., A wearable pH sensor with high sensitivity based on a flexible charge-coupled device. *Nat. Electron.* **2018,** *1* (11), 596-603.
74. Anes, B.; Bettencourt da Silva, R. J. N.; Oliveira, C.; Camões, M. F., Seawater pH measurements with a combination glass electrode and high ionic strength TRIS-TRIS HCl reference buffers – An uncertainty evaluation approach. *Talanta* **2019,** *193*, 118-122.
75. Caldeira, K.; Wickett, M. E., Anthropogenic carbon and ocean pH. *Nature* **2003,** *425* (6956), 365-365.
76. Orr, J. C.; Fabry, V. J.; Aumont, O.; Bopp, L.; Doney, S. C.; Feely, R. A.; Gnanadesikan, A.; Gruber, N.; Ishida, A.; Joos, F.; Key, R. M.; Lindsay, K.; Maier-Reimer, E.; Matear, R.; Monfray, P.; Mouchet, A.; Najjar, R. G.; Plattner, G.-K.; Rodgers, K. B.; Sabine, C. L.; Sarmiento, J. L.; Schlitzer, R.; Slater, R. D.; Totterdell, I. J.; Weirig, M.-F.; Yamanaka, Y.; Yool, A., Anthropogenic ocean acidification over the twenty-first century and its impact on calcifying organisms. *Nature* **2005,** *437* (7059), 681-686.
77. Doney, S. C.; Fabry, V. J.; Feely, R. A.; Kleypas, J. A., Ocean Acidification: The Other CO2 Problem. *Ann. Rev. Mar. Sci.* **2009,** *1* (1), 169-192.
78. Seiter, J. C.; DeGrandpre, M. D., Redundant chemical sensors for calibration-impossible applications. *Talanta* **2001,** *54* (1), 99-106.
79. Dickson, A. G., The measurement of sea water pH. *Mar. Chem.* **1993,** *44* (2), 131-142.
80. Fuhrmann, R.; Zirino, A., High-resolution determination of the pH of seawater with a flow-through system. *Deep Sea Res. Part I Oceanogr. Res. Pap.* **1988,** *35* (2), 197-208.
81. Martz, T. R.; Connery, J. G.; Johnson, K. S., Testing the Honeywell Durafet® for seawater pH applications. *Limnol. Oceanogr. Methods* **2010,** *8* (5), 172-184.
82. Johnson, K. S.; Jannasch, H. W.; Coletti, L. J.; Elrod, V. A.; Martz, T. R.; Takeshita, Y.; Carlson, R. J.; Connery, J. G., Deep-Sea DuraFET: A Pressure Tolerant pH Sensor Designed for Global Sensor Networks. *Anal. Chem.* **2016,** *88* (6), 3249-3256.
83. Bresnahan, P. J.; Martz, T. R.; Takeshita, Y.; Johnson, K. S.; LaShomb, M., Best practices for autonomous measurement of seawater pH with the Honeywell Durafet. *Methods Oceanogr.* **2014,** *9*, 44-60.
84. Clayton, T. D.; Byrne, R. H., Spectrophotometric seawater pH measurements: total hydrogen ion concentration scale calibration of m-cresol purple and at-sea results. *Deep Sea Res. Part I Oceanogr. Res. Pap.* **1993,** *40* (10), 2115-2129.
85. Carter, B. R.; Radich, J. A.; Doyle, H. L.; Dickson, A. G., An automated system for spectrophotometric seawater pH measurements. *Limnol. Oceanogr. Methods* **2013,** *11* (1), 16-27.

86. DeGrandpre, M. D.; Hammar, T. R.; Smith, S. P.; Sayles, F. L., In situ measurements of seawater pCO2. *Limnol. Oceanogr.* **1995,** *40* (5), 969-975.
87. Yao, W.; Liu, X.; Byrne, R. H., Impurities in indicators used for spectrophotometric seawater pH measurements: Assessment and remedies. *Mar. Chem.* **2007,** *107* (2), 167-172.
88. Liu, X.; Patsavas, M. C.; Byrne, R. H., Purification and Characterization of meta-Cresol Purple for Spectrophotometric Seawater pH Measurements. *Environ. Sci. Technol.* **2011,** *45* (11), 4862-4868.
89. Alexander, P. W.; Seegopaul, P., Rapid-flow continuous analysis with ion-selective electrodes. *Anal. Chem.* **1980,** *52* (14), 2403-2406.
90. Hibbert, D. B.; Alexander, P. W.; Rachmawati, S.; Caruana, S. A., Multiple sensor response in segmented flow analysis with ion-selective electrodes. *Anal. Chem.* **1990,** *62* (10), 1015-1019.
91. Borges, E. P.; Martelli, P. B.; Reis, B. F., Automatic Stepwise Potentiometric Titration in a Monosegmented Flow System. *Microchim. Acta* **2000,** *135* (3), 179-184.
92. Caldeira, K.; Wickett, M. E., Ocean model predictions of chemistry changes from carbon dioxide emissions to the atmosphere and ocean. *J. Geophys. Res. Oceans* **2005,** *110* (C9).
93. Dore, J. E.; Lukas, R.; Sadler, D. W.; Church, M. J.; Karl, D. M., Physical and biogeochemical modulation of ocean acidification in the central North Pacific. *Proc. Natl. Acad. Sci.* **2009,** *106* (30), 12235.
94. Byrne, R. H.; Mecking, S.; Feely, R. A.; Liu, X., Direct observations of basin-wide acidification of the North Pacific Ocean. *Geophys. Res. Lett.* **2010,** *37* (2).
95. Sokalski, T.; Ceresa, A.; Zwickl, T.; Pretsch, E., Large Improvement of the Lower Detection Limit of Ion-Selective Polymer Membrane Electrodes. *J. Am. Chem. Soc.* **1997,** *119* (46), 11347-11348.
96. Zdrachek, E.; Bakker, E., Potentiometric Sensing. *Anal. Chem.* **2019,** *91* (1), 2-26.
97. James, H. J.; Carmack, G.; Freiser, H., Coated wire ion-selective electrodes. *Anal. Chem.* **1972,** *44* (4), 856-857.
98. Hulanicki, A.; Trojanowicz, M., Calcium-selective electrodes with pvc membranes and solid internal contacts. *Anal. Chim. Acta* **1976,** *87* (2), 411-417.
99. López-López, M.; Bernal, E.; Moyá, M. L.; Sanchez, F.; López-Cornejo, P., Study of ionic surfactants interactions with carboxylated single-walled carbon nanotubes by using ion-selective electrodes. *Electrochem. Commun.* **2016,** *67*, 31-34.
100. Ping, J.; Wang, Y.; Wu, J.; Ying, Y., Development of an all-solid-state potassium ion-selective electrode using graphene as the solid-contact transducer. *Electrochem. Commun.* **2011,** *13* (12), 1529-1532.

101. Jaworska, E.; Wójcik, M.; Kisiel, A.; Mieczkowski, J.; Michalska, A., Gold nanoparticles solid contact for ion-selective electrodes of highly stable potential readings. *Talanta* **2011,** *85* (4), 1986-1989.

102. Rechnitz, G. A.; Lin, Z.-F., Potentiometric measurements with calcium-selective liquid-liquid membrane electrodes. *Anal. Chem.* **1968,** *40* (4), 696-699.

103. Zdrachek, E.; Bakker, E., Electrochemically Switchable Polymeric Membrane Ion-Selective Electrodes. *Anal. Chem.* **2018,** *90* (12), 7591-7599.

104. Bobacka, J.; Ivaska, A.; Grzeszczuk, M., Electrochemical study of poly(3-octylthiophene) film electrodes I. Electrolyte effects on the voltammetric characteristics of the polymer. Three states of the polymer film. *Synth. Met.* **1991,** *44* (1), 9-19.

105. Chen, T.-A.; Wu, X.; Rieke, R. D., Regiocontrolled Synthesis of Poly(3-alkylthiophenes) Mediated by Rieke Zinc: Their Characterization and Solid-State Properties. *J. Am. Chem. Soc.* **1995,** *117* (1), 233-244.

106. Lindfors, T.; Höfler, L.; Jágerszki, G.; Gyurcsányi, R. E., Hyphenated FT-IR-Attenuated Total Reflection and Electrochemical Impedance Spectroscopy Technique to Study the Water Uptake and Potential Stability of Polymeric Solid-Contact Ion-Selective Electrodes. *Anal. Chem.* **2011,** *83* (12), 4902-4908.

107. Veder, J.-P.; De Marco, R.; Clarke, G.; Chester, R.; Nelson, A.; Prince, K.; Pretsch, E.; Bakker, E., Elimination of Undesirable Water Layers in Solid-Contact Polymeric Ion-Selective Electrodes. *Anal. Chem.* **2008,** *80* (17), 6731-6740.

108. Burnett, R. W.; Covington, A. K.; Fogh-Andersen, N.; Külpmann, W. R.; Lewenstam, A.; Maas, A. H. J.; Müller-Plathe, O.; VanKessel, A. L.; Zijlstra, W. G., Use of Ion-Selective Electrodes for Blood-Electrolyte Analysis. Recommendations for Nomenclature, Definitions and Conventions. **2000,** *38* (4), 363-370.

109. Radu, A.; Anastasova-Ivanova, S.; Paczosa-Bator, B.; Danielewski, M.; Bobacka, J.; Lewenstam, A.; Diamond, D., Diagnostic of functionality of polymer membrane – based ion selective electrodes by impedance spectroscopy. *Anal. Methods* **2010,** *2* (10), 1490-1498.

110. Qi, L.; Jiang, T.; Liang, R.; Qin, W., Polymeric membrane ion-selective electrodes with anti-biofouling properties by surface modification of silver nanoparticles. *Sens. Actuators B Chem.* **2021,** *328*, 129014.

111. Kraikaew, P.; Sailapu, S. K.; Bakker, E., Rapid Constant Potential Capacitive Measurements with Solid-Contact Ion-Selective Electrodes Coupled to Electronic Capacitor. *Anal. Chem.* **2020,** *92* (20), 14174-14180.

112. Reynolds, R. M.; Padfield, P. L.; Seckl, J. R., Disorders of sodium balance. *BMJ* **2006,** *332* (7543), 702.

113. McKee, M.; Exall, S.; Stuckler, D.; Wolff, A., 'Normal' serum sodium concentration among inpatients over 65 admitted to hospital: an observational study. *Postgrad. Med. J.* **2016,** *92* (1083), 21.

114. Grillo, A.; Salvi, L.; Coruzzi, P.; Salvi, P.; Parati, G., Sodium Intake and Hypertension. *Nutrients* **2019,** *11* (9), 1970.

115. Farquhar, W. B.; Edwards, D. G.; Jurkovitz, C. T.; Weintraub, W. S., Dietary sodium and health: more than just blood pressure. *J. Am. Coll. Cardiol* **2015,** *65* (10), 1042-1050.

116. Adrogué, H. J.; Madias, N. E., Hyponatremia. *New Eng. J. Med.* **2000,** *342* (21), 1581-1589.

117. Adrogué, H. J.; Madias, N. E., Hypernatremia. *New Eng. J. Med.* **2000,** *342* (20), 1493-1499.

118. Bataille, S.; Baralla, C.; Torro, D.; Buffat, C.; Berland, Y.; Alazia, M.; Loundou, A.; Michelet, P.; Vacher-Coponat, H., Undercorrection of hypernatremia is frequent and associated with mortality. *BMC Nephrol.* **2014,** *15* (1), 37.

119. Greenberg, A.; Verbalis, J. G.; Amin, A. N.; Burst, V. R.; Chiodo Iii, J. A.; Chiong, J. R.; Dasta, J. F.; Friend, K. E.; Hauptman, P. J.; Peri, A.; Sigal, S. H., Current treatment practice and outcomes. Report of the hyponatremia registry. *Kidney Int.* **2015,** *88* (1), 167-177.

120. Adrogué, H. J., Consequences of Inadequate Management of Hyponatremia. *Am. J. Nephrol.* **2005,** *25* (3), 240-249.

121. Cerdà-Esteve, M.; Cuadrado-Godia, E.; Chillaron, J. J.; Pont-Sunyer, C.; Cucurella, G.; Fernández, M.; Goday, A.; Cano-Pérez, J. F.; Rodríguez-Campello, A.; Roquer, J., Cerebral salt wasting syndrome: Review. *Eur. J. Intern. Med.* **2008,** *19* (4), 249-254.

122. Chauhan, K.; Pattharanitima, P.; Patel, N.; Duffy, A.; Saha, A.; Chaudhary, K.; Debnath, N.; Van Vleck, T.; Chan, L.; Nadkarni, G. N.; Coca, S. G., Rate of Correction of Hypernatremia and Health Outcomes in Critically Ill Patients. *Clin. j. Am. Soc. Nephrol.* **2019,** *14* (5), 656.

123. Sterns, R. H.; Nigwekar, S. U.; Hix, J. K., The Treatment of Hyponatremia. *Semin. Nephrol.* **2009,** *29* (3), 282-299.

124. Julie, R.; Clara Odilia, S.; Irina, C.; Bettina, W.; Ingeborg, S.; Martin, F.; Wiebke, F.; Mirjam, C.-C., The challenges of sodium measurements: indirect versus direct ion-selective method. *Eur. J. Endocrinol.* **2019,** *181* (2), 193-199.

125. Garcia, R. A.; Vanelli, C. P.; Pereira Junior, O. D. S.; Corrêa, J. O. d. A., Comparative analysis for strength serum sodium and potassium in three different methods: Flame photometry, ion-selective electrode (ISE) and colorimetric enzymatic. *J. Clin. Lab. Anal.* **2018,** *32* (9), e22594-e22594.

126. Buzanovskii, V. A., Ion Chromatography, Spectrophotometry, Titrimetry, and Gravimetry Measurements of Sodium Concentration in the Blood. *Meas. Tech.* **2016,** *59* (6), 678-683.

127. Albert, V.; Subramanian, A.; Rangarajan, K.; Pandey, R. M., Agreement of two different laboratory methods used to measure electrolytes. *J. Lab. Physicians* **2011,** *3* (2), 104-109.

128. Burnett, R. W.; Covington, A. K.; Fogh-Andersen, N.; Külpmann, W. R.; Lewenstam, A.; Maas, A. H. J.; Müller-Plathe, O.; Sachs, C.; Siggaard-Andersen, O.; VanKessel, A. L.; Zijlstra, W. G., Recommendations for Measurement of and Conventions for Reporting Sodium and Potassium by Ion-Selective Electrodes in Undiluted Serum, Plasma or Whole Blood. **2000,** *38* (10), 1065-1071.

129. Doku, G. N.; Gadzekpo, V. P. Y., Simultaneous determination of lithium, sodium and potassium in blood serum by flame photometric flow-injection analysis. *Talanta* **1996,** *43* (5), 735-739.

130. Mazzachi, R. D.; Mazzachi, B. C.; Berry, M. N., A Manual Spectrophotometric Method for the Measurement of Serum Sodium and Potassium by Enzyme Activation. **1994,** *32* (9), 709-718.

131. Burnett, D.; Ayers, G. J.; Rumjen, S. C.; Woods, T. F., Sodium Measurements in the Presence of Paraproteins by Four Direct ISE Methods and Flame Photometry Compared. *Ann. Clin. Biochem.* **1988,** *25* (1), 102-109.

132. Berry, M. N.; Mazzachi, R. D.; Pejakovic, M.; Peake, M. J., Enzymatic determination of sodium in serum. *Clin. Chem.* **1988,** *34* (11), 2295-2298.

133. Bruno, A. E.; Barnard, S.; Rouilly, M.; Waldner, A.; Berger, J.; Ehrat, M., All-Solid-State Miniaturized Fluorescence Sensor Array for the Determination of Critical Gases and Electrolytes in Blood. *Anal. Chem.* **1997,** *69* (3), 507-513.

134. Shea, A. M.; Hammill, B. G.; Curtis, L. H.; Szczech, L. A.; Schulman, K. A., Medical costs of abnormal serum sodium levels. *J. Am. Soc. Nephrol.* **2008,** *19* (4), 764-770.

135. Bakker, E., Determination of Unbiased Selectivity Coefficients of Neutral Carrier-Based Cation-Selective Electrodes. *Anal. Chem.* **1997,** *69* (6), 1061-1069.

136. Bakker, E.; Bühlmann, P.; Pretsch, E., The phase-boundary potential model. *Talanta* **2004,** *63* (1), 3-20.

137. Nägele, M.; Bakker, E.; Pretsch, E., General Description of the Simultaneous Response of Potentiometric Ionophore-Based Sensors to Ions of Different Charge. *Anal. Chem.* **1999,** *71* (5), 1041-1048.

138. Morf, W. E.; Simon, W., Cation-Response Mechanism of Neutral Carrier Based Ion-Selective Electrode Membranes. *Helv. Chim. Acta* **1986,** *69* (5), 1120-1131.

139. Crespo, G. A.; Bakker, E., Dynamic electrochemistry with ionophore based ion-selective membranes. *RSC Advances* **2013,** *3* (48), 25461-25474.

140. Pergel, É.; Gyurcsányi, R. E.; Tóth, K.; Lindner, E., Picomolar Detection Limits with Current-Polarized Pb2+ Ion-Selective Membranes. *Anal. Chem.* **2001,** *73* (17), 4249-4253.

141. Makarychev-Mikhailov, S.; Shvarev, A.; Bakker, E., Pulstrodes: Triple Pulse Control of Potentiometric Sensors. *J. Am. Chem. Soc.* **2004,** *126* (34), 10548-10549.

142. Buck, R. P.; Lindner, E., Studies of Potential Generation Across Membrane Sensors at Interfaces and through Bulk. *Acc. Chem. Res.* **1998,** *31* (5), 257-266.

143. Lingenfelter, P.; Bedlechowicz-Sliwakowska, I.; Sokalski, T.; Maj-Zurawska, M.; Lewenstam, A., Time-Dependent Phenomena in the Potential Response of Ion-selective Electrodes Treated by the Nernst− Planck− Poisson Model. 1. Intramembrane Processes and Selectivity. *Anal. Chem.* **2006,** *78* (19), 6783-6791.

144. Sokalski, T.; Lingenfelter, P.; Lewenstam, A., Numerical solution of the coupled Nernst− Planck and Poisson equations for liquid junction and ion selective membrane potentials. *J. Phys. Chem. B* **2003,** *107* (11), 2443-2452.

145. Morf, W. E.; Pretsch, E.; De Rooij, N. F., Computer simulation of ion-selective membrane electrodes and related systems by finite-difference procedures. *J. Electroanal. Chem.* **2007,** *602* (1), 43-54.

146. Radu, A.; Meir, A. J.; Bakker, E., Dynamic diffusion model for tracing the real-time potential response of polymeric membrane ion-selective electrodes. *Anal. Chem.* **2004,** *76* (21), 6402-6409.

147. Nahir, T. M.; Buck, R. P., Transport processes in membranes containing neutral ion carriers, positive ion complexes, negative mobile sites, and ion pairs. *J. Phys. Chem.* **1993,** *97* (47), 12363-12372.

148. Buck, R. P.; Beruhe, T. R., Theta functions; transform tables and examples for electrochemists. *J. Electroanal. Chem. Interf. Electrochem.* **1988,** *256* (2), 239-253.

149. Zook, J. M.; Buck, R. P.; Langmaier, J.; Lindner, E., Mathematical Model of Current-Polarized Ionophore-Based Ion-Selective Membranes. *J. Phys. Chem. B* **2008,** *112* (7), 2008-2015.

150. Zook, J. M.; Buck, R. P.; Gyurcsányi, R. E.; Lindner, E., Mathematical Model of Current-Polarized Ionophore-Based Ion-Selective Membranes: Large Current Chronopotentiometry. *Electroanalysis* **2008,** *20* (3), 259-269.

151. Nahir, T. M.; Buck, R. P., Modified Cottrell behavior in thin layers: Applied voltage steps under diffusion control for constant-resistance systems. *J. Electroanal. Chem.* **1992,** *341* (1), 1-14.